LIGHT-GUIDED LUMPECTOMY: VISUAL AND QUANTITATIVE LOCALIZATION OF BREAST LESIONS

By

Amanda L. Dayton

A DISSERTATION

Presented to the Department of Biomedical Engineering

and the Oregon Health & Science University

School of Medicine

in partial fulfillment of

the requirements for the degree of

Doctor of Philosophy

September 22, 2013

School of Medicine
Oregon Health & Science University

CERTIFICATE OF APPROVAL

This certifies that the Ph.D. dissertation of
Amanda L. Dayton
has been approved

Scott Prahl, Ph.D.	Mentor
Donald Duncan, Ph.D.	Member
Steven Jacques, Ph.D.	Member
Ronald Wolf, M.D.	Member
Monica Hinds, Ph.D.	Member
Tania Vu, Ph.D.	Member

Abstract

In the U.S. in 1996, the last year the National Survey of Ambulatory Surgery was completed, 341,000 outpatient lumpectomies were performed. Positive margins following lumpectomy in approximately 30 %, of procedures, the patient usually undergoes a second surgery to clear the margins. The long term goal of this work was to develop a simple, practical tool to improve the outcome of lumpectomy surgeries. An optical wire was developed to make the breast tissue surrounding a lesion glow red by placing a light source within the lesion.It was hypothesized that light guided lumpectomies could result in a decrease in positive margins, fewer procedures, reduced cost, and better cosmetic outcomes. The goals of the work presented here were to develop an optical wire, clinically evaluate the feasibility of light guided lumpectomies, and to quantitatively determine the distance from the tissue surface to a light source within.

An optical wire was designed with a 3 m optical fiber axially attached to a standard localization wire. After placement of the wire, the lumpectomy could be performed using standard methods but with the additional assistance of being able to see a red glow-ball of light surrounding the lesion. A small clinical study of light guided lumpectomy in 8 patients was conducted. During surgery, a glow-ball of red light provided immediate visualization at the end of the optical wire which the surgeon was able use to estimate proximity to the wire tip. Seven of the eight lumpectomies resulted in negative margins upon pathology review. Use of the optical wire resulted in good clinical outcomes, but it was re-designed to be more comfortable for the patient and easier to use.

The intensity of the visible light during lumpectomy was variable and not a reliable indicator of distance from the light source. In addition to a visual guide, the operating surgeon also wanted to know exactly how far the dissection plane was from the lesion. It was hypothesized that the distance could be determined using the light emitted from the optical wire with frequency domain measurements. In scattering media, sinusoidally

modulated light becomes demodulated and a phase lag develops between the source and the propagating wave.

A multi detector probe is proposed to be used in conjunction with light-guided lumpectomy to give the operating surgeon a quick measurement of distance within the breast without *a-priori* knowledge of the tissue optical properties. An expected relative error of 1 % from the proposed method was determined.

A fiber coupled optical system was assembled to modulate the intensity of a red laser diode with a network analyzer. The detected signal was compared to the source and a phase lag between the two was measured. As expected, the phase lag measured through optical phantoms was found to be in agreement with the diffusion theory approximation and found to be linear as a function of distance from the source with a deviation from linearity of 0.1 deg/mm. Three prophylactic mastectomy specimens were also tested after surgery and before examination by pathology. During the investigations, an optical fiber was inserted stereotactically through a needle and the phase lag from the edge of the tissue to the fiber tip was measured with another optical fiber. The phase lag was used to determine the distance between the fibers. Optical measurements of the distance between source and detector were within 15 % of the actual value.

Acknowledgements

Without the support and encouragement of those around me, I would not have finished this long journey to attain three letters after my name. I have been lucky to work with truly amazing people who made getting through the research an experience we laughed about daily. Thank you Teresa, Rose, Lisa, Becki, Ping Katrina, Ville, Kari, and Gen for your smiling faces and brilliant wit. Thank you.

I extend heartfelt gratitude to Scott Prahl for guiding me through the ups and downs of research. Thank you for teaching me some science, some engineering, some business, some 'mad' presentation skills, and that apple IS better. Mostly, I appreciate that you gave me the freedom to make decisions... and therefore mistakes and then helped me either pick up the pieces or celebrate a success. Thank you.

Don Duncan and Steve Jacques both helped me through my time as a graduate student with their clever insight and commitment to teaching. Both in and out of the classroom, you have both been supportive yet critical and pushed me to consider problems in ways I hadn't considered. Thank you.

I was lucky enough to marry the love of my life, James Dayton. Thank you for your love, your unwavering support, and holding me up when I needed it. I could not have done this without you and would not be the person I am without you. Thank you.

Contents

List of Figures **ix**

List of Tables **xvii**

1 Introduction **1**

1.1 Specific Aims . . . 1

1.2 Significance & Background . . . 1

1.2.1 Significance . . . 1

1.2.2 Background . . . 2

1.3 Current Therapy: Diagnosis . . . 2

1.3.1 Imaging: Mammogram, Ultrasound, Magnetic Resonance . . . 2

1.3.2 Biopsy and Clip Placement . . . 2

1.3.3 Staging . . . 3

1.4 Current Therapy: Treatment . . . 4

1.4.1 Breast Surgery . . . 4

1.4.2 Margins . . . 4

1.4.3 Kopans Wire . . . 5

1.4.4 Partial Breast Irradiation . . . 6

1.5 Rationale . . . 6

2 Light Guided Lumpectomy: Device and Case Report **11**

2.1 Introduction . . . 11

2.2 Benchtop Development . . . 13

2.2.1 Visibility . . . 13

2.2.2 Prophylactic Mastectomy Specimens . . . 15

2.3 Fabrication and Testing . . . 16
2.3.1 Light Delivery . . . 17
2.3.2 Optical Wire Assembly . . . 18
2.4 Clinical Use . . . 19
2.5 Conclusion . . . 21

3 Light Guided Lumpectomy: First Clinical Experience 23
3.1 Introduction . . . 23
3.2 Materials & Methods . . . 25
3.2.1 Optical Wire . . . 25
3.2.2 Wire Localization . . . 26
3.2.3 Light-guided Lumpectomy . . . 27
3.2.4 Pathology . . . 27
3.3 Results . . . 28
3.3.1 Wire Localization . . . 28
3.3.2 Light-guided Lumpectomy . . . 28
3.3.3 Specimen Radiograph . . . 30
3.3.4 Pathology . . . 30
3.4 Discussion . . . 31

4 Light Guided Lumpectomy: Second Generation Device 33
4.1 Introduction . . . 33
4.2 Fabrication . . . 34
4.2.1 Optical Wire Components . . . 35
4.3 Instructions for Use . . . 38
4.3.1 Needle Localization . . . 38
4.3.2 Lumpectomy . . . 38
4.4 Tensile Testing . . . 39
4.5 Sterilization . . . 42
4.5.1 Results . . . 43
4.6 Conclusions . . . 44

5 Measuring Distance in the Frequency Domain: Theory & Simulations **45**
5.1 Introduction . . . 45
5.1.1 Optical Properties of Breast Tissue . . . 45
5.2 Theory . . . 49
5.3 Materials & Methods . . . 52
5.3.1 Boundaries . . . 52
5.3.2 Monte Carlo Model . . . 54
5.4 Results . . . 55
5.4.1 Boundaries . . . 55
5.4.2 Monte Carlo Model . . . 56
5.5 Conclusions . . . 56

6 A self-calibrating distance measurement device **61**
6.1 Introduction . . . 61
6.2 Design . . . 63
6.3 Error Analysis . . . 65
6.3.1 Materials & Methods . . . 65
6.3.2 Results . . . 70
6.4 Conclusions . . . 70

7 Measuring Distance Through Optical Phantoms **75**
7.1 Introduction . . . 75
7.2 Materials & Methods . . . 75
7.2.1 Optical Phantoms . . . 75
7.2.2 Modulation System . . . 78
7.2.3 System Stability . . . 78
7.2.4 Modulation Frequency . . . 79
7.2.5 Diffusion Approximation . . . 79
7.2.6 Linear Phase Response . . . 80
7.2.7 System Offset . . . 81
7.3 Results . . . 81
7.3.1 System Stability . . . 81
7.3.2 Modulation Frequency . . . 83

7.3.3 Diffusion Approximation . . . 85
7.3.4 Linear Phase Response . . . 85
7.3.5 System Offset . . . 86
7.4 Conclusions . . . 86

8 Measuring Distance Through Breast Tissue 89
8.1 Introduction . . . 89
8.2 Materials & Methods . . . 90
8.2.1 Study Design . . . 90
8.2.2 Measurement System . . . 90
8.2.3 Coaxial Measurement Geometry . . . 91
8.2.4 Perpendicular Measurement Geometry . . . 92
8.3 Results . . . 96
8.3.1 Coaxial Measurement Geometry . . . 96
8.3.2 Perpendicular Measurement Geometry . . . 99
8.4 Conclusions . . . 99

9 General Discussion & Conclusions 103
9.1 Light Guided Lumpectomy and First Generation Optical Wire . . . 103
9.2 Second Generation Optical Wire . . . 104
9.3 Intensity Modulation: Modeling & Diffusion Theory . . . 105
9.4 Self Calibrating Distance Measurement Probe . . . 105
9.5 Measuring Distance Through Optical Phantoms . . . 106
9.6 Measuring Distance Through Breast Tissue . . . 107
9.7 Discussion . . . 107

References 109

Appendices 117

A Steam Sterilization Study of the Optical Wire 119

B Code **131**

B.1 Time Resolved Monte Carlo 131

B.2 Fourier Transform of Time Resolved Monte Carlo 139

B.3 Error Analysis of Probe Design 148

B.4 Photon Distribution Monte Carlo 149

B.5 Analysis of Photon Distribution Monte Carlo 157

List of Figures

1.1 *Left:* Digital mammogram revealing micro-calcifications suspicious for ductal carcinoma *in situ* (DCIS). *Right:* The dark, hypo-echoic, irregular shaped mass is DCIS in an image generated by ultrasound. 3

2.1 The optical wire used for light guided lumpectomy. The device consists of a 200 μm optical fiber adhered to a standard Kopans wire. 13

2.2 The simulated relative visibility of light through 30 mm of breast tissue shows a peak near 650 nm. The overall visibility has been normalized to 1. 14

2.3 An example of breast tissue illumination with a red laser, an optical fiber is located 10 mm within the tissue. The glowball of light can be seen surrounding the needle directly above the ruler. Visualized through the skin with room lights on (*top*) the glowball is 2 cm in diameter and 4 cm in diameter with the lights dimmed (*bottom*). 15

2.4 The diameter of visible light through mastectomy tissue as the depth of a 3 mW 633 nm light source was increased. Visible diameter is shown under typical laboratory lighting (lit) conditions and with most laboratory lights off (dark). 16

2.5 To couple light into a bare 200 μm fiber in the operating room, the light from a 633 nm HeNe laser traveled through a neutral density filter wheel and was then focused with an objective onto the fiber face. The fiber was positioned within a fixed SMA connector and held in place with a fiber clamp. The neutral density wheel was used to control the power emitted from the fiber. 17

2.6 *Top* The Kopans wire is the standard wire used in wire guided lumpectomies. It is a thin stainless steel wire bent at its tip to anchor it in tissue once deployed. *Bottom* The assembled optical wire was composed of a Kopans wire with an optical fiber adhered to it with medical grade epoxy (light grey) along the length of the Kopans wire. The epoxy and optical fiber were offset 3 mm from the tip of the Kopans wire. 18

2.7 Orthogonal mammograms of the optical wire placement, *Left* lateral medial projection *Right* cranial caudal projection. The hook end of the wire and the fiber tip are within 3 mm of the biopsy clip within the lesion. One centimeter separates each line on the rules. 19

2.8 After illuminating the optical wire, the lesion was surrounded with light that could be seen through the skin and the incision site. 20

3.1 Red light emission from excised human breast tissue with the source 20 and 50 mm deep as labeled, (*left* room lights on, *middle & right* room lights off). 24

3.2 A light emitting optical wire composed of a 200 μm optical fiber adhered to the length of a standard wire. The light emitting tip of the optical fiber is offset 2–3 mm from the distal, hooked tip of the wire. The ruler is in units of millimeters. 26

3.3 Orthogonal mammograms of one patient after wire localization. The wire was inserted in the lateral to medial direction with its tip in the tumor and approximated to the clip. Rulers are in units of centimeters. 26

3.4 **Top row:** Visibility of a deep (6 cm) glowball near the chest wall as room lighting is increased (*left to right*). **Bottom row:** In practice, (*left*) light guided the surgeon towards the cancer and (*middle & right*) created a visible sphere to remove. The red light can be appreciated well with color images available online. 29

3.5 Orthogonal radiographs of the lumpectomy specimen from the breast shown in Figure 3.3. The optical wire remains approximated to the biopsy clip and centered in the specimen. 29

4.1 **A.** Optical wire with the anchor wire glued within one lumen of the dual lumen tube. The anchor wire is secured within the tube and cannot be removed. The second lumen is open on the proximal end (right) to allow insertion of either a placement wire or optical fiber. The distal end of the lumen (left) is sealed with 1 mm of medical grade glue. The dark lines around the optical wire are depth markers. **B.** Optical Wire with placement wire inside tube. For clarity, drawings are not to scale. **C.** Photograph of actual optical wire. 34

4.2 A profile of the custom extruded dual lumen Pebax 7233 tube. 36

4.3 The set up of the MTS for tensile testing of the bend of the Kopans wire. 40

4.4 The set up of the MTS for tensile testing the strength of the epoxy, indicated in grey, in the optical wire. 40

4.5 The tensile force needed to pull the dual lumen optical wire out of the clamps retaining the samples (n = 8) and the force needed to straighten the bend in standard kopans wires (n = 5). We were not able to pull the optical wire apart, the tensile strength of the optical wire is greater than 12 N. 41

5.1 Created from data published by Spinelli *et al.* (1) and Shah *et al.* (2). The reported absorption of lipid, water, oxygenated hemoglobin and de-oxygenated hemoglobin at physiologic concentrations with the intrinsic variability of healthy tissue indicated by error bars. 47

5.2 Adapted from van Veen *et al.* (3). 48

5.3 Example of the sinusoid sampled at the source and detector at the same time. The amplitude (A) of the wave as well as the DC (dotted lines) decrease upon traveling through a scattering medium and a phase lag, θ, develops. 50

5.4 Top Left: Phase is proportional to distance and the expected slope of measurements in tissue will be between 0.5 and 2 deg/mm. Top Right: Phase is proportional to frequency in the relatively low frequencies shown here. A 70 MHz modulation frequency was chosen to simplify the components of an experimental system. Bottom Left: Phase is a function of the inverse square root of the absorption coefficient. This plot shows the expected range of values reported in the literature for all patients. The oval indicates the expected range in 1 patient. Bottom Right: Phase is a function of the square root of the reduced scattering coefficient. This plot shows the expected range of values reported in the literature for all patients. The oval indicates the expected range in 1 patient. 53

5.5 Diagram of extrapolated boundary condition. 54

5.6 Modulation frequency is 150 MHz, $\mu_a = 0.005\,\mathrm{mm}^{-1}$, $\mu_s' = 1.0\,\mathrm{mm}^{-1}$, $R_{eff} = 0.493$, and the infinite medium phase was calculated as in Equation 5.4 and the extrapolated boundary as in Equaion 5.8. 55

5.7 The results of the time based Monte Carlo simulation and subsequent Fourier Transform. Left: $r = 9\,\mathrm{mm}$, Right: $r = 22\,\mathrm{mm}$. Top row: The photons binned as a function of time. MIddle row: The modulation of the signal as a function of frequency. Bottom row: The phase of the signal as a function of frequency. MC: Monte Carlo data, DT: diffusion theory approximation. 57

5.8 Modulation and phase of Monte Carlo (MC) and diffusion theory (DT) with a modulation frequency of 76 MHz for all source detector separation distances, r with photons launched at 5, 25, & 45 mm. 58

5.9 Modulation and phase of Monte Carlo (MC) and diffusion theory (DT) with a modulation frequency of 153 MHz for all source detector separation distances, r with photons launched at 5, 25, & 45 mm. 59

6.1 The concept of a handheld probe with phase comparators to measure the distance light has traveled through tissue. 62

6.2 In these diagrams the light source (S) is within a scattering medium (shaded) below the probe detectors (D_1, D_0 and D_2). The distance between detectors (l) and the distance from source to detectors (r_1, r_0 and r_3) are drawn as lines. The angle ψ is between the face of the probe and the normal of the light source. The angles α_1, and α_2 are between the face of the probe and the hypotenuse of the triangle formed between the detectors and the source. *left* Probe face is perpendicular to the line between the source and the center detector. *right* Probe face is not perpendicular to the line between the source and the center detector. 63

6.3 The face of the probe has a center detector, D_0, and three surrounding detectors, D_1, D_2 and D_3, each a distance, l, from the center detector and located at 0, 90, and 180 degrees from each other. 64

6.4 The photon distributions for detectors located at (0,0,0), (0,5 mm,0) & (0,10mm,0) when launched from (0,0,15 mm). The left column shows the distributions along the y axis and the right column along the x axis. Photons were launched within a scattering dominant medium and the location of each scattering event of each photon was binned in 1 mm square bins. 68

6.5 The difference between the detectors (0,0,0) and (0,5 mm,0) in the top row, and (0,0,0) and (0,10 mm,0) in the bottom row in both the x (left column) and y (right column) planes. The color bar is in units of percent per mm^3. Negative, blue colors, indicate photons that were collected by the outer detectors and not the central detector while positive, red colors, were collected by the central detector and not the outer. 69

6.6 The absolute value of the relative error in the calculation of r_{0c} using equation 6.11 as a function of the detector angle, ψ, and the actual depth of the source, r_0. Each line between $r_0 = 5$ mm and $r_0 = 50$ mm represents a 5 mm increment in the actual depth of the source. The four plots show the change in error as the distance between detectors, l, is increased from 5 to 10 to 25 to 45 mm. 71

7.1 Three of the polyurethane optical phantoms. 76

7.2 The intensity modulation system. 78

7.3 Two measurement configurations used to measure the phase lag as a function of source detector separation distance, r. 80

7.4 Stability of measured phase. The entire system was shut down and then re-started between measurements data sets 1–4. 81
7.5 The phase was stable over a period of 41 minutes. Data was collected at the time points indicated in the legend while sweeping the modulation frequency of the network analyzer. 82
7.6 Measured phase as a function of distance from the source. Each point represents the mean of 101 phase measurements, error bars are the standard deviation. 83
7.7 Standard Error of the mean, ε, normalized by distance, r, and corresponding slope, β, of phase as a function of distance. 84
7.8 Data: Measured phase lag with source and detector separated by 15mm for frequencies between 0–300 MHz in phantom 2. DT: Diffusion theory approximation generated using Equation 5.4 with the known optical properties of phantom 2. . . . 85
7.9 Linear phase response as a function of distance from source. The source fiber was located within phantom 4 at depths, D, from the side and top of the phantom while the detector fiber was moved along the top of the phantom in 5 mm increments. . . 86
7.10 Linear phase response as a function of distance from the source in 3 phantoms. The lines were drawn to illustrate the system offset, C_a. 87

8.1 The intensity modulation system as used in the perpendicular measurement geometry. Only the location of the needle was changed for the coaxial measurement geometry and is illustrated below. 91
8.2 Coaxial Measurement geometry: The source fiber was stereotactically inserted in the tissue through a needle in a black delrin fiber holder. The detector fiber was placed on the surface in 5 mm increments as indicated by the arrows, r, extending from the source to the surface. 92
8.3 In this diagram the light source (S) is below the probe detectors ($D_{1,2,3}$). The distance between detectors (l) and the distance from source to detectors ($r_{1,2,3}$) are drawn as lines. The angle ψ is between the face of the probe and the normal to the light source. The angles $\alpha_{1,2}$ are between the face of the probe and the hypotenuse of the triangle formed between the detectors and the source. 93
8.4 The face of the probe has a center detector, D_0, and three surrounding detectors, $D_{1,2,3}$, each a distance, l, from the center detector and located at 0, 90, and 180 degrees from each other. 94

8.5 Perpendicular Measurement geometry: A, B, & C are cross sectional views in the plane of the fiber tips. D shows the top view of this geometry. The source fiber was stereotactically inserted in the tissue parallel to the fiber holder at a fixed depth, R=8 or 21 mm, from the bottom of the fiber holder (A, B & C). The needle was placed so it was perpendicular to the holes in the fiber holder and with tip of the fiber in the same plane as the holes at a distance x from the needle insertion point (D). The detector fiber was placed on the surface where r_1, r_0, & r_2 are indicated using the fiber holder. 95

8.6 *Left column:* Tissue. *Right column:* Phantom. *Top row:* The phase lag from the source of light to the probe as a function of the stereotactically measured distance between the two fibers. The lines are fit to Equation 5.6 ($r = \gamma_a \cdot \theta + C_a$) with $C_a = 0$. *Bottom row:* The difference between fit line and data. 97

8.7 The phase lag from the source of light to the probe as a function of the stereotactically measured distance, R between the two fibers in the coaxial configuration for three tissue samples. The intensity of light was modulated at 70 MHz. The different markers each represent the indicated source fiber depth within the tissue. 98

8.8 The calculated distance between source and detector, r_0 is plotted against the stereotactically measured source depth, R. Equation 8.3 was used to determine r_0 where $\bar{\theta}$ is the average of θ_1 and θ_2. The line indicates equality between the ordinate and abscissa. Each plot represents one of the tested separation distances between detector fibers, l=5, 10, 15 mm. 101

A.1 The optical fiber is not intended for inoculation (dunnage). Note: Optical Fiber is packaged in an outer Teflon coil. Each coil is placed inside a paper/film pouch and sealed. Each inner pouch is placed inside an outer pouch and sealed for exposure. . . 127

A.2 Optical wire as provided, intended for inoculation; see diagram below. 127

A.3 After inoculation, the optical wire will be packaged in the sponsor supplied paper/-film pouches. Each inner pouch is sealed and placed inside an outer pouch which is then sealed for exposure. 128

A.4 Optical Wire with placement wire inside tube. The anchor wire is secured within the tube and can not be removed. For clarity, drawing is not to scale. 129

A.5 Optical Wire with placement wire removed from tube. For clarity, drawing is not to scale. 129

List of Tables

3.1 Radiographic and Operative metrics for enrolled patients. IDC: invasive ductal carcinoma, DCIS: ductal carcinoma *in situ*. Breast Comp. was the BI-RADS breast composition score. Wire-to-clip was the distance between the wire tip and the biopsy clip in both the cranio-caudal [CC] and latero-medial [LM] projections. The wire depth was the distance from the wire tip to the skin. The fiber power was controlled by neutral density filters and was the percentage of total laser power used during lumpectomy. The summary column shows the mean and standard deviation. 25

3.2 Pathologic findings following resection(s). IDC: invasive ductal carcinoma, DCIS: ductal carcinoma *in situ*, ADH: atypical ductal hyperplasia (a risk factor for but not a breast cancer). A high nottingham histologic grade of 3 represents poorly differentiated cells that divide more rapidly and tend to spread when compared to moderate (2) and low, (1) grades. 30

3.3 Margin status following resection, shortest margin was measured on the primary lumpectomy specimen. IDC: invasive ductal carcinoma, DCIS: ductal carcinoma *in situ*, $*$: margin focally involved, A: anterior, P: posterior, M: medial, L: lateral, S: superior, I: inferior. 31

3.4 Specimen and lesion dimensions shown in centimeters. The summary column shows the mean and standard deviation. †: residual disease. 31

4.1 Note: + = Positive for Growth (Nonsterile), PC = Positive Control, NA = Not Applicable A common PC was cultured with samples from the 3rd half cycle 44

6.1 For each Monte Carlo simulation at a different source depth the number of photons collected at each detector as well as the distance between detectors, l are shown. The total percent difference is the sum over the total area. The percent missed at (0,0,0) is the sum of the negative values divided by the total and the percent missed at (0,l,0) is the sum of the positive values divided by the total. 72

7.1 Polyurethane phantom dimensions and optical properties measured at 638 nm. The standard deviation of the absorption coefficient was $0.001\,\mathrm{mm}^{-1}$ and the reduced scattering coefficient was $0.01\,\mathrm{mm}^{-1}$. 77

8.1 Summary of data collected in breast tissue sample 3 in the perpendicular configuration. The separation distance between detector fibers, l, is shown as well as the phase lag measured, $\theta_{1,2,3}$ at each detector with modulation frequency, f indicated. Also shown is the stereotactically measured source depth, R and the calculated distance between source and detector, r_0. r_0 was determined by Equation 8.3 where $\bar{\theta}$ is the average of θ_1 and θ_2. The error was calculated as the difference between R and r_0 divided by R. 99

1

Introduction

1.1 Specific Aims

The long term goal of this work was to develop a simple, practical tool to improve the outcome of lumpectomy surgeries. To accomplish this goal, the breast tissue surrounding a lesion was made to glow red by placing a light source at the center of the lesion. The device was called an optical wire and the procedure a light guided lumpectomy. It was hypothesized that light guided lumpectomies could result in a decrease in positive margins and in more uniform margins. This could result in fewer procedures, reduced cost, and better cosmesis.

- Aim 1: Develop an optical wire
- Aim 2: Clinically evaluate the feasibility of light guided lumpectomies
- Aim 3: Determine the distance from the light source to the tissue surface

1.2 Significance & Background

1.2.1 Significance

In the U.S. in 2006, 18,000 inpatient lumpectomies occurred (17) and in 1996, the last year the National Survey of Ambulatory Surgery was completed, 341,000 outpatient lumpectomies were performed. The occurrence of breast conserving surgery has increased in the last decade (5, 7, 8, 18, 19) so the actual number of procedures performed today is likely to be higher. It is estimated that three out of four breast cancer patients are eligible for breast conserving therapy (7). It

has been demonstrated that lumpectomies followed by breast irradiation have equivalent 12 year ipsilateral recurrence rate as mastectomies[1] for tumors less than 4 cm in diameter with negative or positive axillary lymph nodes (20, 21). However, the margin status of lumpectomies is critical to the success of the treatment. If a margin is positive following lumpectomy, the patient usually undergoes a second surgery to clear the margins. This not only creates additional cost but also prolongs the course of treatment.

1.2.2 Background

For small breast cancers and pre-cancerous conditions a lumpectomy, also called breast conserving surgery, is often performed. In this surgical technique, the lesion and surrounding tissue are removed but the remainder of the breast is left intact (4, 5, 6, 7, 8). Many studies have shown that obtaining negative margins[2] at initial lumpectomy decreases the risk of ipsilateral [3] recurrence and the need for additional surgeries. However, the rate of published negative margins ranges from 50–90% (9, 10, 11, 12, 13, 14, 15) and should be improved.

1.3 Current Therapy: Diagnosis

1.3.1 Imaging: Mammogram, Ultrasound, Magnetic Resonance

Today, the imaging techniques of digital mammograms, ultrasound, and magnetic resonance (MR) can detect sub-millimeter calcifications and lesions within the breast as shown in Figure 1.1. Widespread use of screening mammograms began in 1983 and led to an immediate increase in identification of disease followed by a decrease in death rates (16, 22). As a result of screening mammograms, tumors can be found and treated before becoming more advanced disease.

1.3.2 Biopsy and Clip Placement

If a suspicious lesion is found during a screening mammogram, the lesion is biopsied. This biopsy is done under mammographic, ultrasound, or MR guidance depending on which imaging technique the lesion is more pronounced (22) and availability of resources. A biopsy needle is inserted and samples of tissue are removed in and around the lesion. After sampling the area, at least one radio-opaque clip is inserted through the biopsy needle as a permanent indicator of the location of

[1] complete removal of breast
[2] border of lumpectomy specimen is cancer free
[3] in the same breast

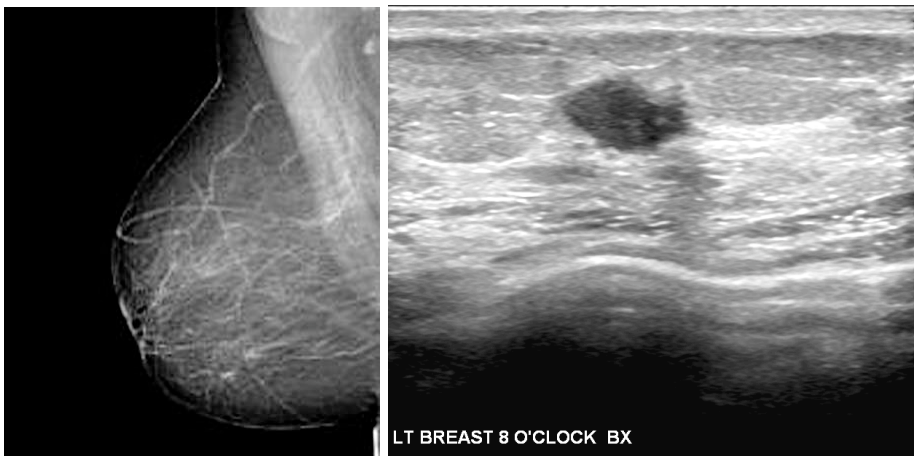

Figure 1.1: *Left:* Digital mammogram revealing micro-calcifications suspicious for ductal carcinoma *in situ* (DCIS). *Right:* The dark, hypo-echoic, irregular shaped mass is DCIS in an image generated by ultrasound.

the biopsy. The clip is detectable with x-ray, ultrasound and MR imaging. Often, the clip is in an X shape for easy identification. The biopsy samples are then histologically examined for breast cancer by a pathologist.

1.3.3 Staging

Upon completion of radiologic and pathologic examination, breast cancer can be diagnosed. The most common forms of breast cancer are ductal and lobular carcinomas. Ductal carcinoma originates in the ducts of the breast and lobular carcinoma originates in the milk producing glands. Breast cancer is classified into four stages according to tumor size and axillary lymph node involvement:

- Stage I - cancers are less than or equal to 2 cm in diameter with no evidence of axillary or distant lymph node involvement,
- Stage II - primary tumors are between 2 and 5 cm in diameter or involve axillary lymph nodes without distant metastasis,
- Stage III - primary tumors are any size with axillary nodes in a matted mass (IIIa), or with chest wall or skin involvement or both (IIIb),
- Stage IV - presence of distant metastasis.

In addition, both ductal carcinoma *in situ* (DCIS) and lobular carcinoma *in situ* (LCIS) are considered pre-cancerous. They are both non-invasive conditions, but if left untreated, DCIS and LCIS are likely (20–50%) to become invasive carcinoma (23, 24, 25, 26, 27, 28). Although LCIS is less understood than DCIS the risk of its progression to invasive cancer is still widely accepted. Treatment decisions are based on the stage of the cancer, genetic testing, family history, age, and patient preferences.

1.4 Current Therapy: Treatment

1.4.1 Breast Surgery

Coinciding with developments in the field of radiology, the surgical treatment of breast cancer has also evolved. Surgical treatment for breast cancer was once a radical mastectomy, which involved removing not only the breast but also most local lymph nodes and the muscles of the chest wall and axilla [1]. Today, modified radical mastectomies or total mastectomies are performed in which the breast is removed but the muscles surrounding the breast are left intact. The axillary lymph nodes are left intact in a total mastectomy, but are removed in a modified radical mastectomy. For small cancers and pre-cancerous conditions a lumpectomy, also called breast conserving surgery, is often performed. In this surgical technique, the lesion and surrounding tissue are removed but the remainder of the breast is left intact (4, 5, 6, 7, 8). Lumpectomy is then followed by radiation therapy.

1.4.2 Margins

Lumpectomy margins are generally classified as positive (0 mm), close (<2 mm), or negative (>2 mm) in practice. Many studies have shown that obtaining negative margins at initial lumpectomy decreases the risk of ipsilateral recurrence and the need for additional surgeries. The rate of published positive margins ranges from 10–50% (9, 10, 11, 12, 13, 14, 15). In addition, a 2 mm margin does not guarantee complete removal of cancer. In one study residual tumor was found in 21% of negative margins upon re-excision (14). However, 10 mm margins are a reasonable goal. In MacDonald *et al.*, 455 nonrandomized patients with DCIS were treated with excision alone. After adjusting for all other predictors the likelihood of local recurrence for patients with margins less than 10 mm was

[1] armpit

5.39 times as much as that for patients with margins of 10 mm or more (95% confidence interval, 2.7–10.6 times) (29).

Lumpectomy outcomes are influenced by surgical experience. One study of 660 lumpectomies illustrated the significant difference that experience and skill level make when removing wire localized non-palpable tumors. The rate of negative margins was evaluated with multivariate analysis at one institution. It was found that attending surgeons and senior residents achieved negative margins more than 83% of the time, while junior residents assisted by another resident only achieved 61% clearance. There was no difference between skill level for palpable tumors (30).

1.4.3 Kopans Wire

More than 25 years ago Daniel Kopans introduced the hookwire technique to simplify the preoperative localization of breast cancers (31). The hookwire is a 20–25 cm long thin wire bent at the tip to form a V shaped hook and is now referred to as the Kopans Wire. In practice, a radiologist places a needle in a tumor using either x-ray or ultrasound guidance then slides the Kopans wire, hook end first, through the needle. Once the hook has moved past the end of the needle it springs open in the middle of the tumor and retains its position. Blue dye may also be injected in the area of the tumor to serve as a secondary indication of tumor location during surgery. The dye is however, irregular, difficult to control, and not particularly useful unless the wire migrates. The needle is removed and the wire external to the skin is taped in place to prevent displacement of the wire. Proper placement is confirmed with orthogonal mammograms and the patient is sent to the operating room.

The surgery is guided by the Kopans wire. The surgeon views the mammograms and observes the general location of the tumor and wire. During the operation the wire is followed. Before reaching the end of the wire, the surgeon must deviate from the wire and then re-approach it to excise the tissue surrounding its tip. The exact point to deviate from and approach the wire is unclear and can cause the resection to be scalloped (i.e., the deviation or approach was either too close or too far from the tumor and was consequently repeated). In a scalloped resection, positive margins can be found in the tissue flap created by the misguided deviation/approach.

The surgeon is implicitly encouraged to follow a non-ideal surgical approach to the tumor. The radiologist places the wire parallel to the chest wall because it is the safest and most accurate method of localization (22). However, skin tension lines radiate concentrically from the nipple and are the cosmetically ideal placement of surgical incisions. Often, to avoid following the wire from

the skin to the tumor, surgeons will anticipate the location of the tip in order to properly place the skin incision. After this incision is made, the wire is cut near the skin, pulled into the incision and followed to the tumor.

1.4.4 Partial Breast Irradiation

Lumpectomy with a subsequent 6 weeks of breast irradiation is the current standard of care for breast conserving therapy (8). However, partial breast irradiation is in phase II clinical trials and looks promising as an alternative to the current treatment (32).

In this procedure, a balloon is placed in the lumpectomy cavity prior to surgical close. After recovery from surgery, the patient is treated with high dose rate brachytherapy through the balloon. This procedure is attractive to patients because the course of treatment only lasts 5–6 days (as opposed to 6 weeks). Long term follow up is needed but local recurrence is in the range of 0–2% (32, 33). The most common contraindications of partial breast irradiation are when the lumpectomy bed is within 1 cm of the skin or is not spherical in shape (32).

1.5 Rationale

Chapter 2 describes the first generation optical wire as well as the first clinical implementation of the device. With a long term goal of reducing the number of repeat lumpectomies due to positive margins, an optical wire was designed to be used as a visual localization technique during lumpectomy surgery. The wire was designed and tested so that a 200 μm optical fiber was axially attached to a Kopans wire with medical grade epoxy. The tip of the optical fiber was offset 3 mm from the tip of the Kopans wire. The idea was that the optical wire could be placed by a radiologist in exactly the same manner as a Kopans wire with the tip of the wire within the lesion to be removed. After placement of the wire, the lumpectomy surgery could be performed using standard methods with a Kopans wire but with the additional assistance of being able to see a red glow-ball of light surrounding the lesion. It was determined that red light (specifically 630–660 nm) would be the most visible wavelength after traveling through breast tissue. A light delivery system was designed and the optical wire was tested in prophylactic mastectomy specimens to confirm the red light was visible through 30–50 mm of breast tissue. After bench top testing was completed, the optical wire was used clinically in one 65 year old patient undergoing lumpectomy. Given the known location and approximate size of the lesion from previous imaging, the surgeon was able

to identify the area of breast tissue to remove. The glow-ball provided immediate visualization at the end of the optical wire which the surgeon was able use to estimate proximity to the wire tip. Pathology analysis provided final confirmation of negative margin status.

Given the successful clinical implementation of the optical wire, Chapter 3 presents a clinical study of 8 patients where an optical wire was used during lumpectomy surgery. Patients with non-palpable breast cancer ($<$ 2 cm diameter) undergoing lumpectomy for biopsy-proven radiographically identifiable disease were eligible. Patients were between the ages of 41 & 68 diagnosed with either invasive ductal carcinoma or ductal carcinoma *in situ*. Each wire was placed within 4 mm of the lesion by a radiologist. The light emitted from the optical wire was used in each surgery to assist in locating the area of tissue to be removed. This allowed the surgeon to choose a direct plane of dissection towards the lesion that would result in good cosmetic appearance. In addition, after approaching the area to be removed, the glow-ball was used to dissect around the lesion. Seven of the eight lumpectomies resulted in negative margins upon pathology review.

In Chapter 4, the optical wire was re-designed to create a second generation device. Although the optical wire study resulted in good clinical outcomes, the wire itself needed to be made more comfortable for the patient and more user friendly for both the radiologist placing the wire as well as the operating surgeon and engineer operating the light source. Since the first generation optical wire had 3 m of optical fiber permanently attached to the Kopans wire, it required extra time to be placed by the radiologist, then the fiber had to be wound and carefully taped to the patient's chest. Once the patient was in the operating room, the fiber had to be carefully untaped and unwound, then manually coupled and aligned with the red laser. None of the fibers broke in the clinical testing that was performed, however, it was likely to occur due to the fragile nature of the small fiber. To address the issue of potential fiber breakage and in an overall effort to make the device more comfortable for the patient and easier to use, a second generation optical wire was designed, tested, and manufactured. The second generation device was designed with a custom extruded Pebax dual lumen tube with dimensions of 0.0196×0.0334 inches ($500 \times 850\,\mu$m). One lumen of the tube was permanently adhered to a Kopans wire and the other lumen was left open so a fiber could be slid in and out. This second generation device allowed the radiologist to place the wire without the fiber attached. The second generation device was more comfortable for the patient because the fiber did not have to be attached to the patient between placement and surgery. From both the radiologist and patient perspective, the optical wire was simply a larger diameter Kopans wire. During surgery, the optical fiber could be placed within one lumen of the dual lumen tube

and taped in place during the surgery. The second generation device underwent thorough tensile testing and third party sterility validation. It was found to be robust and sterilizable with steam.

Chapter 5 is a discussion of breast tissue optics, the theory behind using an intensity modulated point source to approximate distance through tissue, and Monte Carlo models created to test the theory. The optical properties of breast tissue, both cancerous and normal have been studied for nearly 20 years. Due to inherent variations in breast tissue the reduced scattering (μ_s') and absorption (μ_a) coefficients have a wide variance in the literature. Frequency domain measurements are based on sinusoidally modulating a light source, usually within a bandwidth of hundreds of megahertz. Upon photon propagation through highly scattering material, such as tissue, the sinusoidal signal becomes demodulated, both the amplitude (A) of the wave and the average intensity (DC) decrease and a phase lag develops between the source and the propagating wave. The diffusion approximation to the Boltzmann equation (83) is used to model the propagation of a modulated light source through a highly scattering medium (84). Both the diffusion approximation and Monte Carlo models were provided the same results for phase lag through scattering media. The diffusion approximation with and without a boundary condition was used to show that at source depths of more than 5 mm no boundary condition was needed to provide an estimate of phase lag.

A method is proposed in Chapter 6 to measure the distance light has traveled from a point source within scattering media to the surface. Ideally, a small light-sensing probe could be used in conjunction with light-guided lumpectomy. The probe could give the operating surgeon a quick measurement of the distance from the dissection plane to the light source within the breast. In addition, the probe should be hand-held, about the size of a marker, indicate direction to the source and provide accurate distance readings. The primary goal of this measurement probe was to determine the distance from light source to probe without a-priori knowledge of the tissue optical properties. A major problem of measuring the distance from a light source within heterogeneous breast tissue to a detector on the surface is the optical properties will most likely change as the distance does. Therefore, the probe would be required to adjust to changing optical properties without need of a lengthy calibration. This was accomplished by designing a probe with multiple detectors centered around a primary detector. A known distance between the detectors as well as phase measurements at each detector allow for a direct measurement of the distance between the light source and the primary detector without the need to know or measure the optical properties of the breast tissue. An expected maximum error of 4 % from the proposed method was determined.

Chapter 7 presents a modulated optical system and data that corresponds to the diffusion theory approximation. A fiber coupled optical system was assembled to modulate the intensity of a red laser diode with a network analyzer. The diode could be modulated from 0–350 MHz, and was primarily operated at 70 MHz. The network analyzer was used to create a modulated signal as well as detect an incoming signal. The detected signal was compared to the source and a phase lag between the two was measured. A series of optical phantoms were created to mimic the optical properties of breast tissue and utilized to test the optical system. The modulated optical system was found to be stable. In addition, the phase lag measured through optical phantoms was found to be in agreement with the diffusion theory approximation and found to be linear as a function of distance from the source.

In Chapter 8, the modulated optical system was tested in breast tissue to measure the distance from a point source to the surface. Optical phantoms are very useful for characterizing optical devices, but are far more homogeneous than real tissue. The system was tested in *ex vivo* breast tissue to ensure it measures distance through breast tissue. Three prophylactic mastectomy specimens were tested after surgery and before examination by pathology. During the investigations, an optical fiber was inserted stereotactically through a needle and the phase lag from the edge of the tissue to the fiber tip was measured with an optical probe. The phase lag was used to determine the distance from the tip of the fiber optic to the probe. A linear response of phase to distance from the source in both tissue and phantom was found. As expected, the variance of the data collected in tissue was greater than in the phantom. The feasibility of using the probe described in Chapter 6 to determine distance in tissue samples was tested. Optical measurements of the distance between source and detector were within 15 % of the actual value.

2

Light Guided Lumpectomy: Device and Case Report

2.1 Introduction

We describe the development, design, fabrication and testing of an optical wire to assist in the surgical removal of small lesions during breast-conserving surgery. We modified a standard localization wire by adding a 200 micron optical fiber alongside it: the resulting optical wire fit through an 18 gauge needle for insertion in the breast. The optical wire was anchored in the lesion by a radiologist under ultrasonic and mammographic guidance. At surgery, the tip was illuminated with an eye-safe, red, HeNe laser and the resulting glowball of light in the breast tissue surrounded the lesion. The surgeon readily visualized the glowball in the operating room. This glowball provided sufficient feedback to the surgeon that it was used (1) to find the lesion and (2) as a guide during resection. Light guided lumpectomy was a simple enhancement to traditional wire localization that could improve the current standard of care for surgical treatment of small, non-palpable breast lesions.

For small breast cancers and pre-cancerous conditions a lumpectomy, also called breast conserving surgery, is often performed. In this surgical technique, the lesion and surrounding tissue are removed but the remainder of the breast is left intact. More than 340,000 lumpectomies were performed in 2006 in the U.S. (17, 37) and this number has increased steadily over the last decade (5, 7, 8, 18, 19). In this paper, we describe the development of a device to assist surgeons in removing small non-palpable breast lesions found during radiologic screening.

[1]This chapter is slightly modified from the Journal of Biomedical Optics (36)

In 1980, Kopans introduced the hookwire technique to improve the pre-operative localization of breast lesions (31). The hookwire is a 20–25 cm long thin wire bent at the tip to form a V-shaped hook and is now referred to as the Kopans Wire. In practice, a radiologist places a needle in a lesion using either X-ray or ultrasound guidance then slides the Kopans wire, hook end first, through the needle. Once the needle is removed, the hook springs open and is anchored at the lesion site. The wire external to the skin is taped in place to prevent its displacement. Proper localization is confirmed with orthogonal mammograms and the patient is sent to the operating room.

The surgery is guided by the anchored Kopans wire. The surgeon views the mammograms and observes the general location of the lesion and wire. Since the end of the wire is in the lesion, the surgeon uses the wire to find the small non-palpable lesion. The surgeon will try to remove the lesion with the disease free surrounding tissue; consequently before reaching the end of the wire, the surgeon must deviate from the wire and then re-approach it to excise the tissue surrounding its tip. The exact point to deviate from and approach the wire is unclear and can cause the resection to be scalloped (i.e., the cut was either too close or too far from the lesion and the distance needed to be corrected). At a minimum, if diseased tissue is found within 2 mm of the surface of the resected tissue, the borders are positive and a second surgery is indicated. Scalloped borders are irregular and can result in positive margins.

The radiologist places the wire parallel to the chest wall because it is the safest and most accurate method of localization (22). However, this approach is not necessarily ideal for the surgeon. Often, to avoid following the wire from the skin to the lesion, surgeons will anticipate the location of the tip to properly place the skin incision. After this incision is made, the wire is cut near the skin, pulled into the incision and followed to the lesion. Despite the wire guidance, these procedures are often repeated due to positive margins. The rates of published positive margins range from 10–50% (9, 10, 11, 12, 13, 14, 15).

We hypothesized that the standard wire guided lumpectomy could be improved by using light. The standard Kopan's wire would be replaced by an optical wire that illuminated the breast and produced a glowball of light that surrounded the lesion. This glowball might assist surgeons in both locating and resecting non-palpable lesions by providing a visible, spherical target. The optical wire would be placed by a radiologist using the same technologies as are currently used for Kopans wires. To maintain the current standard of care, the optical wire consisted of a Kopans wire attached to a 200 μm optical fiber with medical grade epoxy as shown in Figure 2.1. This paper is a description of the device and case report on its use.

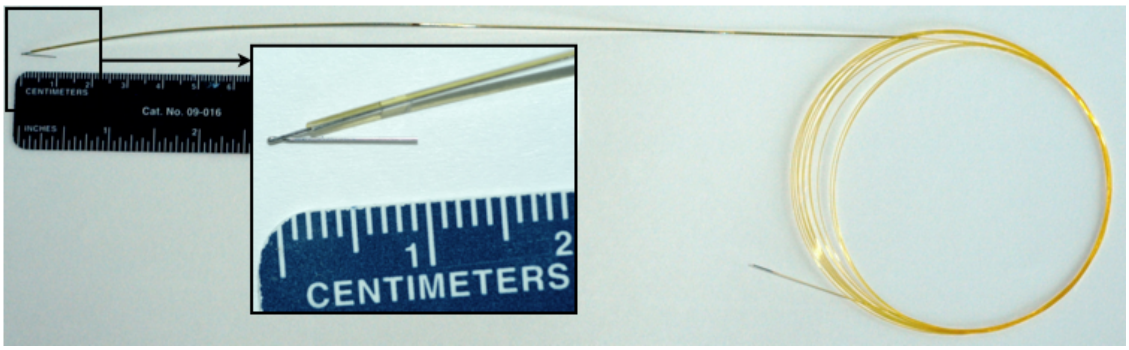

Figure 2.1: The optical wire used for light guided lumpectomy. The device consists of a 200 μm optical fiber adhered to a standard Kopans wire.

2.2 Benchtop Development

2.2.1 Visibility

One primary goal of light-guided lumpectomy was to ensure visibility of the glowball during surgery with no need for eye protection or imaging devices. To maximize light penetration through tissue, the illumination would ideally be at an infrared wavelength such as 800 nm. In fact, this wavelength works well when semiconductor-based sensors are used to detect light but is well outside the range of sensitivity of the human eye (400–700 nm). The 800 nm wavelength can be seen using infrared night vision goggles, but this is impractical in the operating room. Instead, one must find a wavelength that maximizes light penetration (longer wavelengths) and also maximizes visibility (shorter wavelengths). The visibility of light transmission through breast tissue might be estimated as the product of the light transmitted through 10 mm of breast tissue and the sensitivity of the human eye. Both normal and diseased breast tissue (3, 38, 39, 39, 40, 41, 42, 43) have reduced scattering coefficients (μ_s') that range from 0.5–2.0 mm^{-1}. The absorption coefficient (μ_a) of breast tissue in the visible range of the spectrum is dominated by hemoglobin.

The spectral behavior of scattering was assumed to be

$$\mu_s' = 0.4 \left(\frac{\lambda}{650\,\text{nm}} \right)^{-0.7} \text{mm}^{-1}$$

where λ is the wavelength. This was based on van Veen *et al.* (3) from intra-operative optical properties of normal breast tissue. The absorption coefficient (μ_a) was determined by a nominal

hemoglobin concentration of 2% with 80% oxygenation. A point source diffusion model (44)

$$\frac{3(\mu_a + \mu_s)}{4\pi r} \exp(-r\sqrt{3\mu_a(\mu_a + \mu_s')})$$

was used to determine the fraction of light emitted by the optical fiber that passed through $r = 30\,\text{mm}$ of simulated breast tissue. This fraction was then multiplied by the CIE 1951 standards of luminous efficiency for the (light adapted) photopic eye (45) to obtain an estimate of relative visibility as a function of wavelength (Figure 2.2). In this graph, the dramatic increase in visibility at 600 nm is caused by a decrease in light absorption by blood. The decrease in visibility approaching 700 nm is due to the sensitivity of the human eye. The optimal wavelength was conveniently around 633 nm and a red HeNe laser could be used. The scotopic (dark adapted) response (not shown) is shifted slightly to the left of the photopic curve.

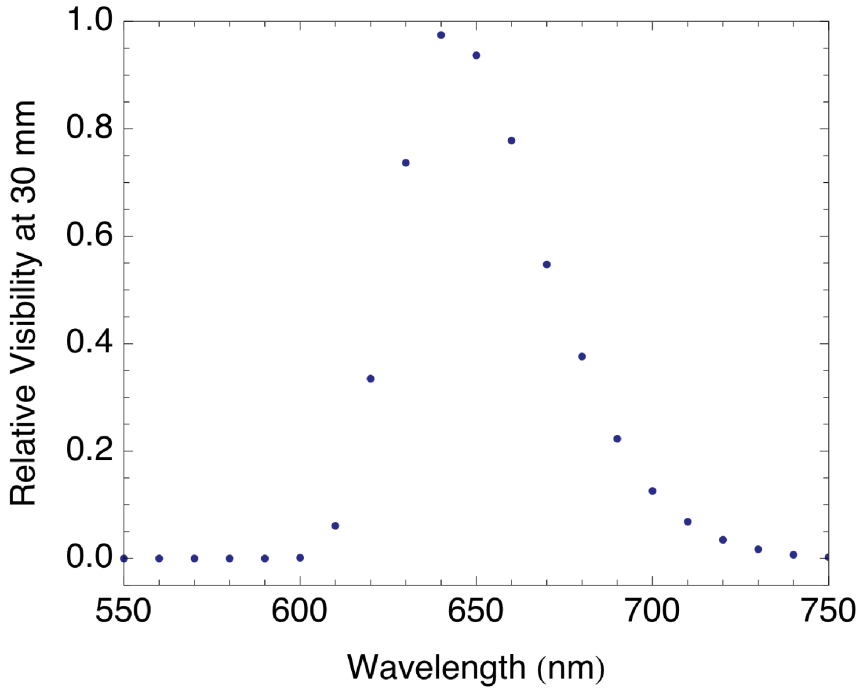

Figure 2.2: The simulated relative visibility of light through 30 mm of breast tissue shows a peak near 650 nm. The overall visibility has been normalized to 1.

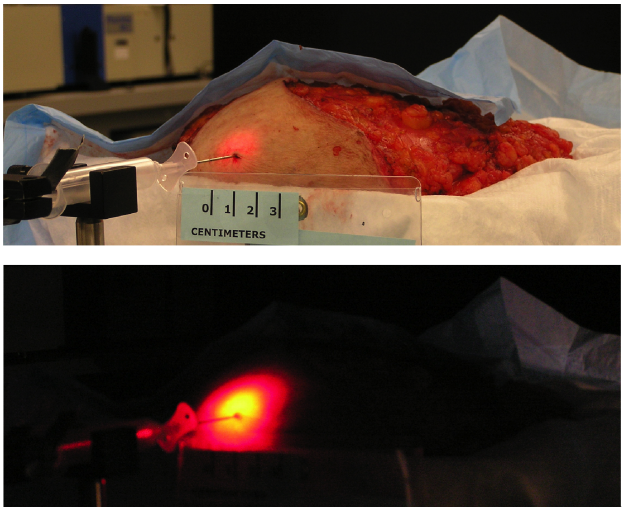

Figure 2.3: An example of breast tissue illumination with a red laser, an optical fiber is located 10 mm within the tissue. The glowball of light can be seen surrounding the needle directly above the ruler. Visualized through the skin with room lights on (*top*) the glowball is 2 cm in diameter and 4 cm in diameter with the lights dimmed (*bottom*).

2.2.2 Prophylactic Mastectomy Specimens

Based on the estimated visibility and the work of Hussman (46) where 635 nm light was visible through several centimeters of breast tissue, a pre-clinical study was established under Providence Health & Services IRB protocol #06-29B. Following informed consent, three subjects undergoing prophylactic mastectomy were enrolled in the study. Immediately after the surgery was completed, but before pathological evaluation, the cancer-free mastectomy specimen was brought to the lab for evaluation. Green (543 nm, 8 mW HeNe laser), red (633 nm, 15 mW HeNe laser) and white (Oriel tungsten lamp) light was stereotactically delivered within the tissue through an 800 μm optical fiber. Approximately 3 mW of light was emitted from the fiber for each light source. Visibility was evaluated at 5 mm intervals from 5–60 mm depth under bright (300 lx) and dim (2 lx) room lighting conditions. The diameter of the light centered around the source fiber and emitting from the tissue was measured for each source, depth, and room lighting condition with a ruler and the eye as a detector. The green light was visible only under dim room lights at 5 mm depth and under no other conditions. In a dim room, the red and white light had a diameter of 50 mm at source depths of 5–30 mm; the light could be seen at a depth of 50 mm but not at 60 mm. In a bright room, the red and white light had a diameter of 20 mm at source depths of 5–10 mm; the visible diameter was reduced at longer depths and could be seen at 30 mm depth but not at any deeper locations,

Figure 2.4. The white light appeared red after traveling though 10 mm of tissue. Viewing the light through skin reduced the visibility distance by about half that of when skin was not present. The intensity gradient towards the source was easily visualized, Figure 2.3.

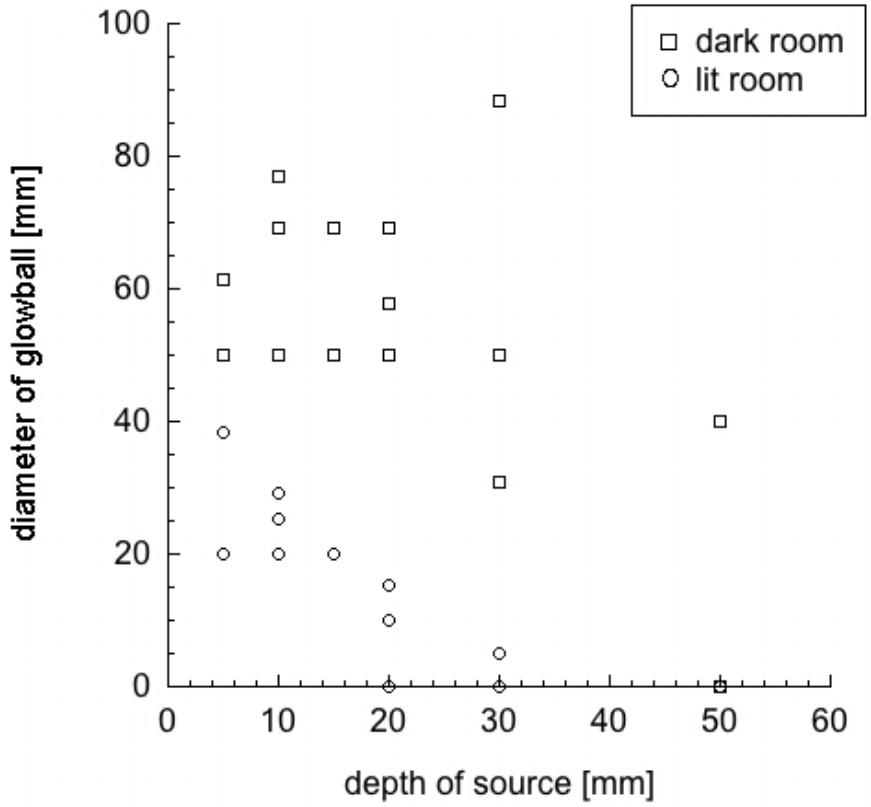

Figure 2.4: The diameter of visible light through mastectomy tissue as the depth of a 3 mW 633 nm light source was increased. Visible diameter is shown under typical laboratory lighting (lit) conditions and with most laboratory lights off (dark).

2.3 Fabrication and Testing

Based on these promising *ex vivo* results we designed and built an optical wire for use during surgery. Ideally, the procedure used by the radiologist for placing the optical wire would be identical to that used for a Kopans wire; unfortunately, the added bulk of the optical fiber required that the needle size be increased from 21 to 18 gauge. This was the only change from the standard procedure used by the radiologist for placing the wire.

The diameter of the Kopans wire was 250 μm and the diameter of the optical wire was 457 μm,

Figure 2.1. The optical fiber had to be displaced from the tip of the Kopans wire by 3 mm for the assembly to pass through the 18 gauge needle. The entire length of the optical wire had to fit through the needle, which meant that the end of the optical fiber was bare and could have no connectors to facilitate light coupling. To be able to position the laser away from the sterile field in the operating room, a 3 m length of optical fiber was chosen.

2.3.1 Light Delivery

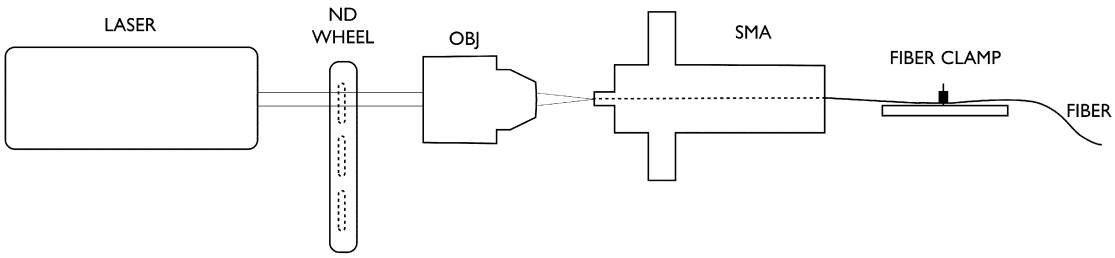

Figure 2.5: To couple light into a bare 200 μm fiber in the operating room, the light from a 633 nm HeNe laser traveled through a neutral density filter wheel and was then focused with an objective onto the fiber face. The fiber was positioned within a fixed SMA connector and held in place with a fiber clamp. The neutral density wheel was used to control the power emitted from the fiber.

For the glowball to be visible during lumpectomy, laser light had to be reproducibly coupled into a bare fiber. In addition, the light emitting end of the fiber was within breast tissue so light output could not be measured directly. To accomplish reproducible light coupling, the laser system was designed to be aligned with a separate 20 cm standard optical fiber. The intensity of the light emitting from the fiber was controlled with a neutral density filter set so the glowball could be made smaller or larger.

The laser light was focused by a 10× objective (0.3 NA). The focal spot was located at a 200 μm SMA connector which the optical fiber could slide through, (see Figure 2.5). To position the fiber, it was pushed through the SMA connector towards the objective then pushed back into the SMA connector with a 2 mm diameter rod so that the fiber face was in plane with the front of the SMA connector. To prevent the fiber from moving, a fiber holder was used to secure the fiber in place.

A three meter optical fiber was characterized before attaching it to the Kopans wire. The system was aligned with a 20 cm long segment of the same fiber used in the optical wire. At the free end of this standard fiber, a silicon optical sensor (Coherent, OP-2VIS) and power meter (Coherent, FieldMax II–TO) were used to measure the output. The SMA connector was translated in the

plane perpendicular to the axis of the fiber until the light output was maximized. The standard fiber, aligned and then re-placed in the SMA 5 times, coupled 4.4 ±0.6 mW. After the standard fiber was aligned, the system was not changed except for removal of the standard fiber and placement of the optical wire fiber. The 3 m optical wire fiber coupled 2.7 ±0.4 mW over 5 different placements. Due to the small standard deviation of the power output, it was assumed that the system could be aligned in the operating room using the standard optical fiber and then replaced by the optical wire fiber to achieve the power output given above.

2.3.2 Optical Wire Assembly

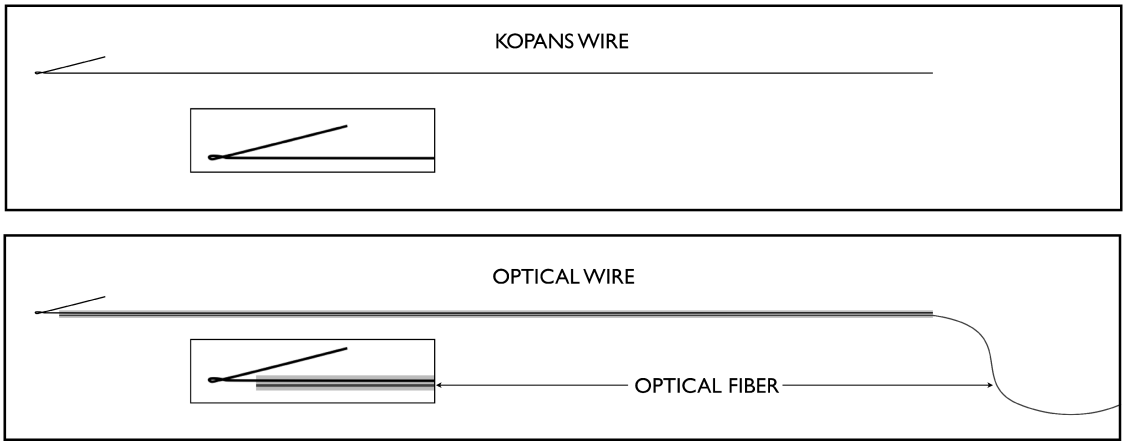

Figure 2.6: *Top* The Kopans wire is the standard wire used in wire guided lumpectomies. It is a thin stainless steel wire bent at its tip to anchor it in tissue once deployed. *Bottom* The assembled optical wire was composed of a Kopans wire with an optical fiber adhered to it with medical grade epoxy (light grey) along the length of the Kopans wire. The epoxy and optical fiber were offset 3 mm from the tip of the Kopans wire.

After the fiber was characterized, the optical wire was assembled, Figure 2.6. The proximal 247 mm of a Kopans wire (Cook Medical, DKBL-25-9.0) and the distal 247 mm of the characterized optical fiber (CeramOptec, Optran WF 200/220 P) were placed within a 457 μm inner diameter teflon tube so that the fiber tip was 3 mm from the bent end of the Kopans wire. Using a 30 gauge blunt tip needle, the medical grade epoxy (LOCTITE 3921) was slowly dispensed into the teflon tube. To cure the epoxy once the tube was filled, a ultraviolet light source (Dymax Light Welder, 3010EC) irradiated every 4 cm of the assembly for two minutes. The teflon tube was slowly slid off of the optical wire leaving the Kopans wire attached to the optical fiber.

The tip of the fiber was 3 mm from the tip of the Kopans wire. The epoxy was solid and uniformly distributed over its 247 mm length. The device was packaged and sterilized by hydrogen peroxide (STERRAD).

2.4 Clinical Use

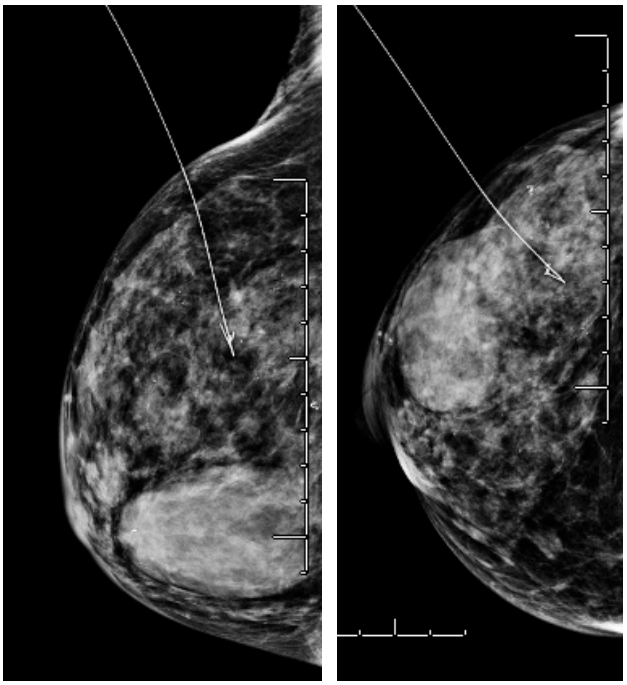

Figure 2.7: Orthogonal mammograms of the optical wire placement, *Left* lateral medial projection *Right* cranial caudal projection. The hook end of the wire and the fiber tip are within 3 mm of the biopsy clip within the lesion. One centimeter separates each line on the rules.

A 65 year old female provided informed consented and was enrolled in a phase I clinical trial of light guided lumpectomy under Providence Health & Services IRB protocol #07-11A. Prior to enrollment, a biopsy of the lesion had proven positive for ductal carcinoma *in situ* and a radio-opaque clip was inserted at the site of the biopsy. Using sterile technique and local lidocaine, the radiologist used an 18 gauge needle to place the optical wire 40 mm into the upper outer aspect of the right breast next to the clip using ultrasound. With the tip of the optical wire anchored within millimeters of the clip, the needle was removed from the breast and the optical fiber was wound, placed between gauze and taped to the subject's skin. The localization of the lesion was confirmed with two orthogonal X-ray mammograms, Figure 2.7.

The subject was taken to the operating room where she received general anesthetic and was endotracheally intubated. The laser system was aligned using the standard fiber. The optical wire fiber was untaped from the subjects skin and uncoiled. The free end of the optical wire fiber was coupled to the laser assembly and the rest of the fiber was secured with tape to prevent it from moving.

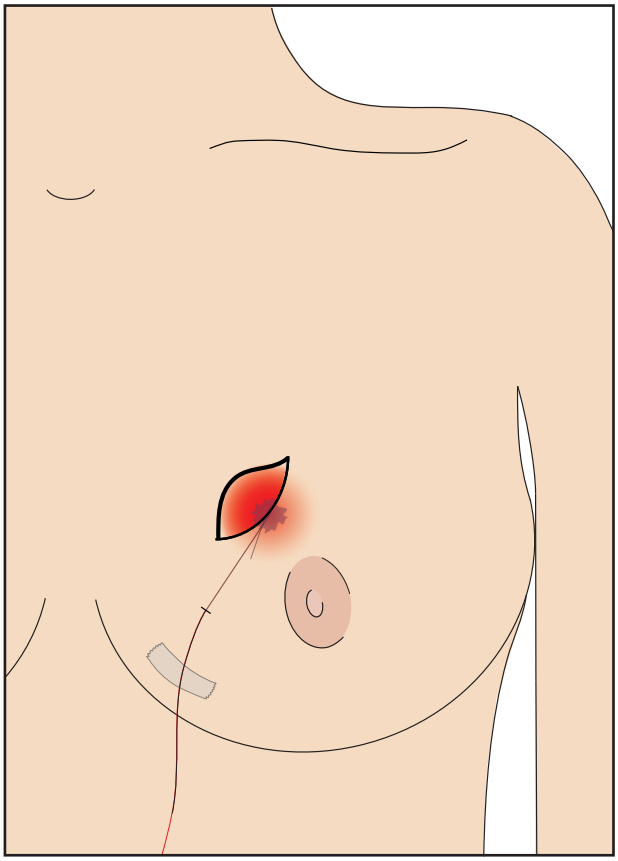

Figure 2.8: After illuminating the optical wire, the lesion was surrounded with light that could be seen through the skin and the incision site.

In the operating suite, the optical wire was illuminated (1–4 mW of power were coupled into the fiber during the porcedure) and an incision was made in the upper outer quadrant where the surgeon knew the lesion was located. The room lights were turned down until the glowball was visualized by the investigators (no secondary detectors were used), Figure 2.8. Using the glowball to indicate direction, the surgeon made sharp dissection superior, medial and lateral following the light gradient. The direction of the optical wire tip was readily determined by gentle palpation of

surrounding tissue. By switching the neutral density filters, the intensity and therefore the size of the glowball was gradually reduced as determined by the surgeon. The surgeon then began dissecting around the glowball to resect the lesion. After the specimen was completely excised, the wire was cut and the specimen sides were inked with different colors to indicate orientation. The specimen was sent for orthogonal radiographs in which the clip and wire were centrally located in the specimen so the incision was closed. The subject tolerated the procedure well with no known complications.

This procedure demonstrated the feasibility of light guided lumpectomies. The specimen was $25 \times 56 \times 35$ mm in the anterior-posterior $\times$ medial-lateral $\times$ superior-inferior aspects. The subject had histologically negative margins (>10 mm) and the surgeon found the glowball helpful in both localizing the non-palpable lesion as well as resecting a relatively spherical specimen of the appropriate size.

2.5 Conclusion

Light guided lumpectomy may enable new approaches during surgery that may lead to improved cosmetic results for the subject. Currently, surgeons need to "follow the wire" either from its skin entry site (selected by the radiologist) or from a nearby incision. A circum-areolar incision often has enhanced cosmetic results, but finding the tip of a traditional Kopans wire when using such an approach can be challenging.

Light guided lumpectomy may provide simple, practical benefits to the current practice of breast conserving surgery. In this subject, the optical wire seemed to help the surgeon find and resect a non-palpable breast lesion. The tip of the optical wire was known to be within the lesion as it was placed with imaging guidance so that it localized a biopsy proven ductal carcinoma *in situ*. Given the known location and approximate size of the lesion from previous imaging, the surgeon was able to identify the area of breast tissue to remove. The glowball provided immediate visualization at the end of the optical wire which the surgeon was able use to estimate proximity to the wire tip. As a confirmation that the lesion appeared to be contained in the lumpectomy specimen, orthogonal radiographs were taken of the specimen to provide immediate feedback to the surgeon before the incision was closed. Pathologic analysis provided final confirmation of the margin status.

Although encouraging, this is a case report and in order to improve clinical outcomes, the light guided lumpectomy will need to demonstrate improved margin status following resection of small lesions. If successful in improving clinical outcomes, the slightly larger needle used for localization

and the dimmed lights in the operating room should prove to be small adjustments to the procedure. If the optical wire can reduce the number of procedures that result in positive margins, and therefore reduce the number of repeated lumpectomies it may not only improve patient outcomes but reduce the cost of treating breast cancer. However, this remains an open question that is being addressed in a prospective, randomized, controlled trial.

3

Light Guided Lumpectomy: First Clinical Experience

3.1 Introduction

Despite numerous advances, lumpectomy remains a challenging procedure. We report on the early use of light-guided lumpectomy. Eight patients with non-palpable breast cancer undergoing lumpectomy for biopsy-proven and radiographically identifiable cancer were enrolled in the study. An optical wire was designed that incorporated a standard hook-wire with an optical fiber. The optical wire was placed in the same manner as a hook-wire. During light-guided lumpectomy, an eye safe laser illuminated the optical wire and created a sphere of light surrounding the cancer. The results were that light was visible at the beginning of each surgery and facilitated approaching the cancer without using the wire. Dissection around the sphere of light kept the wire tip within the surgical specimen. Three of eight initial surgical specimens had focally positive margins. Additional cavity shaves were performed during five lumpectomies and resulted in negative margins in seven of eight patients. Light-guided lumpectomy is a minor change to breast conserving surgery that can be easily incorporated into clinical practice. Further investigation into the clinical benefit of light-guided lumpectomy is warranted.

Surgical management of breast cancer has been evolving over the last two decades. It is estimated that three out of four breast cancer patients are eligible for breast conserving therapy (7) and the occurrence of breast conserving surgery has increased in the last decade (5, 7, 8). In 2006, 347,000 lumpectomies and 70,000 mastectomies were performed in the U.S. (17, 37).

[1]This chapter is slightly modified from the Journal of Biophotonics (47)

It has been demonstrated that lumpectomies with negative margins followed by breast irradiation have equivalent 12 year ipsilateral recurrence rate as mastectomies for tumors less than 4 cm in diameter with negative or positive axillary lymph nodes (21). Upon 20 year follow up, disease-free and overall survival following lumpectomy with negative margins and x-ray irradiation were not statistically different from those treated with mastectomy (48). However, margin negative lumpectomy remains challenging (30, 49). Margin status is critical to success of the treatment with most studies reporting 20–40% positive margins following lumpectomy (50, 51). If a margin is positive following lumpectomy, the patient usually undergoes a second surgery to clear the margins. Positive margins not only increase risk of ipsilateral breast tumor recurrence (50, 52) but also prolong the course of treatment, create additional cost and potentially affect the cosmetic result. One suggested explanation for the high positive margin rate is lack of tumor visibility during surgery (49).

The feasibility of using low-power eye-safe light as a beacon in breast tissue, has been demonstrated (36). Figure 3.1 shows the light distribution at the surface of excised human breast tissue when the light source was 20 and 50 mm deep in both a lit and dark room. Similar observations have been reported where red light could be seen through several centimeters of breast tissue (46). We were initially concerned that the diffuse glowball (30-60 mm in diameter) would make it difficult to determine the center. However, gentle pressure on the breast tissue clearly indicated the direction to the source by reducing the distance between the source and the surface. The path between the source and the location of the pressure appeared brighter that the surrounding areas of tissue.

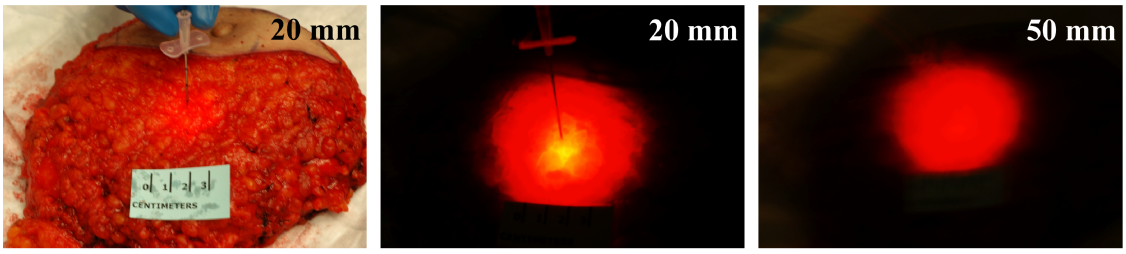

Figure 3.1: Red light emission from excised human breast tissue with the source 20 and 50 mm deep as labeled, (*left* room lights on, *middle & right* room lights off).

A visible glowball of light centered within a tumor may be able to assist in both locating and resecting it. This is a report on the first eight uses of light-guided lumpectomy. Light was used as a simple method for isolating the tissue volume surrounding a breast cancer.

3.2 Materials & Methods

Eight patients provided informed witnessed consent and were enrolled in an institutional review board approved study. Patients with non-palpable breast cancer (< 2 cm diameter) undergoing lumpectomy for biopsy-proven radiographically identifiable disease were eligible. We did not exclude patients based on type of breast cancer, neoadjuvant chemotherapy, or age. Patients were recruited from the patient population of one surgeon at one institution. Patients were between 41 and 68 years old undergoing lumpectomy to remove ductal carcinoma *in situ* (3 patients) or invasive ductal carcinoma (5 patients), Table 3.1. One patient was treated with neoadjuvant chemotherapy prior to lumpectomy. Five patients underwent sentinel lymph node biopsy at the time of lumpectomy.

Patient	1	2	3	4	5	6	7	8	Summary
Age [years]	67	51	65	41	61	68	53	59	58 ± 9
Initial Diagnosis	IDC	IDC	DCIS	IDC	IDC	IDC	DCIS	DCIS	
Breast Comp.	3	3	4	4	2	2	2	1	3 ± 1
Wire-to-Clip [cm]									
CC	0.5	0.1	0.2	0.1	0.4	0.4	0.6	0.5	0.4 ± 0.2
LM	0.4	0.1	0.2	0.8	0.1	0.1	0.2	0.2	0.3 ± 0.2
Wire Depth [cm]	5	5	4	6	5	5	3	6	5 ± 1
visible through skin	No	Yes	No	Yes	No	Yes	Yes	Yes	
fiber power [%]	100	100	100	30	30	100	30	70	70 ± 35

Table 3.1: Radiographic and Operative metrics for enrolled patients. IDC: invasive ductal carcinoma, DCIS: ductal carcinoma *in situ*. Breast Comp. was the BI-RADS breast composition score. Wire-to-clip was the distance between the wire tip and the biopsy clip in both the cranio-caudal [CC] and latero-medial [LM] projections. The wire depth was the distance from the wire tip to the skin. The fiber power was controlled by neutral density filters and was the percentage of total laser power used during lumpectomy. The summary column shows the mean and standard deviation.

3.2.1 Optical Wire

Optical wires (36) instead of hook-wires (31) were used to localize tumors. Each optical wire was composed of a biocompatible polyimide sheathed 200 μm optical fiber (Optran WF 200/220 P, CeramOptec, East Longmeadow, MA) attached to a 20 cm long Kopans breast lesion localization wire (DKBL-20-9.0, Cook Medical Inc., Bloomington, IN) using medical-grade ultraviolet-curing acrylic (Loctite 392, Henkel Corporation, Bay Point, CA). The outer diameter of the optical wire was 457 μm. The total length of the optical fiber was 3 meters. The light emitting end of the optical fiber was offset 2–3 mm in the proximal direction from the tip of the Kopans wire to allow the entire optical wire to pass though an 18 G needle (Figure 2.1).

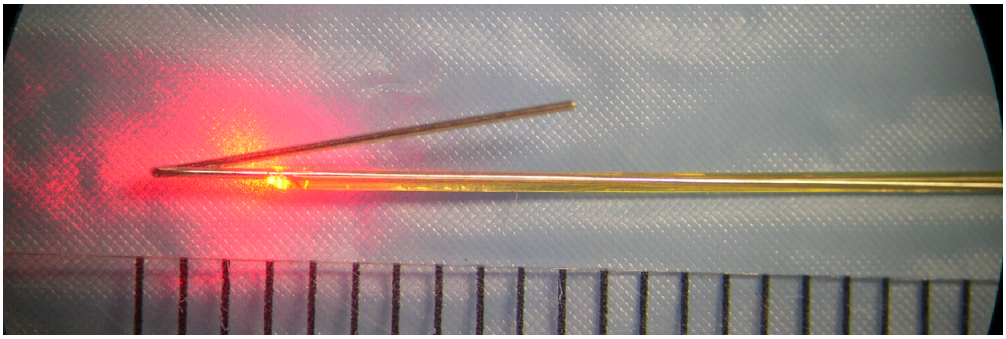

Figure 3.2: A light emitting optical wire composed of a 200 μm optical fiber adhered to the length of a standard wire. The light emitting tip of the optical fiber is offset 2–3 mm from the distal, hooked tip of the wire. The ruler is in units of millimeters.

3.2.2 Wire Localization

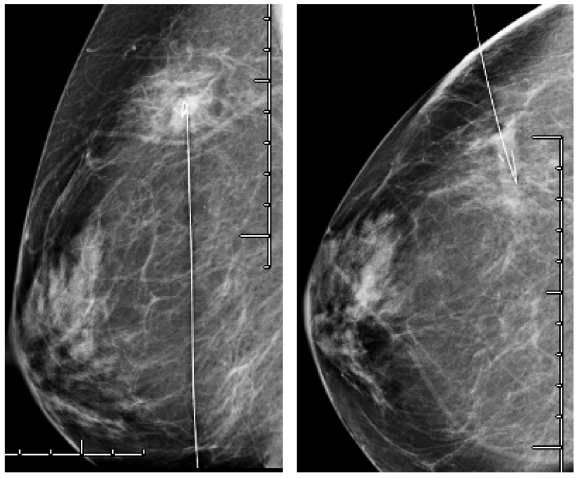

Figure 3.3: Orthogonal mammograms of one patient after wire localization. The wire was inserted in the lateral to medial direction with its tip in the tumor and approximated to the clip. Rulers are in units of centimeters.

The center of the tumor was targeted during localization. An 18G needle was placed in the breast using either mammography or ultrasound guidance. The optical wire was advanced through the needle until the spring hook was aligned with the tip of the needle. Imaging confirmation of placement within the tumor was achieved and the needle was removed allowing the hook to deploy. Orthogonal mammograms were taken to verify the location of the wire relative to the tumor and to the previously placed biopsy clip, Figure 3.3. Finally, the external portion of the optical wire

was secured to the breast with gauze and tape.

Breast density was recorded based on the Breast Imaging-Reporting and Data System (BI-RADS) breast composition score of 1–4. Where 1 indicates almost entirely fat, 2 indicates scattered fibroglandular densities, 3 indicates heterogeneously dense, and 4 indicates extremely dense tissue.

3.2.3 Light-guided Lumpectomy

Once in the operating room, patients were placed under anesthesia and the tape holding the optical wire in place was removed. The optical wire was connected to a 633 nm HeNe laser with less than 2 mW of light coupled into the fiber. Because the light emitting end of the fiber was within the breast, exact measurements of light output were not possible. However, each fiber had been previously validated to emit 1–2 mW of light. At this low power, laser goggles were not needed, heating of the tissue was calculated to be less than 1 °C, and there was no risk of tissue damage from the light. The light from the laser was focused into the optical fiber using lenses. In lumpectomies 4–8, neutral density filters were used to reduce the intensity of light and consequently the apparent size of the glowball. The filters transmitted either 100, 70, 30, 10 or 1 % of the maximum light. Each surgery was started with 100% of the light, the room lights were dimmed in attempt to visualize the red light before making an initial incision. If visible, the brightest area on the skin indicated the shortest approach to the cancer. At the operating surgeon's discretion, the filter was adjusted to change the glowball size around the cancer to approximately 3–4 cm in diameter.

Once the primary specimen had been resected, its six margins were inked by the operating surgeon with six different colors to indicate orientation. The specimen was sent to radiology to confirm that it contained the clip and apparent cancer. Orthogonal radiographs were taken of the specimen with orientation marked on the images. If specimen radiographs or gross appearance of the cavity margins in surgery were suspicious, additional cavity shavings were performed, inked for orientation and sent to pathology.

3.2.4 Pathology

Each specimen submitted to pathology was placed in formalin, grossly examined, sectioned and stained with hematoxylin and eosin. Additional immunoperoxidase staining was performed for estrogen receptor, progesterone receptor, and human epidermal growth factor receptor 2. Cancers were staged according to the American Joint Committee on Cancer Tumor Node Metastasis (TNM) classifications. The specimen size, cancer size, margin status, and pathologic diagnosis

were recorded. Margins were considered *positive* for invasive ductal carcinoma if tumor cells were within 1 mm, *close* within 2 mm, and *negative* greater than 2 mm from the margin. Margins were considered *positive* for ductal carcinoma *in situ* if tumor cells were within 2 mm, *close* within 3 mm and *negative* greater than 3 mm from the margin(53).

3.3 Results

3.3.1 Wire Localization

Each optical wire was placed within a few millimeters of the biopsy clip. In the cranio-caudal projection, the distance from the wire tip to the biopsy clip was 4 ± 2 mm and in the latero-medial projection 3 ± 2 mm. The length of wire within the breast was 50 ± 10 mm. The time of the localization procedure was 21 ± 16 min. The BI-RADS breast composition scores were between 1 & 4, Table 3.1.

3.3.2 Light-guided Lumpectomy

The glowball was used as a guide in all eight lumpectomies. In 5 patients, with the room lights dimmed, red light was visualized before the first skin incision and provided a clear approach to the targeted tumor. In all patients, the light was readily visualized after skin incision so the light rather than the wire dictated the surgical plane. The cancer was approached by sharp dissection towards the brighter light. This was particularly useful for a deep tumor near the chest wall in patient 4. In patients 4–8, the intensity of light was reduced to make the glowball smaller after approach. While keeping the light centered, dissection around the glowball was made. A consistent border around the glowball was obtained by excising along a plane of similar light intensity. After the optical wire and surrounding tissue were removed, the cavity was re-examined. In 5 patients, additional margins were removed due to either suspicious appearance of the cavity or review of specimen radiograph, Table 3.3. Figure 3.4 demonstrates the effect of room lighting on visibility of the glowball (top row), as well as how the glowball was used in locating (bottom row, left) and removing the tissue specimen (bottom row, middle & right). The time from first incision to removal of the specimen was 17 ± 6 min and the laser was on for 17 ± 7 min.

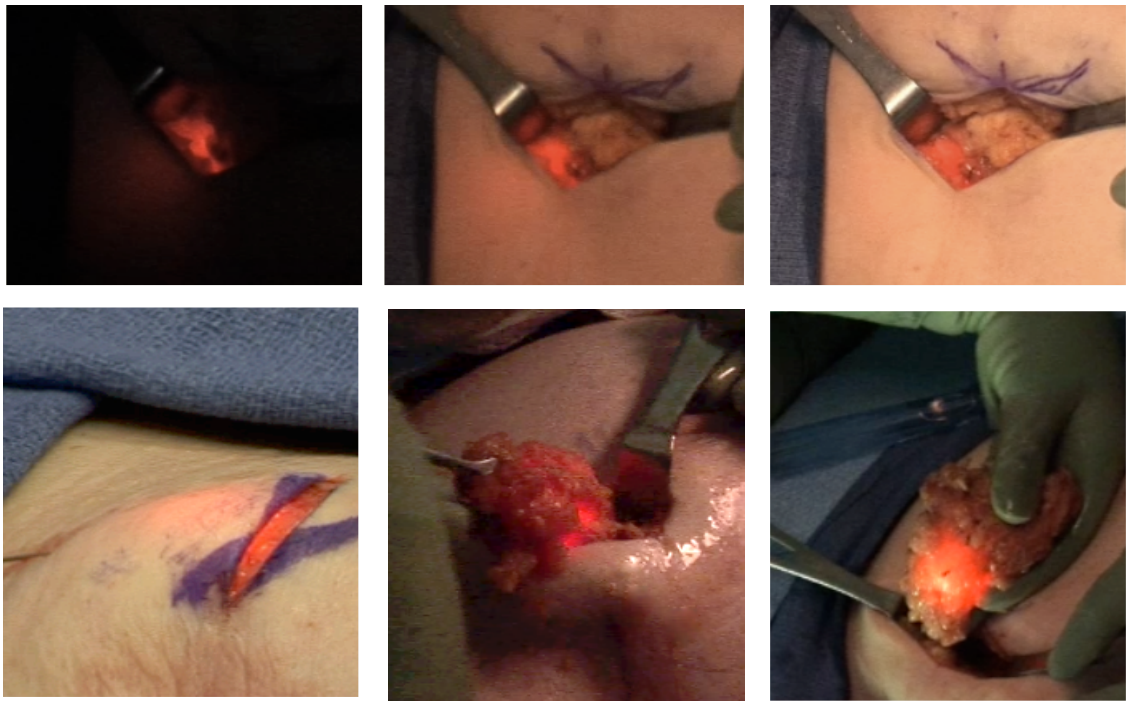

Figure 3.4: Top row: Visibility of a deep (6 cm) glowball near the chest wall as room lighting is increased (*left to right*). **Bottom row:** In practice, (*left*) light guided the surgeon towards the cancer and (*middle & right*) created a visible sphere to remove. The red light can be appreciated well with color images available online.

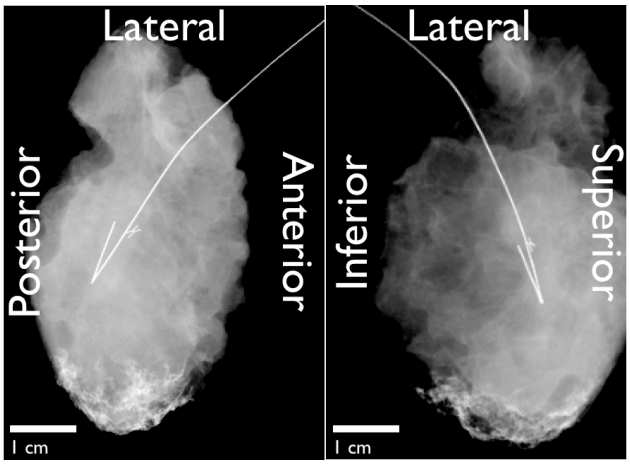

Figure 3.5: Orthogonal radiographs of the lumpectomy specimen from the breast shown in Figure 3.3. The optical wire remains approximated to the biopsy clip and centered in the specimen.

3.3.3 Specimen Radiograph

Each specimen was imaged with orientation marked on orthogonal radiographs. The clip was retained in all eight specimens. Figure 3.5 shows the specimen radiograph for the same patient in Figure 3.3. The clip and optical wire were centrally located in the specimen.

3.3.4 Pathology

Although all patients were diagnosed with either IDC or DCIS following core needle biopsy, upon final diagnoses, one patient had only atypical ductal hyperplasia & lobular carcinoma *in situ* remaining in the breast both of which indicate increased risk for breast cancer, Table 3.2. All four of the patients who underwent sentinel node biopsy were negative for lymph node metastasis. The Nottingham histologic grade for each patient is also shown in Table 3.2. A high (3) grade classifies poorly differentiated cells that tend to spread and divide more rapidly than moderate (2) and low (1) grades.

Of the primary (light-guided) resections, 3 focally positive margins (1 DCIS, 2 IDC) and 5 negative margins were found. Removal of additional tissue by cavity shaving at the time of initial surgery resulted in negative margins in all but one patient as shown in Table 3.3. No tumor cells were found in any of the additional margins. In the patient with a positive margin, the primary specimen was excised from the anterior skin to the posterior fascia and additional tissue was excised along the inferior margin at the time of initial surgery. DCIS was found at the anterior and inferior margins, but no skin had been removed at the anterior margin which resulted in re-excision at a later date.

The dimensions of the primary specimens and cancers are shown in Table 3.4.

Patient	1	2	3	4	5	6	7	8
Final Diagnosis	IDC & DCIS	IDC & DCIS	ADH & LCIS	IDC	IDC & DCIS	IDC & DCIS	IDC & DCIS	DCIS
Node Status [+ / total]	0/3	0/1	0/0	0/1	0/1	0/2	0/0	0/0
IDC grade	1	2		3	3	3	2	
DCIS grade	2	3			3	3	3	1

Table 3.2: Pathologic findings following resection(s). IDC: invasive ductal carcinoma, DCIS: ductal carcinoma *in situ*, ADH: atypical ductal hyperplasia (a risk factor for but not a breast cancer). A high nottingham histologic grade of 3 represents poorly differentiated cells that divide more rapidly and tend to spread when compared to moderate (2) and low, (1) grades.

Patient	1	2	3	4	5	6	7	8
Shortest IDC Margin [mm]	0	5		3	5	0	>5	5
Shortest DCIS Margin [mm]	1					>5	0	
Involved Margin(s)	S*					A*	A* I	
Cavity Shave(s)	S L			A M L S I		A S	I	A M
Neoplasm in Cavity Shave(s)	no			no		no	no	no

Table 3.3: Margin status following resection, shortest margin was measured on the primary lumpectomy specimen. IDC: invasive ductal carcinoma, DCIS: ductal carcinoma *in situ*, $*$: margin focally involved, A: anterior, P: posterior, M: medial, L: lateral, S: superior, I: inferior.

Patient		1	2	3	4	5	6	7	8	Summary
Specimen Size:	Ant.-Post.	3.2	2.5	2.5	2.6	3.8	2.5	3.0	4.5	3.1 ± 0.7
	Med.-Lat.	6.2	3.5	5.6	7.5	5.0	4.8	7.0	8.0	6.0 ± 1.5
	Sup.-Inf.	4.6	4.5	3.5	5.0	4.0	4.5	4.5	6.5	4.6 ± 0.8
Cancer Size:	Ant.-Post.	1.9	0.7		$0.3^{\dagger}$	1.7	1.3	1.9	$0.5^{\dagger}$	1.5 ± 0.5
	Med.-Lat.	1.7	0.6			1.5	1.1	0.9		1.1 ± 0.4
	Sup.-Inf.	0.9	0.5			1.1	0.9	0.7		0.8 ± 0.2

Table 3.4: Specimen and lesion dimensions shown in centimeters. The summary column shows the mean and standard deviation. †: residual disease.

3.4 Discussion

Light-guided lumpectomy is a feasible technique for resecting non-palpable breast tumors that was easily incorporated into standard practices. Placement of the optical wire was identical to a standard hook-wire. Lumpectomy was facilitated by illumination of tissue as well as a hook-wire. Dissection towards the bright light provided a direct path to the tumor. Once an incision was made in the skin the red light was visible in all patients. The light was visible at 6 cm below the skin which may prove to be particularly useful for deep cancers or for resecting tumors within large breasts. After approach, the glowball provided a visible sphere to dissect around. Ideally, measurements of the distance from the specimen surface to the wire tip would be available to the operating surgeon and is an active area of investigation (54).

The low power laser was comparable to a laser pointer used for presentations; the surgical staff did not need special eye protection. At 1–2 mW of light, the glowball was not visible through the skin in three cases due to either room lighting, fiber coupling or strong attenuation by the skin. All enrolled patients were fair-skinned caucasians, therefore it was unlikely skin color affected visibility between patients. Higher scattering in skin than breast tissue was the presumed cause of

attenuation. It is possible that the light will not be visible prior to skin incision in patients with darker skin pigmentation due to increased attenuation of the visible light. I believe the disadvantage of increased light attenuation in darker skin was outweighed by the the ease of using a visible light source. If infra-red light was used an imaging system would be needed during the entire procedure, which would complicate the surgical field and potentially increase operating time.

This technique relies on correct placement of the wire tip and relatively uniform absorption and scattering within the tissue to create a sphere of light. It has been reported that the absorption and scattering of cancerous and normal breast tissue differ. In the review by Leff *et al.*, malignant breast tissue has higher absorption than normal tissue for visible red light by approximately two fold (55) and could affect glow ball sphericity. For example, if the wire tip were placed medial to a 2 cm lesion, the light on the lateral side of the lesion coiuld be attenuated more than on the medial side. However, the position of the tip to the lesion is known prior to lumpectomy. In addition, a wavelength range of 630-640 nm was selected where absorption by hemoglobin is low, approximately $0.04\,\mathrm{cm}^{-1}$ (55), to minimize visual differences between healthy and diseased tissue.

Light-guided lumpectomy does not identify tissue as cancerous, but allows a spherical volume of tissue to be readily resected. It has not been demonstrated that more spherical specimens result in fewer positive margins. However, more spherical specimens may enable treatment with existing partial breast x-ray irradiation and provide a relatively continuous (non-fractured) surface for pathologic examination.

4

Light Guided Lumpectomy: Second Generation Device

4.1 Introduction

Although the study presented in Chapter 3 resulted in promising clinical outcomes, the wire itself was made to be more comfortable for the patient and more user friendly for the radiologist, operating surgeon and engineer operating the light source. Since the first generation optical wire had 3 m of optical fiber permanently attached to the Kopans wire, it required extra time to be placed by the radiologist, then the fiber had to be wound and carefully taped to the patient's chest. Once the patient was in the operating room, the fiber had to be carefully untaped and unwound, then manually coupled and aligned with the red laser. None of the fibers broke in the clinical testing that was performed, however, it was likely to occur due to the fragile nature of the small fiber. To address the issue of potential fiber breakage and in an overall effort to make the device more comfortable for the patient and easier to use, a second generation optical wire was designed, tested, and manufactured. The second generation device was designed with a custom extruded Pebax dual lumen tube with dimensions of $480 \times 818\,\mu$m. One lumen of the tube was permanently adhered to a Kopans wire and the other lumen was left open so a fiber could be slid in and out. This second generation device allowed the radiologist to place the wire without the fiber attached. The second generation device was more comfortable of the patient because the fiber did not have to be attached to the patient between placement and surgery. From both the radiologist and patient perspective, the optical wire was simply a larger diameter Kopans wire. During surgery, the optical fiber could be placed within one lumen of the dual lumen tube and taped in place during the surgery.

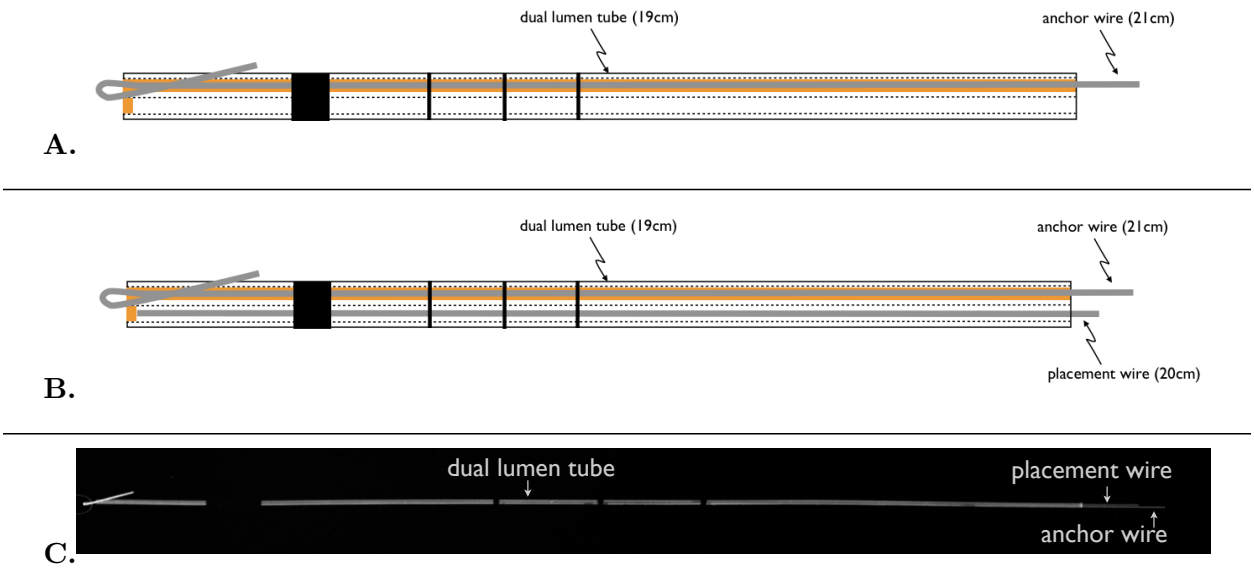

Figure 4.1: **A.** Optical wire with the anchor wire glued within one lumen of the dual lumen tube. The anchor wire is secured within the tube and cannot be removed. The second lumen is open on the proximal end (right) to allow insertion of either a placement wire or optical fiber. The distal end of the lumen (left) is sealed with 1 mm of medical grade glue. The dark lines around the optical wire are depth markers. **B.** Optical Wire with placement wire inside tube. For clarity, drawings are not to scale. **C.** Photograph of actual optical wire.

This chapter is organized to present the fabrication of the optical wire, describe how the wire will be used, and finally to describe the strength testing and sterility validation of the wire.

4.2 Fabrication

The optical wire was re-designed for the comfort of the patient and the ease of use for the surgeon and the engineer. For each device, a sterilely packaged Cook Kopans wire was cut 21 cm from the hook tip and the cut end polished flat, this resulted in the anchor wire. The anchor wire was glued within the entire length of one lumen of a custom extruded dual lumen tube using 1.5 μL of medical grade epoxy. The other lumen of the tube was sealed at its distal end with 1 mm of epoxy and holds a placement wire during needle localization, see Figure 4.1. The purpose of the placement wire was to ensure no air pockets exist within the lumen of the tube during sterilization. It is possible an air pocket within the lumen could not get up to temperature during sterilization.

During surgery, the placement wire is removed and replaced with the optical fiber. One end of

an optical fiber, is connected to a low power red laser. The power of the light emitting from other end is measured with a sterile power meter. The optical fiber is then pushed into the empty lumen. The tube and fiber are taped to the patients skin to prevent them from moving. The surgery can now be guided by the red glowball of light. If, for any reason, the illumination of tissue failed, the optical wire could be used as a standard Kopans wire to guide the surgery.

4.2.1 Optical Wire Components

The Kopans wire has been used routinely for 25 years to localize breast tumors in humans. It is manufactured by Cook Medical Inc. and distributed worldwide. As distributed, a Kopans localization wire is composed of two parts, a 21 G needle and a spring hookwire that slides through the needle. The needle is not used with the optical wire because it is too small. The localization needles used were 18G (as opposed to the standard 21G) to allow the optical wire to advance through the needle. The standard hookwire is 20-25cm long, 250 microns in diameter; its tip is bent to form a V. The V-shape serves as the hook and anchors the wire in place once the hook extends past the tip of the needle as it is withdrawn by the radiologist.

The placement wire was cut from the long straight portion of a Kopans wire in this study. It is 20 cm long.

The dual tube was custom designed and extruded for this device. The tubing was clear and made from the polymer Pebax 7233, a poly vinyl chloride with USP class VI approval. Pebax 7233 is widely used for catheters in the medical device industry. The tubing had two lumens, each 300 μm in diameter with an overall dimension of 480$\times$818 μm, Figure 4.2. There are 4 depth marks on the outside of the dual lumen tube as shown in Figure 4.1. The first begins 2 cm and ends 3 cm from the distal end. This mark is intended to be used as an optional depth reference during surgery. The other three marks indicate correct alignment during needle localization. When a mark aligns with the luer end of the localization needle, the end of the optical wire is located at the sharp end of the needle. The three marks correspond to needle lengths of 5, 7, & 9 cm. The three needle lengths are provided so the radiologist can choose an appropriate one at their discretion. The ink was applied with a pad printing technique and was a USP Class VI approved ink (Marabu Tampapur TPU) used for marking medical devices and catheters.

The optical fiber (CeramOptec) was composed of a silica core and cladding, both of which are surrounded by a polyimide jacket. All of the materials in the optical fiber are biocompatible. The fiber is resistant to breakage above a bend radius of 11 mm. The fiber was 190 μm in diameter and

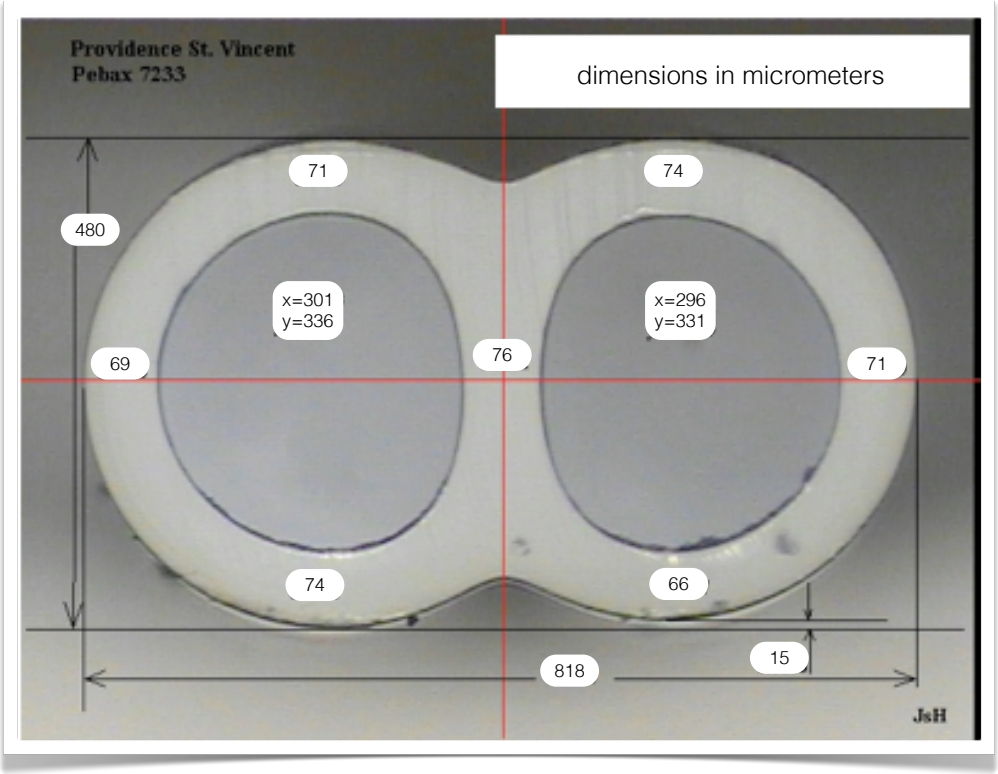

Figure 4.2: A profile of the custom extruded dual lumen Pebax 7233 tube.

easily slides into one lumen of the optical wire. The optical fiber had a standard SMA connector on one end to facilitate light coupling with the laser.

An ultraviolet light curing acrylic (Loctite 3921) was used to glue the Kopans wire within the tube. It is classified as a medical device adhesive by EN/ISO 10993 Biological Tests. Loctite 3921 is sterilizable by both hydrogen peroxide and steam techniques. It readily adheres to plastics and metals. The epoxy is cured with a 365 nm light source at 200 $\mathrm{mW/cm^2}$ for 1 minute. A two-minute cure time was used to ensure all epoxy was cured.

The components of the device were all made in ISO 9001 approved facilities and are all either FDA approved and / or have USP Class VI approval for use in a medical device. The components were assembled aseptically and then the optical wire and optical fiber were packaged and sent for sterilization using steam processing.

4.3 Instructions for Use

4.3.1 Needle Localization

1. Remove the optical wire from sterile packaging. Do not use device if the package has been damaged or opened.
2. Place needle according to standard practice so it is within the lesion.
3. Place the optical wire as a standard Kopans wire would be placed.
4. Following placement of the optical wire, care should be taken to tape the wire and optical fiber to the skin. DO NOT severely bend the wire.
5. Final optical wire placement should be confirmed by appropriate imaging.
6. Under no circumstances should the optical wire be pulled out without surgical intervention.

4.3.2 Lumpectomy

1. Remove optical fiber from packaging. Attach SMA end to laser, while maintaining sterility of bare end.
2. Remove tape from the optical wire and patient.
3. Drape patient and prepare area for surgery
4. Remove the straight wire from the tube of the optical wire.
5. Place the optical fiber inside the tube and advance 19 cm until it stops.
6. Securely tape the optical wire and fiber to the skin of the patient.
7. The hookwire should be used as a guide for the surgeon, not a retractor.
8. Extra care should be taken to avoid cutting or breaking the optical fiber.
9. Depending on the depth of the optical wire, the glowball may not be visible with all room lights on. Adjust room lights until red light can be visualized.
10. A manual power supply controls the laser illumination and can be adjusted as the surgeon requests.

11. Follow the intensity gradient of the red light until the room lights can be turned on and the glowball visualized.

12. Resect a sphere around the glowball by following the intensity gradient of light.

13. Once the resection is complete the fiber may be removed and the optical wire can be cut and pulled through the breast tissue if needed.

14. Measure the optical power output of the fiber.

4.4 Tensile Testing

Tensile testing of the Kopans wire bend was performed and considered the primary failure point of the wire. If the wire were placed within a breast and then retracted, the hooked end would straighten until breakage or displacement occurred. To find the strength of the bend, each of five Kopans wires were placed in a MTS machine to simulate the wire being pulled out of tissue as shown in Figure 4.3. The straight portion of the wire was clamped in place and attached to a 100 lb force load cell. The hooked end was placed over the base of a triangular shaped steel rod more than ten times the diameter of the wire to ensure the rod did not bend during testing. The clamp holding the rod was displaced at 2 mm/s so the wire was pulled in tension and the angle of the bend increased from 15–90° degrees. The maximum force was recorded.

The resulting mean force to straighten the bend of the wire was 3.02 N with a standard deviation of 0.13 N. This is similar to about a 300 g mass pulling on the wire. This measurement was used as a design threshold; the optical wire needed to be as strong or stronger than 3 N in tension.

To test the glue strength between the wire and the tube, the amount of glue was reduced from 1.5 to 0.5 μL. Eight samples were made with wire glued inside the tube, cured under UV light for 2 minutes, and then steam sterilized 3 times at 132°C for 30 minutes. The samples were then loaded into the MTS machine and tested in tension as shown in Figure 4.4 where epoxy is indicated in grey. The straight portion of the tube / wire assembly was clamped in place and attached to a 100 lb force load cell. The hooked end of the wire was placed over a straight steel rod more than ten times the diameter of the wire to ensure the rod did not bend during testing. The clamp holding the wire was displaced at 2 mm/s so the wire was pulled in tension but the bend in the wire would not change angle.

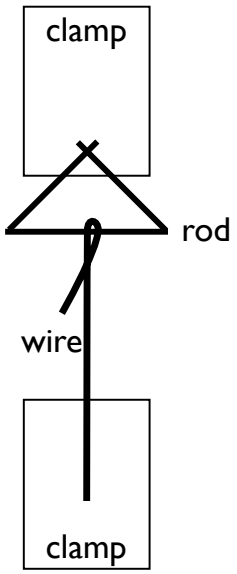

Figure 4.3: The set up of the MTS for tensile testing of the bend of the Kopans wire.

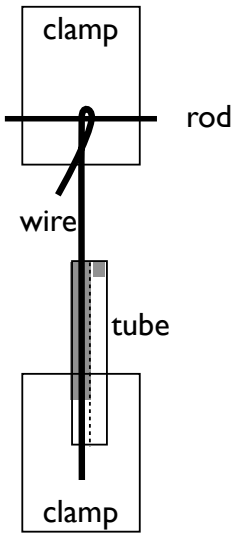

Figure 4.4: The set up of the MTS for tensile testing the strength of the epoxy, indicated in grey, in the optical wire.

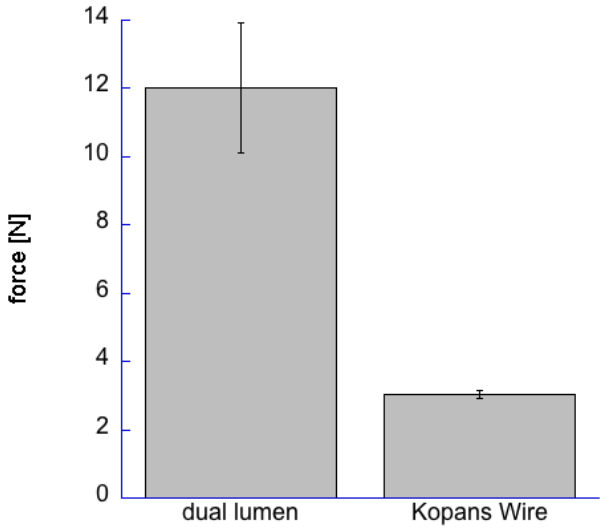

Figure 4.5: The tensile force needed to pull the dual lumen optical wire out of the clamps retaining the samples (n = 8) and the force needed to straighten the bend in standard kopans wires (n = 5). We were not able to pull the optical wire apart, the tensile strength of the optical wire is greater than 12 N.

We were not able to pull the wire out of the tube, because the clamps retaining the samples failed. The mean force of the clamp on the tube was 12 N with a standard deviation of 2 N, therefore, the force it would take to pull the wire out of the tube is greater than 12 N. This force is significantly greater than the force required to straighten the bend in the anchor wire, 3 N, (Student's t-test, $p < 0.001$). Figure 4.5 shows a factor of safety of at least 4.

4.5 Sterilization

The purpose of this study was to verify the effectiveness of steam sterilization for the Optical Wire Device. The intent of this study was to develop guidelines for steam sterilization and to provide assurance of sterility using 132°C with prevacuum air removal.

Due to the small lumen size in the optical wire, sterility within the lumen had to be verified following steam sterilization. The temperature, time and type of steam sterilization cycle were determined. NAMSA was contacted to consult and conduct the sterility validation.

This study was conducted per NAMSA Protocol 09G_54391_02 (see Appendix A for a complete description), in accordance with AAMI TIR12:2004 *Designing, Testing, and Labeling Reusable Medical Devices for Reprocessing in Healthcare Facilities: A Guide for Device Manufacturers and ISO 17665-1:2006 Sterilization of health care products Moist heat Part 1: Requirements for the development, validation and routine control of a sterilization process for medical devices.*

A total of ten Optical wires were each inoculated with 0.01 mL of SPORTROL *Geobacillus stearothermophilus* spore suspension (Lot S77112) in accordance with NAMSA Test Specification T0007359-02. The spore suspension had a certified *D*-value of 1.9 minutes. The suspension was serially diluted with sterile water for injection (SWFI) to obtain 2.6 x 10^4 spores/optical wire. Inoculated devices were allowed to dry for a minimum of four hours in a laminar airflow (LAF) hood. Prior to and post inoculation, enumeration of the inoculum suspension was performed to ensure the delivery population.

This study utilized biological indicators (products inoculated with 10^6 *Geobacillus stearothermophilus* spores[1]) to demonstrate that the biological indicator challenge was successfully sterilized using three consecutive half cycles.

For each of three half cycles, three dry inoculated optical wires were individually double-pouched. In addition, three optical fibers inside Teflon coils were individually double pouched. Although the Optical Fibers were not deemed most difficult to sterilize, they were present in each cycle exposure to simulate practical sterilization configuration during routine processing. Three double-pouched optical wires and three double-pouched optical fibers were placed inside the autoclave chamber. Each inner pouch contained a steam chemical indicator strip.

[1]Different populations may have been utilized depending on the D-value in order to represent a minimum of a six $\log_{10}$ reduction. See Section 5.1.2 of NAMSA Protocol 09G_54391_02 for explanation of D-value equivalent populations.

Three autoclave exposures (half cycles) were conducted for three minutes at 132°C with prevacuum air removal, four pulses, and no dry time. All half cycles were performed without dry time to represent worst-case scenario.

Following each half cycle, three inoculated optical wires were aseptically removed from their pouches and individually tested for sterility to determine the presence of surviving spores. One unexposed inoculated device was also sterility tested for use as a positive control. Samples were cultured in 400 mL of soybean casein digest broth (SCDB) in accordance with NAMSA Sterility Test Specification T0007360-01. Cultures were incubated at 55-60°C until positive for growth or for seven days. All procedures were conducted with good manufacturing practices in conformance with ISO 13485:2003.

4.5.1 Results

Successful completion of three half cycle exposures at 132°C prevacuum confirmed that the half cycles provided a minimum of a six $\log_{10}$ reduction of the biological indicator spore population. This qualifies the full cycle at 132°C for a minimum of six minutes using prevacuum air removal in a double-pouched configuration.

The combination of verified population and D-value of the *G. stearothermophilus* spore suspension was found to be acceptable per protocol.

$$\log_{10}(\mathit{ChallengePopulation}) \cdot \mathit{D\text{-}value} \geq 6$$

$$\log_{10}(2.6 \times 10^4) \cdot 1.9 = 8.4$$

The population verification of the inoculum suspension confirmed that each device was inoculated with a mean population of 2.6 x 10^4 spores per device.

The sterilization parameters for each of three cycle exposures were recorded and verified to be in compliance:

Parameter	**Half Cycle 1**	**Half Cycle 2**	**Half Cycle 3**
Temperature, °C	132	132	132
Pressure, psig	27-28	27-28	27-28
Steam Exposure Duration, Minutes	3.02	3.02	3.02
Cycle Duration, Minutes	19.00	26.80	25.57

Tests of sterility resulted in no growth of the inoculated product. The positive control resulted in growth, as expected. Although not an indicator of sterility, all chemical indicators demonstrated a color change from yellow to dark brown.

132°C Prevacuum, 3 minutes			
Half Cycle	1	2	3
Inoculated Product	0+ /3	0+ /3	0+ /3
Inoculated Product PC	NA	NA	1+ /1

Table 4.1: Note: + = Positive for Growth (Nonsterile), PC = Positive Control, NA = Not Applicable
A common PC was cultured with samples from the 3rd half cycle

The results of this study demonstrated the ability of three steam half cycles to sterilize biological indicators with 10^6 (or D-value equivalent population) Geobacillus stearothermophilus spores and therefore, provides assurance of sterility of not less than 10^6 following a six minute full cycle exposure at 132°C using prevacuum air removal, no dry time, in a double-pouched configuration.

4.6 Conclusions

An optical wire was designed and manufactured for use in light-guided lumpectomy. The wire is placed in exactly the same manner as a standard Kopans wire, and allows operating surgeons to use a glow-ball of light as a guide to find and resect lesions. The glue of the optical wire was tested in tension and found to have at least a margin of safety 4 times stronger than than the bend of a standard Kopans wire. Since a Kopans wire was incorporated into the optical wire, the optical wire fails under tension exactly as a Kopans wire. Due to the risk of the small lumens of the tubing trapping air and not reaching temperature during steam sterilization, the sterility of the inner lumen was verified. All of nine optical wires were found to be sterile after challenge with innoculum and steam sterilization. A steam sterilization cycle of 6 minutes at 132°C using prevacuum air removal was validated in a double pouched configuration.

5

Measuring Distance in the Frequency Domain: Theory & Simulations

5.1 Introduction

This chapter presents a discussion of breast tissue optics, the theory behind using an intensity modulated point source to approximate distance through tissue, and Monte Carlo models created to test the theory. Frequency domain measurements are based on sinusoidally modulating a light source. Upon photon propagation through highly scattering material, such as tissue, the sinusoidal signal becomes demodulated, both the amplitude (A) of the wave and the average intensity (DC) decrease and a phase lag develops between the source and the propagating wave. In most of the biomedical optics literature the propagation of light is modeled when light enters and leaves tissue. In this body of work, the light is modeled with a source embedded in the tissue and collected after it exits the tissue. The diffusion approximation to the Boltzmann equation (83) was used to model the propagation of a modulated light source through a highly scattering medium (84). Both the diffusion approximation and Monte Carlo models provided the same results for phase lag through scattering media. The diffusion approximation with and without a boundary condition was used to show that at source depths of more than 5 mm no boundary condition was needed to provide an estimate of phase lag.

5.1.1 Optical Properties of Breast Tissue

The optical properties of breast tissue, both cancerous and normal have been studied for nearly 20 years. Due to inherent variations in breast tissue the reduced scattering (μ_s') and absorption (μ_a)

coefficients vary in the literature. The reduced scattering coefficient ranges from 0.5 to 2 mm^{-1} and the absorption coefficient ranges from 0.005 to 0.015 mm^{-1} in the red to near infrared region (NIR) of the light spectrum (1, 2, 3, 56, 57, 58, 59, 60, 61, 62, 63, 64, 65, 66, 67, 68, 69, 70, 71, 72, 73, 74, 75, 76, 77, 78, 79). The main chromophores in the spectra of breast tissue are water, lipid, and hemoglobin (oxygenated and de-oxygenated). The absorption spectra for these chromophores is shown in Figure 5.1 (80, 81). It is important to know the inherent variations of these chromophores in healthy tissue to establish a baseline for device development. In addition, the visibility of light through tissue is dependent on these chromophores. As shown in Chapter 2, Figure 2.2, the peak visibility of light through breast tissue is at 650 nm. A laser diode operating at 638 nm was chosen. This laser was the closest to 650 nm I found that operated at low power and could be incorporated into the optical system that I built.

Intra-subject variation in optical properties and chromophores was examined in the healthy breasts of 5 women by Shah *et al.* (2). The variation over a 30 mm line was only 5–10% for μ_s', oxygen saturation, and lipid content. Water content ranged from 10–20%. Hemoglobin ranged from 2–16%. The intrinsic spatial heterogeneity of breast tissue was 20–40% for μ_a and 5–12% for μ_s'. Water content and total hemoglobin concentration varied by as much as 30–40% and lipid content decreased as a function of age with variation near 30% for 20 year old women and as little as 10% for 65 year old women. Similar results were obtained in another study of 52 healthy volunteers by Durduran *et al.* (66).

Cerussi *et al.* (78) report a quasi isobestic point at 930 nm that is insensitive to changes in lipid and water content. In other spectroscopic studies (3, 67, 70) the absorbance spectra support an insensitivity at 930 nm as well. Most of the reported studies evaluate bulk optical properties of *in vivo* breast tissue, these studies are aimed at screening for breast cancer and are therefore non-invasive. An exception to note is van Veen *et al.* (3) whose measurements were intra-operative and were not made through the skin, Figure 5.2. The region between 900 and 930 nm also seems to be insensitive to malignant vs. normal tissue. A goal of biomedical optics has been to distinguish benign, normal, and malignant disease in the breast, however adequate specificities or sensitivities have yet to be achieved in large clinical trials.

Healthy breast tissue varies greatly in composition, from lipid rich to predominantly fibrous. Radiographically, women who are post menopausal have breasts that are more fibrous. The structure of the breast influences the reduced scattering coefficient. In 2001 Cerussi *et al.* (82) demonstrated

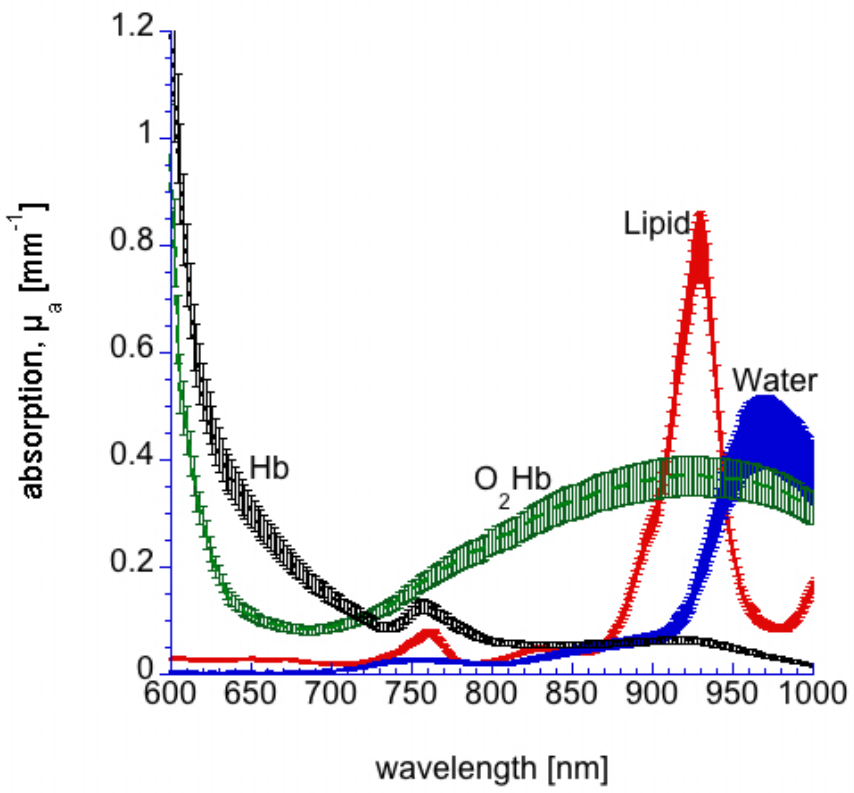

Figure 5.1: Created from data published by Spinelli *et al.* (1) and Shah *et al.* (2). The reported absorption of lipid, water, oxygenated hemoglobin and de-oxygenated hemoglobin at physiologic concentrations with the intrinsic variability of healthy tissue indicated by error bars.

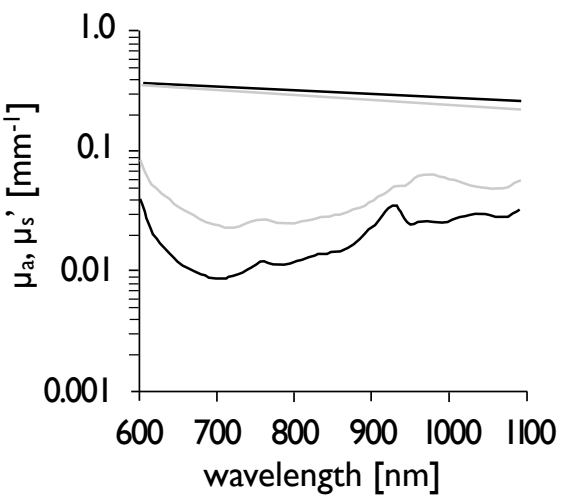

(a) Example of intraoperative malignant (gray) and normal (black) tissue spectra from one patient. Note the region of insensitivity at 930 nm in the absorbance spectra and the very small variation in the reduced scattering along the entire range.

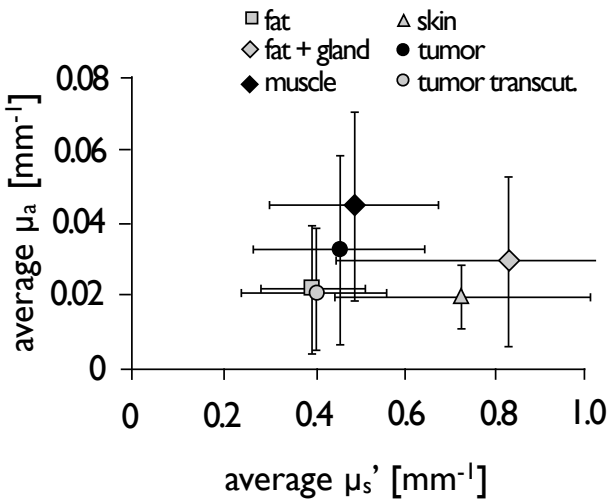

(b) The average absorption versus reduced scattering of 312 measurements on 24 patients at 650 nm. Note the difference skin makes in the reduced scattering. Error bars are standard deviations.

Figure 5.2: Adapted from van Veen *et al.* (3).

a correlation between the scatter power B taken from $\mu'_{s0} = a(\frac{\lambda}{\lambda_0})^{-B}$ and the lipid to water content of the breast. Where a is a constant, λ is the wavelength of interest, and λ_0 is a reference wavelength. Twenty-eight healthy volunteers were measured using a frequency domain system with source to detector spacing of 22 mm. Cerussi *et al* demonstrated that as lipid content decreases, fibrous tissue and water increase. Pifferi *et al.* (67) also demonstrated the same trend in a smaller study. The reduced scattering coefficient was quite sensitive to light collection geometries in both reflection and transmission measurements. Inter subject variation for a and B was between 20 and 30% for six patients.

Compression of the breast has also been shown to influence optical properties. For breasts under 3 lbs of compression a 13±10% (mean ± standard deviation) drop in hemoglobin concentration was demonstrated (79). Changes in pressure on the breast can have a significant effect on blood and water content of the tissue being measured (67, 79).

The majority of the cited papers here made measurements in the frequency domain. The work in these papers is sensitive to changes in water, lipid, hemoglobin, light collection and compression. The review article by Leff *et al.* (55) suggests that optical imaging of breast tissue is a promising adjunct to screening mammography but large clinical trials are needed to demonstrate the sensitivity and specificity of the technology.

5.2 Theory

Frequency domain measurements are based on sinusoidally modulating a light source, usually within a bandwidth of hundreds of megahertz, normally 100–2000 MHz. Upon photon propagation through highly scattering material, such as tissue, the sinusoidal signal becomes demodulated, both the amplitude (A) of the wave and the average intensity (DC) decrease and a phase lag develops between the source and the propagating wave, as shown in Figure 5.3.

The diffusion approximation to the radiative transport equation (83) is used to model the propagation of a modulated light source through a scattering medium (84). The approximation holds true when scattering events are much more common than absorption events and when photons have propagated some distance from the source. The diffusion approximation has been shown to be accurate beyond one mean free path (85) and is given by:

$$S(r,t) = \frac{1}{c}\frac{\partial}{\partial t}\phi(r,t) - D\nabla^2\phi(r,t) + \mu_a\phi(r,t) \tag{5.1}$$

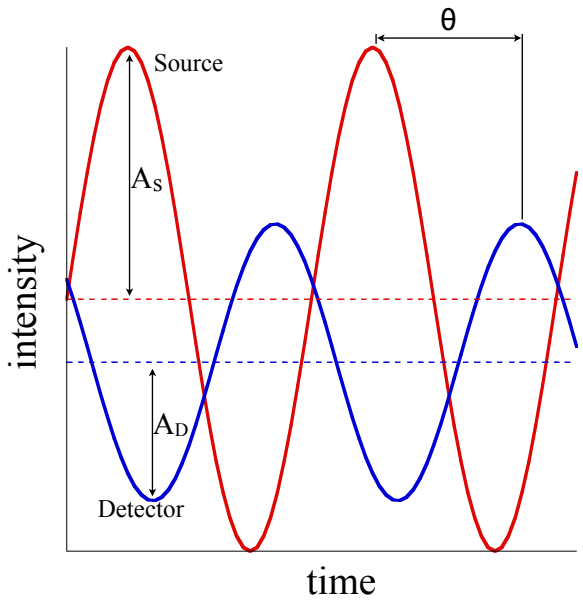

Figure 5.3: Example of the sinusoid sampled at the source and detector at the same time. The amplitude (A) of the wave as well as the DC (dotted lines) decrease upon traveling through a scattering medium and a phase lag, θ, develops.

where $S(r,t)$ is the photon source [W/m^3], c is the speed of light in medium [m/t], $\phi(r,t)$ is the fluence rate [W/mm^2], $D = \frac{1}{3(\mu_s' + \mu_a)}$, μ_a is the absorption coefficient [1/m] and μ_s' is the reduced scattering coefficient [1/m] and equals $\mu_s(1-g)$ where g is the anisotropy and μ_s is the scattering coefficient. For an isotropic short pulse point source in an infinite homogeneous medium, the source can be approximated by a Dirac delta function and the fluence rate is given by (84):

$$\phi(r,t) = c(4\pi Dct)^{-\frac{3}{2}} \exp\left(-\frac{r^2}{4Dct} - \mu_a ct\right) \tag{5.2}$$

If the source is modulated at a frequency ω, the Fourier transform of the above equation can be used to obtain the fluence rate (86)

$$\phi(r,t) = \frac{c}{4\pi\alpha r}\left[e^{-r\sqrt{b/\alpha}} + M_s e^{-r\sqrt{(b+i\omega)/\alpha}} e^{i\omega t}\right] \tag{5.3}$$

where $b = \mu_a c$, $\alpha = Dc$, $\omega = 2\pi f$, $M_s = \frac{AC_s}{DC_s}$, AC_s is the amplitude of the source wave and DC_s is

the mean power of the source. The phase and modulation of the fluence rate are given by (86)

$$\theta(r,\omega) = -r\sqrt{\frac{b}{\alpha}}\left(1+\frac{\omega^2}{b^2}\right)^{1/4}\sin\left(\frac{1}{2}\tan^{-1}\frac{\omega}{b}\right) \tag{5.4}$$

and

$$M(r,\omega) = M_s\exp\left(-r\sqrt{\frac{b}{\alpha}}\left[\left(1+\frac{\omega^2}{b^2}\right)^{1/4}\cos\left(\frac{1}{2}\tan^{-1}\frac{\omega}{b}\right)-1\right]\right) \tag{5.5}$$

If the optical properties of the medium do not need to be explicitly determined, Equations 5.4 & 5.5 can both be approximated by a linear equation and solved for distance, r

$$r = \gamma_a\cdot\theta + C_a \tag{5.6}$$

and

$$r = \gamma_b\cdot\ln(M) + C_b \tag{5.7}$$

where

$$\gamma_a = \sqrt{\frac{b}{\alpha}}\left(1+\frac{\omega^2}{b^2}\right)^{1/4}\sin\left(\frac{1}{2}\tan^{-1}\frac{\omega}{b}\right)$$

$$\gamma_b = M_s\exp\left(-r\sqrt{\frac{b}{\alpha}}\left[\left(1+\frac{\omega^2}{b^2}\right)^{1/4}\cos\left(\frac{1}{2}\tan^{-1}\frac{\omega}{b}\right)-1\right]\right)$$

and C_a & C_b are offsets introduced by the instrumentation of the measurement system and are not dependent on the medium.

In order to compare it with experimental results, the phase lag was explored in the majority of this document. The measurement system described in Chapters 7 & 8 was unable to measure the DC component of a modulated wave. Therefore a measurement of the modulation (A/DC) was not attainable so the phase lag was measured and used to calculate distance.

Figure 5.4 shows the relationship of phase as a function of distance, frequency, absorption coefficient and reduced scattering coefficient. Phase is proportional to distance and the expected slope of measurements in tissue was between 0.5 and 2 deg/mm. Phase was proportional to frequency in the relatively low frequencies shown here. A 70 MHz modulation frequency was chosen to simplify the components of an experimental system. Phase is a function of the inverse square root of the absorption coefficient. This plot shows the expected range of values reported in the literature for all

patients. The oval indicates the expected range in 1 patient which could result in a 2–4 mm error in distance. Phase is a function of the square root of the reduced scattering coefficient. This plot shows the expected range of values reported in the literature for all patients. The oval indicates the expected range in 1 patient which could result in 1–2 mm error in distance.

5.3 Materials & Methods

5.3.1 Boundaries

Traditionally in biomedical optics, a light source is placed outside of the tissue and several approximations have been derived to account for the refractive index mis-match at the boundary of the tissue. In the case of light-guided lumpectomy, the light source is within the tissue and a refractive index mis-match is only where the light exits the tissue. This section describes the process used to determine the effect of the tissue boundary in light-guided lumpectomies.

Farrell *et al.* (87) described a refractive index mis-match between tissue and air for steady state diffuse reflectance. This extrapolated boundary method was expanded to handle a modulated light source and solved for both the phase and modulation in the geometry shown in Figure 5.5 by Haskell *et al.* (88) where:

$$\theta = k_{imag} r_0 - \arctan(IMAG/REAL) \tag{5.8}$$

$$M = (REAL^2 + IMAG^2)^{1/2}/dc \tag{5.9}$$

where $k_{imag} = \sqrt{\frac{3}{2}\mu_a\sigma_{tr}}\left[\sqrt{1+(\omega\tau)^2}-1\right]^{1/2}$, $\tau = \frac{1}{\mu_a c}$, $\sigma_{tr} = \mu_s' + \mu_a$ is the linear transport coefficient, and $l_{tr} = 1/\sigma_{tr}$ is the transport mean free path. The remaining quantities are given by

$$REAL = \frac{\exp(-k_{real} r_0)}{r_0} - \cos[k_{imag}(r_{0b} - r_0)]\frac{\exp(-k_{real} r_{0b})}{r_{0b}} \tag{5.10}$$

and

$$IMAG = \sin[k_{imag}(r_{0b} - r_0)]\frac{\exp(-k_{real} r_{0b})}{r_{0b}} \tag{5.11}$$

and

$$dc = \frac{\exp(-r_0/\delta}{r_0} - \frac{\exp(-r_{0b}/\delta}{r_{0b}} \tag{5.12}$$

where ρ is the lateral distance on the surface, l_{tr} is the depth of the simulated source, $k_{real} = \sqrt{\frac{3}{2}\mu_a\sigma_{tr}}\left[\sqrt{1+(\omega\tau)^2}+1\right]^{1/2}$, $r_0 = (l_{tr}^2 + \rho^2)^{1/2}$, $r_{0b} = [(2z_b + l_{tr})^2 + \rho^2]^{1/2}$ and $z_b = \frac{1+R_{eff}}{1-R_{eff}}\frac{2}{3}l_{tr}$.

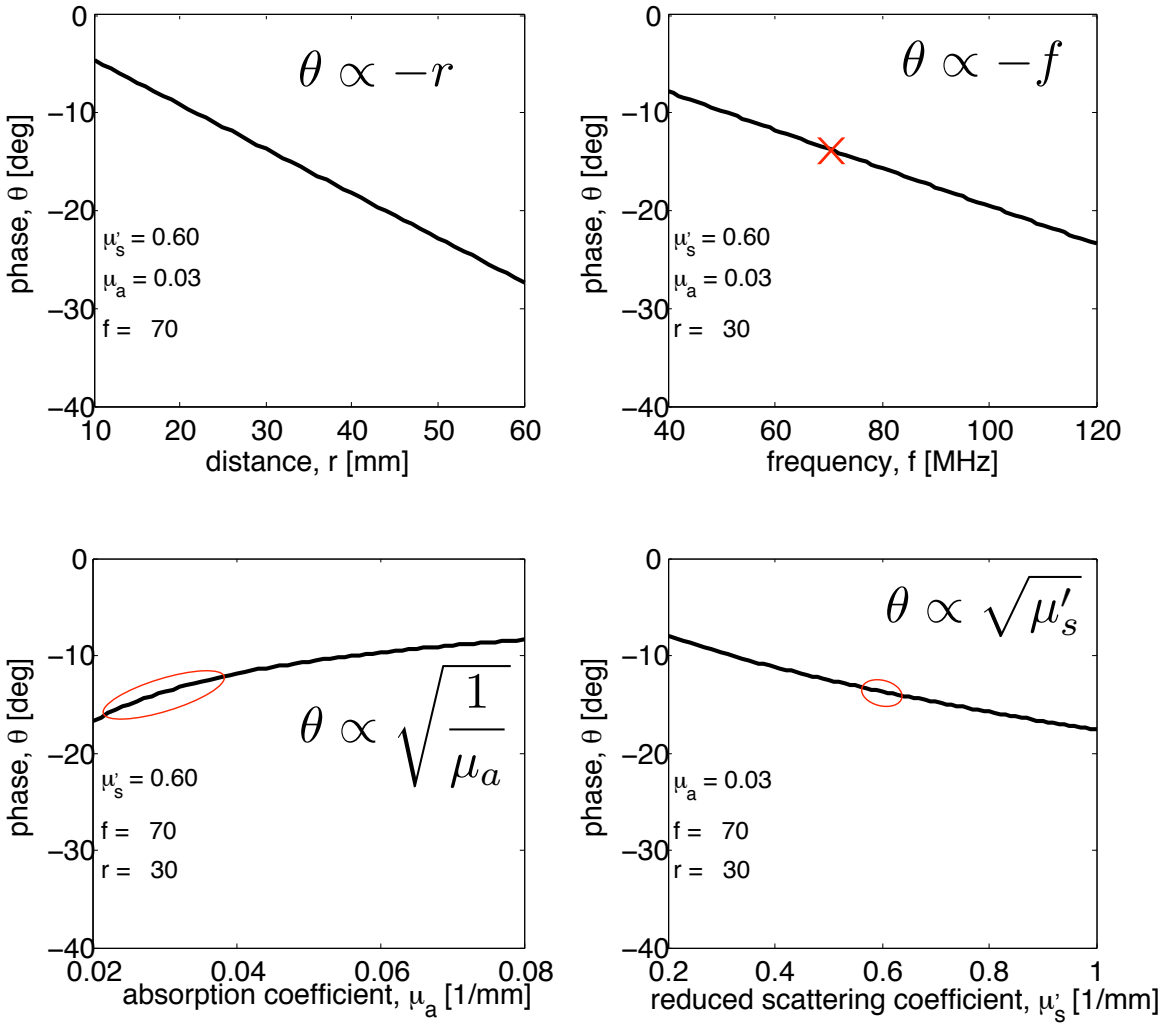

Figure 5.4: Top Left: Phase is proportional to distance and the expected slope of measurements in tissue will be between 0.5 and 2 deg/mm. Top Right: Phase is proportional to frequency in the relatively low frequencies shown here. A 70 MHz modulation frequency was chosen to simplify the components of an experimental system. Bottom Left: Phase is a function of the inverse square root of the absorption coefficient. This plot shows the expected range of values reported in the literature for all patients. The oval indicates the expected range in 1 patient. Bottom Right: Phase is a function of the square root of the reduced scattering coefficient. This plot shows the expected range of values reported in the literature for all patients. The oval indicates the expected range in 1 patient.

R_{eff} is the fraction of the source that becomes the irradiance when light is incident on the surface of the scattering medium (88).

The extrapolated boundary condition is illustrated in Figure 5.5. The phase lag from the source to the boundary of a simulated scattering medium was calculated with a modulation frequency of 150 MHz, $\mu_a = 0.005\,\mathrm{mm}^{-1}$, $\mu_s' = 1.0\,\mathrm{mm}^{-1}$, and $n = 1.40$. The infinite medium solution in Equation 5.4 was compared to the bounded solution in Equation 5.8. In addition, the source was simulated on the surface as well as within the medium. With the real source incident on the surface, l_{tr} was the mean free path and was the position of the simulated point source within the medium. With the real source within the medium (as is the case for light-guided lumpectomy), l_{tr} was the actual source depth.

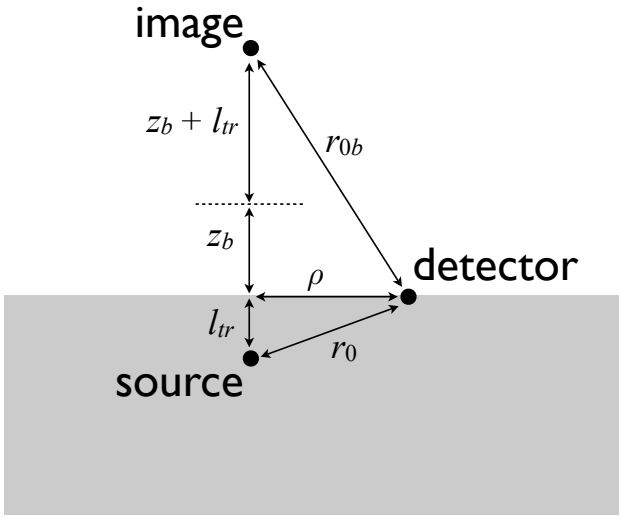

Figure 5.5: Diagram of extrapolated boundary condition.

5.3.2 Monte Carlo Model

A time-resolved Monte Carlo simulation (89) was modified (Appendix B.1) so photons were isotropically launched within a scattering / absorbing medium. Photons that reached the surface of the medium were binned according to distance from the source, r_0, and time elapsed, t. Simulations were run with a modulation frequency of 150 MHz, $\mu_a = 0.001\,\mathrm{mm}^{-1}$, $\mu_s' = 1.5\,\mathrm{mm}^{-1}$, $n = 1.48$, 2 mm radial bins, and source depths of 5, 25 and 45 mm.

A Fourier transform of the Monte Carlo results was performed in Matlab (Appendix B.2). The phase and modulation were found for each distance, r over a broad frequency range. In addition, Equations 5.8 & 5.9 were used to find the analytical approximation of the phase and modulation using the same input variables.

5.4 Results

5.4.1 Boundaries

The extrapolated boundary condition created a nearly constant offset in the phase when the source was incident on the surface and $\rho > 15\,\text{mm}$ as shown in Figure 5.6a. However, when the source was located within the medium, the effect of the boundary was negligible when $\rho > 5\,\text{mm}$ as shown in Figure 5.6b. This justifies the use of a infinite medium solution to phase lag when the source is within the medium and beyond 5 mm deep.

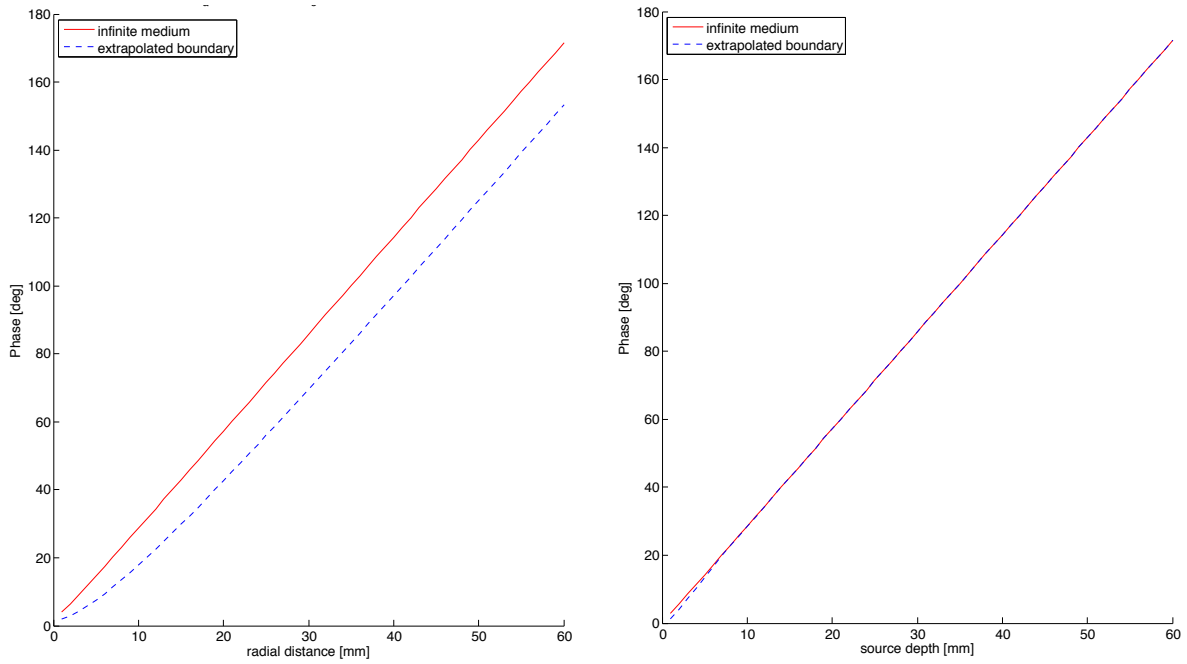

(a) Source on surface,where l_{tr} is mean free path and ρ is the radial distance from the source .

(b) Source within medium, where l_{tr} is the depth of the source and $\rho = 0$.

Figure 5.6: Modulation frequency is 150 MHz, $\mu_a = 0.005\,\text{mm}^{-1}$, $\mu_s' = 1.0\,\text{mm}^{-1}$, $R_{eff} = 0.493$, and the infinite medium phase was calculated as in Equation 5.4 and the extrapolated boundary as in Equaion 5.8.

5.4.2 Monte Carlo Model

Figure 5.7 shows two representative results of the Monte Carlo simulation, corresponding phase modulation and diffusion theory approximation at source detector separation distances of 9 & 22 mm. As expected, the pulse width broadened and amplitude decreased as photons traveled further (top row). The modulation and phase of both the simulated data and diffusion theory matched closely (middle and bottom rows). The modulation and phase at 76 & 153 MHz were plotted as a function of distance for each of the three source depths in Figures 5.8 & 5.9. Close agreement between the two analyses was found. However at a source depth of 45 mm the noise in the Monte Carlo results was significant. Running Monte Carlo simulations with more photons would likely result in reduced noise.

5.5 Conclusions

Both the phase and modulation of an intensity modulated light source can be modeled with the diffusion approximation. In an infinite medium, phase has a linear dependence on distance from the source with the slope of the line dependent on the frequency of modulation and the optical properties of the medium. However, the optical properties of the medium do not need to be explicitly determined in order to calculate the distance from the source as shown in Equation 5.6.

In most work in biomedical optics the effect of a boundary on the behavior of light must be carefully considered. Farrell described the extrapolated boundary method for handling a refractive index mis-match. Haskell expanded on Ferrell's method to solve for the phase of a modulated light source at a boundary. Both of these methods model a light source incident on the surface of a scattering medium and detect light that has escaped the medium some distance from the source. The models both place an imaginary point source within the medium and a negative point source outside the medium. Haskell's method was used to model the phase of a modulated light source propagating through an infinite medium and a bounded medium. The effect of the boundary was negligible when the light source was more than 5 mm from a boundary. This meant an infinite medium analysis of the phase lag twas sufficient to determine the distance between source and detector during light-guided lumpectomy.

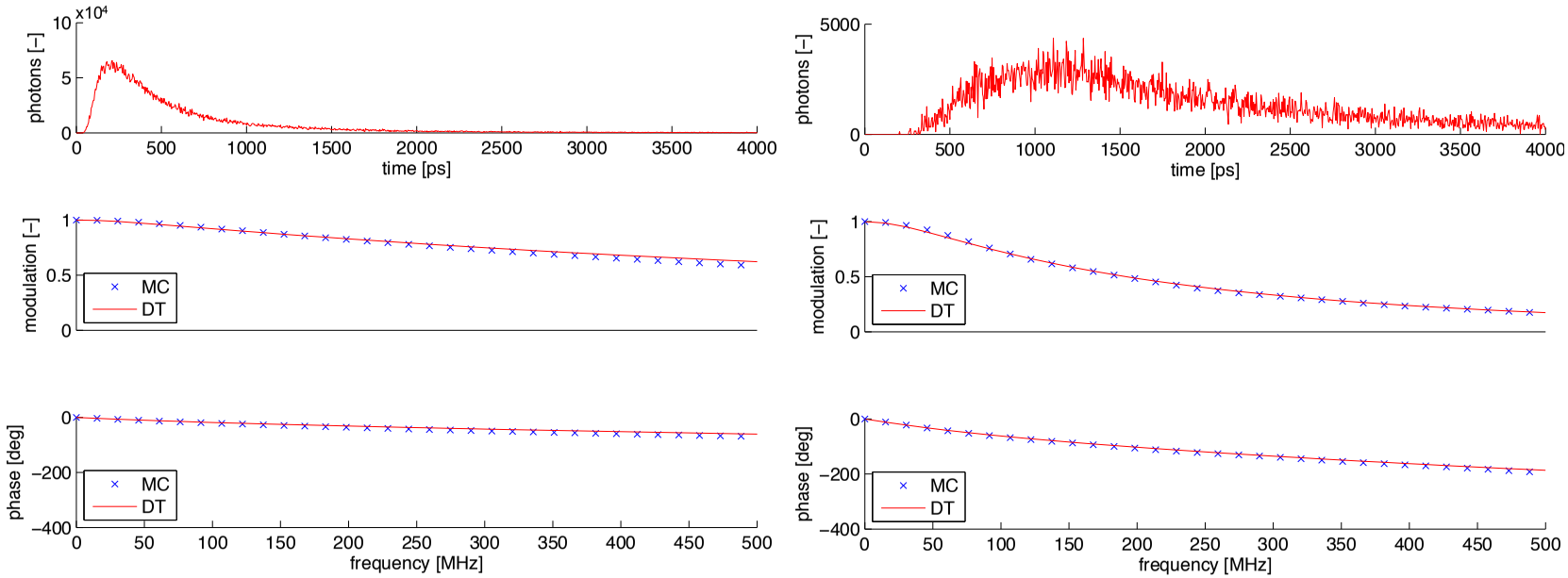

Figure 5.7: The results of the time based Monte Carlo simulation and subsequent Fourier Transform. Left: $r = 9\,\text{mm}$, Right: $r = 22\,\text{mm}$. Top row: The photons binned as a function of time. MIddle row: The modulation of the signal as a function of frequency. Bottom row: The phase of the signal as a function of frequency. MC: Monte Carlo data, DT: diffusion theory approximation.

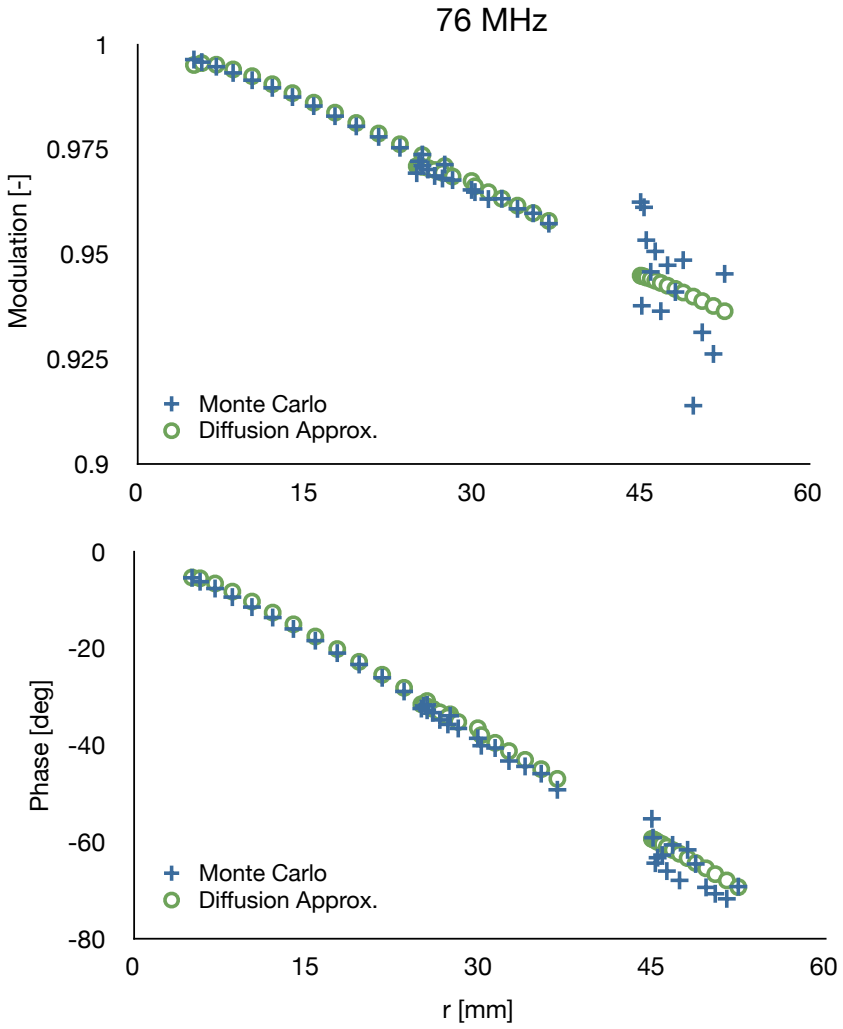

Figure 5.8: Modulation and phase of Monte Carlo (MC) and diffusion theory (DT) with a modulation frequency of 76 MHz for all source detector separation distances, r with photons launched at 5, 25, & 45 mm.

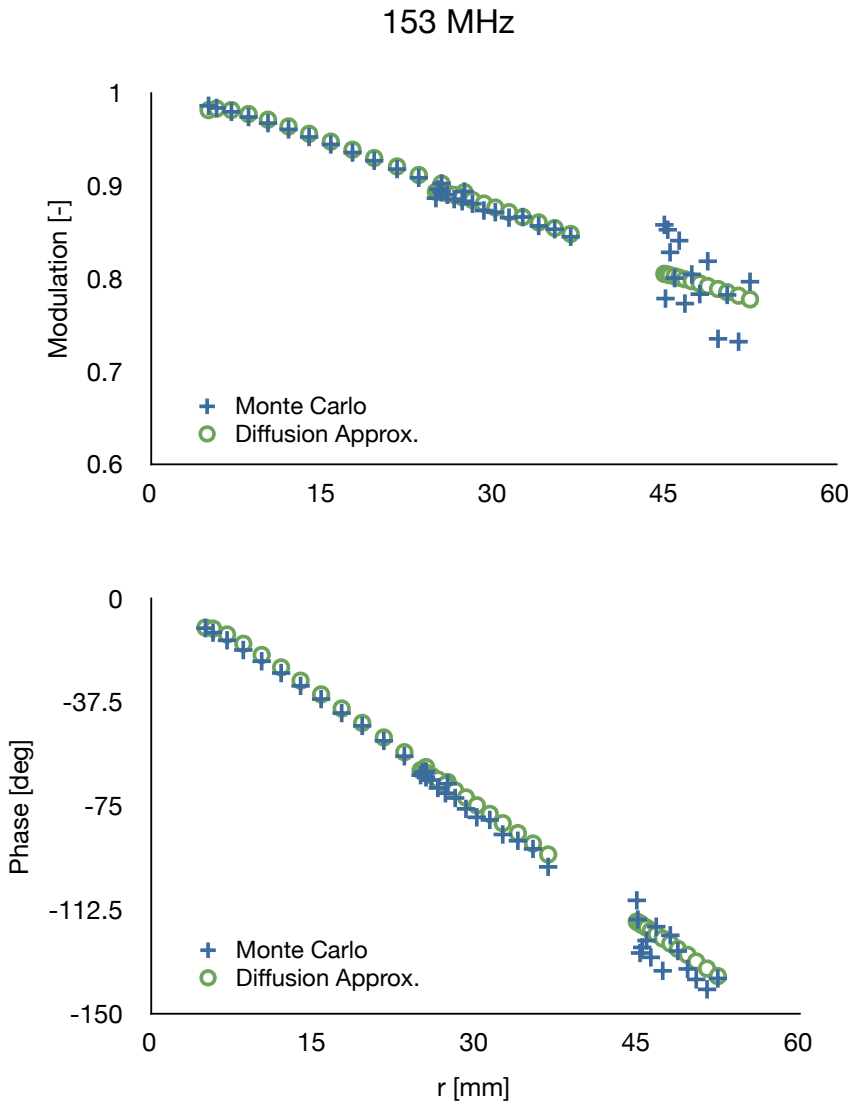

Figure 5.9: Modulation and phase of Monte Carlo (MC) and diffusion theory (DT) with a modulation frequency of 153 MHz for all source detector separation distances, r with photons launched at 5, 25, & 45 mm.

6

A self-calibrating distance measurement device

6.1 Introduction

In this chapter a device to measure the distance from a light source within a scattering medium to a probe on the surface of the medium is presented. The idea is illustrated in Figure 6.1, where a hand held probe could be used during light-guided lumpectomy to measure the distance from the tip of the optical wire to the dissection plane. The primary constraints were: 1) only a single pre-surgery calibration would be required 2) the probe should be insensitive to changes in the properties of the tissue and 3) minimal changes to the optical wire presented in Chapters 2, 3, & 4 would be needed.

Since the optical properties of the medium do not need to be explicitly determined, the solutions of the radiative transport equation for phase and modulation can both be approximated by a linear equation and solved for distance, r as in Equation 5.6

$$r = \gamma_a \cdot \theta + C_a$$

or Equation 5.7

$$r = \gamma_b \cdot \ln(M) + C_b$$

where

$$\gamma_a = \sqrt{\frac{b}{\alpha}} \left(1 + \frac{\omega^2}{b^2}\right)^{1/4} \sin\left(\frac{1}{2} \tan^{-1} \frac{\omega}{b}\right)$$

$$\gamma_b = M_s \exp\left(-r\sqrt{\frac{b}{\alpha}}\left[\left(1+\frac{\omega^2}{b^2}\right)^{1/4}\cos\left(\frac{1}{2}\tan^{-1}\frac{\omega}{b}\right)-1\right]\right)$$

and c is the speed of light in medium, $D = \frac{1}{3(\mu_s'+\mu_a)}$, μ_a is the absorption coefficient and μ_s' is the reduced scattering coefficient and equals $\mu_s(1-g)$ where g is the anisotropy and μ_s is the scattering coefficient, $b = \mu_a c$, $\alpha = Dc$, $\omega = 2\pi f$, $M_s = \frac{AC_s}{DC_s}$, AC_s is the amplitude of the source wave and DC_s is the mean power of the source. It is important to note that C_a & C_b are offsets introduced by the instrumentation of the measurement system and are not dependent on the medium. The ability to isolate the distance between source and detector, r, provided an opportunity to design a simple probe to be used with light-guided lumpectomy. Phase lag will be discussed further in this chapter.

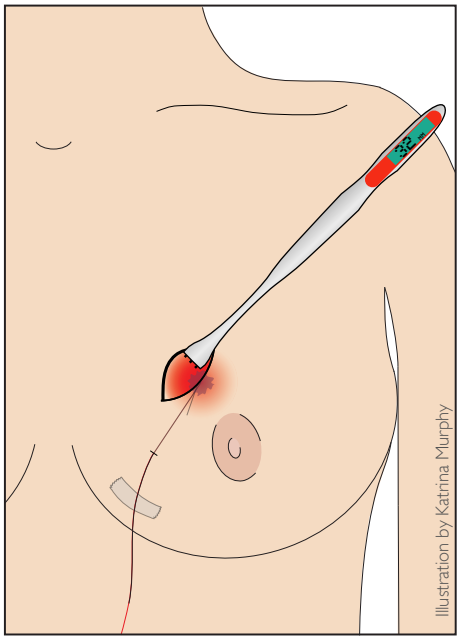

Figure 6.1: The concept of a handheld probe with phase comparators to measure the distance light has traveled through tissue.

6.2 Design

Figure 6.2 is a cross section of the light path from the source, S, to the detectors, D_1, D_0 and D_2. The distance to be measured, r_0, is from the source to the middle of the probe. The detectors D_1 & D_2 are separated from D_0 by a distance l. Ideally, the angle, ψ, between r_0 and the face of the probe is ninety degrees as shown on the left. However, in reality the angle, ψ will deviate from ninety degrees as shown on the right. The error from the geometry on the right will be examined later in this chapter. A phase lag between the source and each detector is measured.

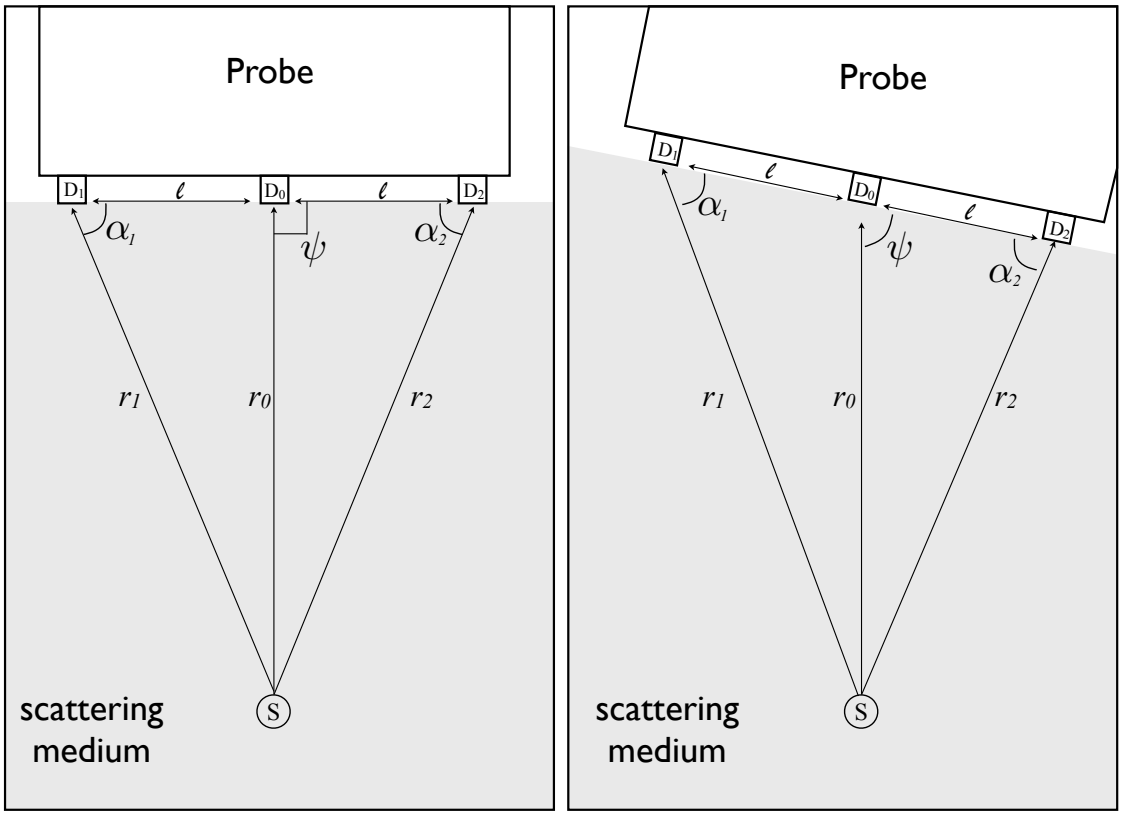

Figure 6.2: In these diagrams the light source (S) is within a scattering medium (shaded) below the probe detectors (D_1, D_0 and D_2). The distance between detectors (l) and the distance from source to detectors (r_1, r_0 and r_3) are drawn as lines. The angle ψ is between the face of the probe and the normal of the light source. The angles α_1, and α_2 are between the face of the probe and the hypotenuse of the triangle formed between the detectors and the source. *left* Probe face is perpendicular to the line between the source and the center detector. *right* Probe face is not perpendicular to the line between the source and the center detector.

Figure 6.3 is the cross section of the face of the probe with a third outer detector, D_3, orthogonal

to the line between the other three detectors. The detectors shown are the minimum needed to determine the distance; in reality many more detectors could be used to reduce error in the measurement.

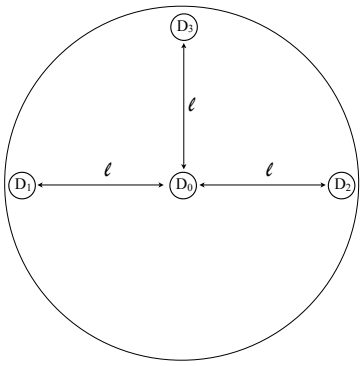

Figure 6.3: The face of the probe has a center detector, D_0, and three surrounding detectors, D_1, D_2 and D_3, each a distance, l, from the center detector and located at 0, 90, and 180 degrees from each other.

From Equation 5.6 $r = \gamma_a \cdot \theta + C_a$, the distance is linearly dependent on the measured phase and C_a is dependent on the measurement system and not the properties of the tissue being measured. Since C_a depends on the phase lag introduced by the instrumentation of the modulated light source and is constant, it can be determined and subtracted from the measured phase at each detector. This leaves the distance dependent only on the phase lag introduced by the scattering of light through the breast.

When the position of the probe is adjusted so that r_1, r_2 and r_3 (not shown) are equal the phase lag measured at the detectors are also equal $\theta_1 = \theta_2 = \theta_3$. In this orientation, the probe is pointing directly at the source, and a measurement of the distance, r_0, from the source to the middle detector can be made independent of the optical properties of the tissue. If the mean of the phase at the outer detectors is calculated $\bar{\theta} = (\theta_1 + \theta_2 + \theta_3)/3$, it follows that the distance, r_0 can be calculated directly from $\bar{\theta}$, θ_0, and the distance between detectors, l, where:

$$\alpha_1 = \arcsin \frac{\theta_0}{\bar{\theta}} \tag{6.1}$$

and

$$r_0 = l \cdot \tan \alpha \tag{6.2}$$

$$r_0 = l \cdot \frac{\theta_0}{\sqrt{\bar{\theta}^2 - \theta_0^2}} \tag{6.3}$$

6.3 Error Analysis

The above holds true when the face of the probe is positioned pointing directly at the light source, i.e. $\psi = 90\,\text{deg}$, and centered so that the phase at the outer detectors are equal. In reality, such probe could be quite frustrating to use due to the precision of placement required. The sensitivity of the design to the distance between detectors, l, and to the angle, ψ, were tested. In addition, the distribution of photons seen at each detector will be slightly different due the heterogeneity of tissue. Monte Carlo modeling was used to assess how different the photon distributions at each detector were.

6.3.1 Materials & Methods

Sensitivity to ψ

Consider the problem of misalignment caused by detectors 1 and 2 not at exactly equal distances from the source. The angle ψ may be written $\psi = \pi/2 + \varepsilon$. When $r_1 = r_2$ the angle $\varepsilon = 0$, however for other values of ε the distances $r_1 \neq r_2$. Since the average value of the distance

$$\bar{r} = \frac{r_1 + r_2}{2} \tag{6.4}$$

is used to find the distance r_0

$$r_0 = l \cdot \frac{r_0}{\sqrt{\bar{r}^2 - r_0^2}} \tag{6.5}$$

(because θ_i is proportional to r_i). The relative error in r_0 is

$$\frac{\Delta r_0}{r_0} = \frac{r_0 - \bar{r}}{r_0} = \frac{r_0 - (r_1/2 + r_2/2)}{r_0} \tag{6.6}$$

using

$$r_1 = \sqrt{l^2 + r_0^2 - 2lr_0\cos(\pi/2 + \varepsilon)} \tag{6.7}$$

$$r_2 = \sqrt{l^2 + r_0^2 - 2lr_0\cos(\pi/2 - \varepsilon)} \tag{6.8}$$

Substituting these values into Equation 6.6 and keeping only terms of $O(\varepsilon^3)$ yields

$$\frac{\Delta r_0}{r_0} \approx -\frac{1}{2}\frac{\rho_0^2}{1+\rho_0^2}\varepsilon^2 \tag{6.9}$$

where $\rho_0 = r_0/l$. Because the error is negative, any misaiming of the device will result in a distance measurement that is larger than actual distance. As long as the depth is at least twice the separation $\rho_0 > 2$, the fraction $\rho_0^2/(1+\rho_0^2) > 0.8 \approx 1$ can be ignored and the relative error is just

$$\frac{\Delta r_0}{r_0} \approx -\frac{1}{2}\varepsilon^2 \tag{6.10}$$

which means that as long as the deviation angle $\varepsilon < 8°$ there will be a less than 1% relative error in the calculated value of r_0.

A Matlab (Student Version 7.10.0, R2010a) program was written to find the error in the calculated source depth r_{0c} independent of any error in the phase measurement, Appendix B.3. The variables of actual source depth, r_0, l, and ψ were varied. Simulated data was first created where ψ was incremented by, ε from $\frac{\pi}{2}$ to π radians for each depth, r_0 and probe separation distance, l.

Both Equations 6.8 & 6.8 were used to calculate the depth of the source. The average distance, $\bar{r} = (r_1 + r_2)/2$, was used to find the calculated depth of the source.

$$r_{0c} = l \cdot \frac{r_0}{\sqrt{\bar{r}^2 - r_0^2}} \tag{6.11}$$

Finally, the relative error of the calculation was found using:

$$\frac{\Delta r_0}{r_0} = \frac{r_0 - r_{0c}}{r_0} \tag{6.12}$$

Photon distribution

Since tissue is inherently heterogenous, measurement of the source depth could be affected by the differences in the distribution of photons collected by each detector. A Monte Carlo code (89) was modified to track the location of each photon collected by the surface detectors and is shown in Appendix B.4. Photons were launched from within the medium at source depths of z = 5–45 mm in 10 mm increments while x and y coordinates were held at zero.

Detectors were placed at the surface of a semi-infinite scattering medium at (0,0,0), (0,5 mm,0) & (0,10 mm,0). The program saved the location of each scattering event for each photon that was collected. Matlab was then used to create a 2 dimensional histogram of the photons collected, Appendix B.5. Bin size was $1\,\mathrm{mm}^3$. For example, Figure 6.4 shows the distribution of photons launched at $z = 15\,\mathrm{mm}$ and collected at the three detectors. The photons were collected in the positive y direction and mirrored around the y axis. The absorption coefficient was $0.004\,\mathrm{mm}^{-1}$, scattering coefficient was $1.3\,\mathrm{mm}^{-1}$, anisotropy was 0.9, refractive index was 1.5, and 500,000 photons were launched. There were 249, 211, & 172 photons collected at y = 0, 5, & 10 mm respectively.

To determine the difference between the photon distributions, the photon counts were normalized to sum to 1 and the distribution with the detector at (0,0,0) was subtracted from the distributions at (0,5 mm,0) and (0,10 mm,0). The subsequent 2D histograms were plotted in both the x and y planes and indicate the differences in the sampled volume for each detector.

Figure 6.5 shows the difference between the detectors in both the x and y planes. The plots in the y plane indicate the volumes sampled more by the outer detectors in blue and by the central detector in red. In this simulation the difference in the sampled volumes depends directly on the positions of the detectors. The plots in the x plane show no dependence on detector location and serve as a baseline for the error in the simulation.

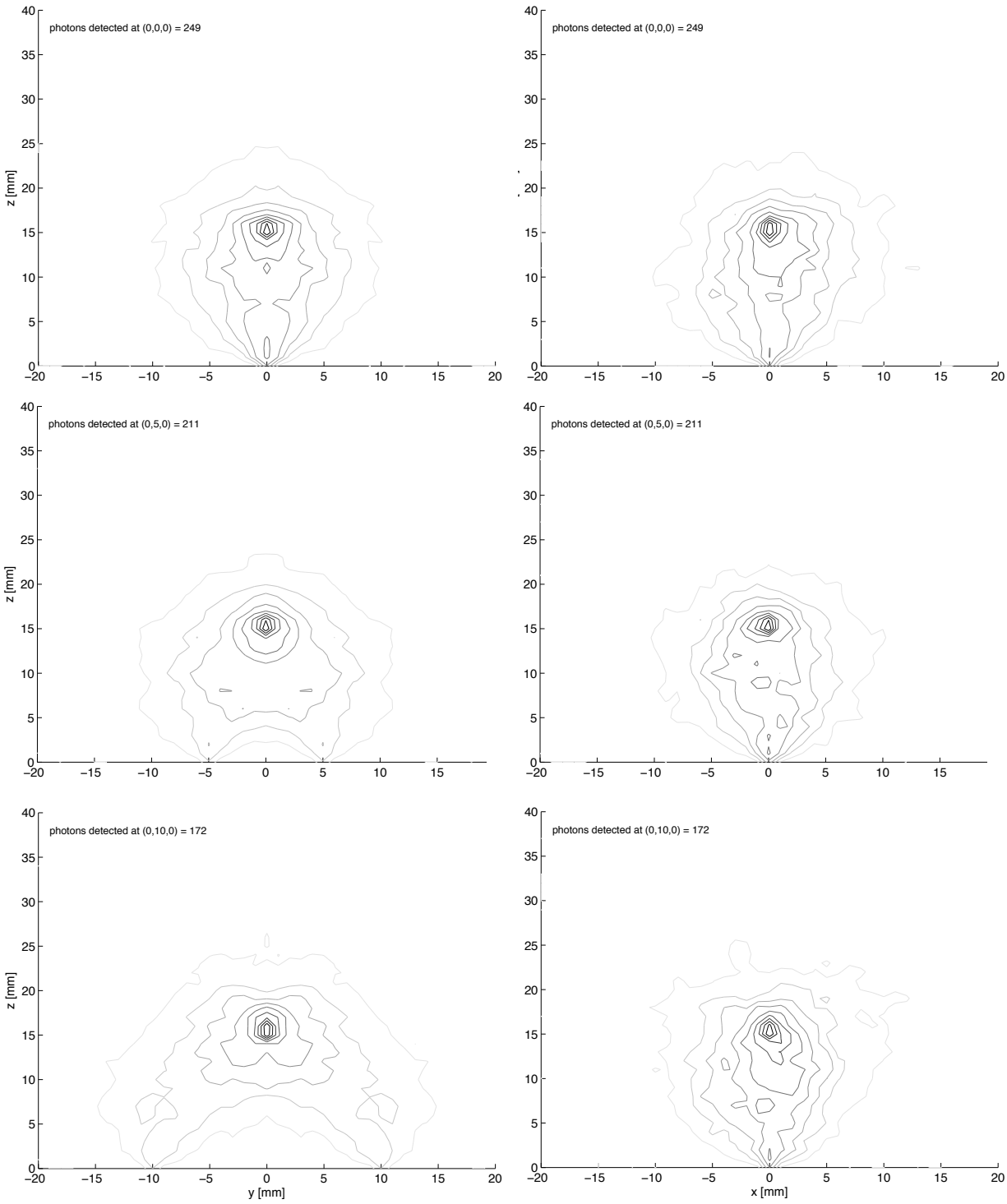

Figure 6.4: The photon distributions for detectors located at (0,0,0), (0,5 mm,0) & (0,10mm,0) when launched from (0,0,15 mm). The left column shows the distributions along the y axis and the right column along the x axis. Photons were launched within a scattering dominant medium and the location of each scattering event of each photon was binned in 1 mm square bins.

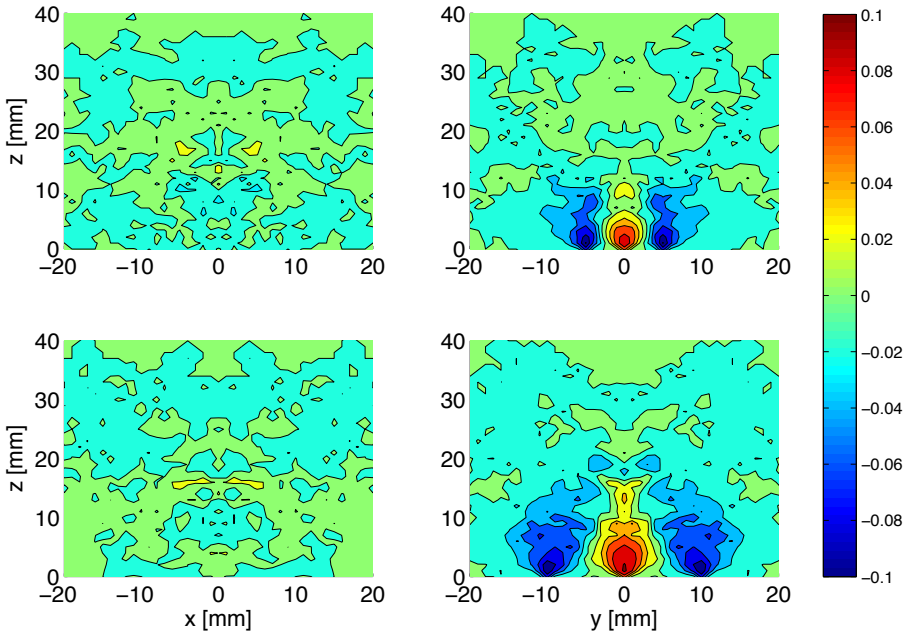

Figure 6.5: The difference between the detectors (0,0,0) and (0,5 mm,0) in the top row, and (0,0,0) and (0,10 mm,0) in the bottom row in both the x (left column) and y (right column) planes. The color bar is in units of percent per mm^3. Negative, blue colors, indicate photons that were collected by the outer detectors and not the central detector while positive, red colors, were collected by the central detector and not the outer.

6.3.2 Results

Angle of probe

Figure 6.6 shows the absolute value of the relative error in the calculation of r_{0c} using equation 6.11 as a function of the detector angle, ψ, and the actual depth of the source, r_0. Each line between $r_0 = 5\,\text{mm}$ and $r_0 = 50\,\text{mm}$ represents a 5 mm increment in the actual depth of the source. The four plots show the change in error as the distance between detectors, l, is increased from 5 to 10 to 25 to 45 mm. The error is not significantly reduced until l approaches 45 mm which is too large for practical use during a surgery. For $\psi = 105\,^\circ$, or a $15\,^\circ$ deviation from normal, relative error is less than 4 % for all values of l and less than 1 % for an $8\,^\circ$ deviation.

Photon Distribution

After normalizing by the number of scattering events, the difference between the central detector and the detector at y=l and are given in Table 6.1. Also shown are the number of photons binned per detector for each simulation and the percent difference at each detector. For example, at a source depth of 25 mm, 340 photons were collected at (0,0,0), 308 at (0,5 mm,0) and 265 at (0,10 mm,0). In the XZ plane with l=5 mm there was a 5.0 % difference between (0,0,0) and (0,5 mm,0) with 52 % of that difference as negative values (space that was sampled by photons collected at (0,5 mm,0) and not at (0,0,0)) and 48 % as positive values (space that was sampled by photons collected at the center and not the outer detectors). In contrast, the YZ plane at the same depth and l resulted in a 9.2 % difference between photon distributions with approximately two thirds of that negative and one third positive.

6.4 Conclusions

Ideally, a probe such as the one shown in Figure 6.1 could be used in conjunction with light-guided lumpectomy to give the operating surgeon a quick measurement of the distance from the dissection plane to the source of the light within the breast. The probe could either be disposable or be placed in a clear sterile cover and re-used. In addition, the probe should be hand-held, about the size of a marker, indicate direction to the source and provide accurate distance readings.

The primary goal of this measurement probe was to determine the distance from light source to probe without *a priori* knowledge of the tissue optical properties. A major problem of measuring the distance from a light source within heterogeneous breast tissue to a detector on the surface

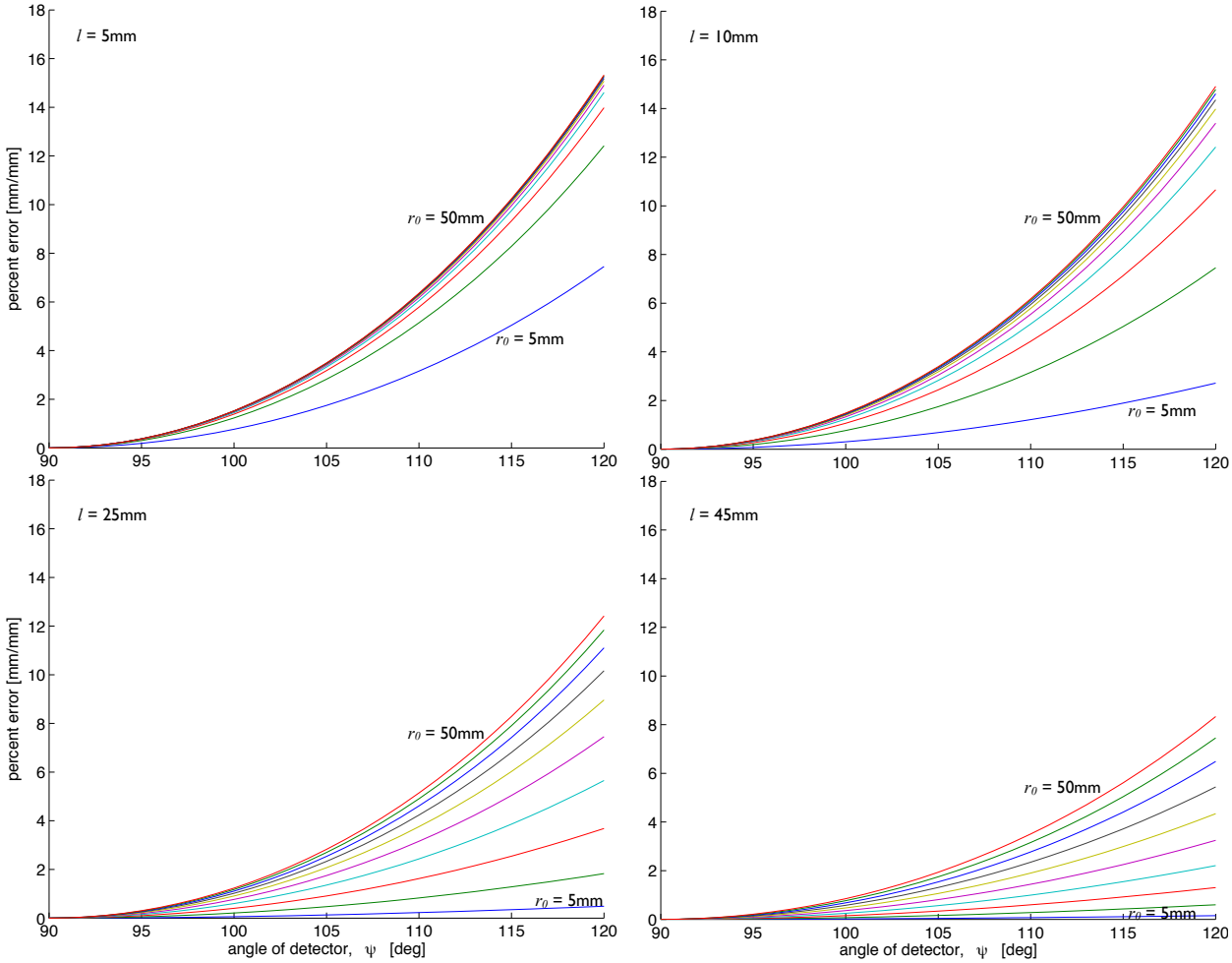

Figure 6.6: The absolute value of the relative error in the calculation of r_{0c} using equation 6.11 as a function of the detector angle, ψ, and the actual depth of the source, r_0. Each line between $r_0 = 5\,\text{mm}$ and $r_0 = 50\,\text{mm}$ represents a 5 mm increment in the actual depth of the source. The four plots show the change in error as the distance between detectors, l, is increased from 5 to 10 to 25 to 45 mm.

depth (mm)	plane	photons (0,0,0)	photons (0,5 mm,0)	photons (0,10 mm,0)	l (mm)	total percent difference	percent missed at (0,0,0)	percent missed at (0,l,0)
5	x	1945	895	270	5	7.2	57	43
5	x	1945	895	270	10	13.2	56	44
5	y	1945	895	270	5	21.6	75	25
5	y	1945	895	270	10	34.5	70	30
15	x	249	211	172	5	5.9	46	54
15	x	249	211	172	10	6.1	46	54
15	y	249	211	172	5	12.9	70	30
15	y	249	211	172	10	21.3	75	25
25	x	340	308	265	5	5.0	52	48
25	x	340	308	265	10	5.0	50	50
25	y	340	308	265	5	9.2	72	28
25	y	340	308	265	10	18.3	78	22
35	x	186	174	162	5	7.0	49	51
35	x	186	174	162	10	6.9	51	29
35	y	186	174	162	5	10.5	73	27
35	y	186	174	162	10	15.6	76	24
45	x	74	78	50	5	11.0	46	54
45	x	74	78	50	10	13.0	50	50
45	y	74	78	50	5	12.8	59	41
45	y	74	78	50	10	18.5	69	31

Table 6.1: For each Monte Carlo simulation at a different source depth the number of photons collected at each detector as well as the distance between detectors, l are shown. The total percent difference is the sum over the total area. The percent missed at (0,0,0) is the sum of the negative values divided by the total and the percent missed at (0,l,0) is the sum of the positive values divided by the total.

of the tissue is the optical properties of the tissue will change as the probe is moved to different locations on the breast. Since the proposed probe does not rely on a determination of the bulk optical properties of the sampled volume, it is well suited to accommodate the changing optical properties of the breast tissue.

Phase was modeled in a homogeneous medium and the expected error was less than 4 % with a detector separation of 5 mm or greater and with the face of the probe less than 15 degrees from normal to the light source. In addition, the difference between detected photon distributions will be less than 8 % with $l = 5$ mm and for source depths beyond 15 mm. This does not mean there will be a 8 % error in the phase measurement, but that the volume sampled by the detectors is only 8 % different with the majority of the difference near the detectors. In the case of light-guided lumpectomy, this is ideal because the probe should be able to measure the distance to the source

but be insensitive to the position of the light source within the lesion. For example, if the source were placed near the anterior edge of a lesion and the probe was pointing towards the source from the lateral side of the lesion the volume surrounding the lesion will still be sampled equally by the detectors. As long the the lesion is at least 10–15 mm deep, the difference in the photon distributions is unlikely to affect phase measurement.

This probe was designed to be used primarily during a lumpectomy and may not be ideal for measurements through the skin. Both scattering and absorption in the skin will significantly decrease the amount of light reaching the probe. There will be an especially dramatic decrease in signal with high melanin content. A dark spot on the skin such as a freckle, mole, or part of the areola will also create error in the distance measurement with this probe. A goal of future work is to determine the number of detectors needed to minimize error while maintaining the small size of the probe.

In addition to error from skin pigment, perturbations in the breast tissue such as calcifications, fibrous tissue, cysts, or bleeding could cause error in the distance measurement. If the perturbation is within 10 mm of the probe and affecting some but not all of the detectors, error will be introduced. One way to minimize the error caused by perturbations would be to use a probe with more than 4 detectors. Perhaps 10–20 detectors or even a fiber bundle could be implemented. Since the average phase lag of the outer detectors is being compared to the central detector, the error will be reduced with the addition of more detectors. More work is needed to determine how perturbations in the tissue will influence the phase lag measured at the detectors.

Prior to evaluation in a clinical setting, this probe needs to be further developed. Experiments in phantoms and computer modeling should be conducted to determine how many detectors are ideal. Device development with the goal of a prototype for use in the operating room also needs to occur. The probe should be hand held with visual and perhaps audio feedback of the distance measured. During a lumpectomy, the probe will likely be used after a skin incision is made as the surgeon is approaching the lesion. It is intended to be an adjunct to the glow-ball during light-guided lumpectomy and will probably be used a few times during the surgery to give the distance from the lesion. After a clinical prototype is ready, a trial in prophylactic mastectomy specimens should be conducted to verify the accuracy of the device when measuring distance in breast tissue. If the mastectomy trial is successful, a larger clinical trial should be conducted to determine if the positive margin rate of lumpectomies could be reduced with light-guided lumpectomy.

7

Measuring Distance Through Optical Phantoms

7.1 Introduction

To test the linear dependence of phase on distance and to evaluate the feasibility of the device proposed in Chapter 6 optical phantoms were made to simulate breast tissue and a modulated optical system was assembled. The fiber coupled optical system was assembled to modulate the intensity of a red laser diode with a network analyzer. The diode could be modulated from 0–350 MHz, and was primarily operated at 70 MHz. The network analyzer was used to create a modulated signal as well as detect an incoming signal. The detected signal was compared to the source and a phase lag between the two was measured. A series of optical phantoms was used to test the system stability, select an ideal modulation frequency, verify the system measurements correspond to the diffusion approximation, verify a linear relationship between phase and distance, and determine the phase lag of the system independent of the scattering medium.

7.2 Materials & Methods

7.2.1 Optical Phantoms

Polyurethane phantoms to simulate tissue were created. India ink (PRO ART, Beaverton, OR) and titanium dioxide, TiO_2 (Sigma, St. Louis MO) were added to polyurethane components (BJB Enterprises, Inc.), which were then mixed and allowed to cure (90). Polyurethane was made from two components; component A was unreacted polyurethane and component B was catalyst. India

ink was mixed with component A and TiO_2 was mixed with component B. Each component was then placed in a vacuum chamber for degassing, the solutions were held at a reduced pressure until all visible air bubbles were drawn out of solution. The two components, A:B, were then mixed in a 100:85 weight ratio respectively. After mixing, the uncured polyurethane was degassed again and cast into a mold.

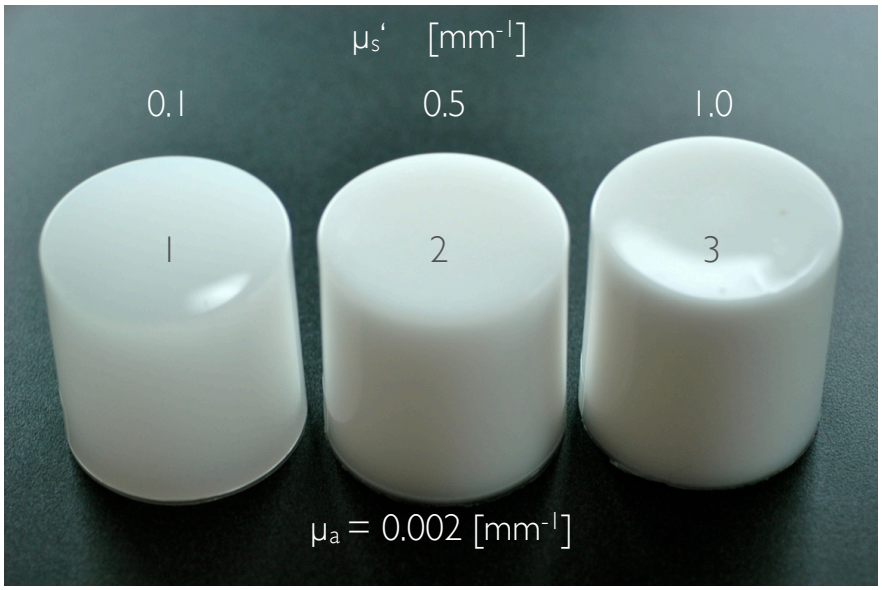

Figure 7.1: Three of the polyurethane optical phantoms.

Cylindrical phantoms were cast approximately 60 mm in diameter and 60 mm in height, a larger phantom was also cast approximately 100 mm in diameter and 100 mm in height. Thin phantoms approximately 60 mm in diameter and 3 mm thick were cast from each mixture, one with only scatterer, one with only absorber and one with both scatterer and absorber. Holes were drilled axially in the cylindrical phantoms to allow optical fibers to be used as sources and detectors within the medium.

The index of refraction, $n = 1.468$, was measured with a refractometer on cured polyurethane.

To determine the optical properties, integrating sphere measurements were made on the thin phantoms. A Xenon light source was coupled to a 1 mm diameter fiber and used to make both reflectance and transmittance measurements with an integrating sphere (203.2 mm diameter sphere, 44.5 mm diameter sample port, 6.4 mm entrance port, 0.05 mm diameter illumination beam). The light inside the integrating sphere was measured using a 1 mm diameter fiber to couple light into a spectrometer (ISA Horiba) and then a PMT (Products for Research, Inc.). Dark noise, M_{dark},

and 100%, M_{100}, signals were measured for reflectance and transmission. A certified reflectance standard (Labsphere) was used for the 100 % reflectance measurements. The signal, M through the phantom was normalized as follows corresponding to either reflectance, R, or transmission, T (90).

$$R = \frac{M - M_{dark}}{M_{100} - M_{dark}} \qquad T = \frac{M^{'} - M^{'}_{dark}}{M^{'}_{100} - M^{'}_{dark}} \tag{7.1}$$

Three reflectance and three transmission measurements were taken on each sample. The inverse adding-doubling method (90) was used to calculate the absorption coefficient, μ_a, and the reduced scattering coefficient $\mu_{s'}$ from the normalized R and T measurements.

The dimensions and optical properties of each phantom are shown in Table 7.1. Phantom 1, 2, & 3 are shown in Figure 7.1. Using the integrating sphere method (90), the absorption coefficient was found to be 0.002 mm^{-1} for phantoms 1, 2, & 3 and the reduced scattering coefficient was 0.1, 0.5, & 1.0 mm^{-1} respectively. The absorption coefficient was found to be 0.005 mm^{-1} for phantom 4 and the reduced scattering coefficient was 1.3 mm^{-1}. For all the phantoms the standard deviation of the absorption coefficient and reduced scattering coefficient were 0.001 mm^{-1} and 0.01 mm^{-1} respectively.

ID		diameter [mm]	height [mm]	μ_a [mm^{-1}]	μ'_s [mm^{-1}]
1		60	60	0.002	0.1
	1_a	60	3	0.002	0.1
	1_b	60	3	0	0.1
	1_c	60	3	0.002	0
2		60	60	0.002	0.5
	2_a	60	3	0.002	0.5
	2_b	60	3	0	0.5
	2_c	60	3	0.002	0
3		60	60	0.002	1.0
	3_a	60	3	0.002	1.0
	3_b	60	3	0	1.0
	3_c	60	3	0.002	0
4		100	100	0.005	1.3
	4_a	60	3	0.005	1.3
	4_b	60	3	0	1.3
	4_c	60	3	0.005	0

Table 7.1: Polyurethane phantom dimensions and optical properties measured at 638 nm. The standard deviation of the absorption coefficient was 0.001 mm^{-1} and the reduced scattering coefficient was 0.01 mm^{-1}.

7.2.2 Modulation System

A system was assembled as shown in Figure 7.2. A computer running LabView (National Instruments, v. 2009) was used to control a network analyzer (Hewlett Packard, 8752C) which generated a radio frequency (RF) signal. The RF signal was delivered to a laser diode mount (ThorLabs,TCLDM9) on which an 638 nm laser diode (Sanyo, DL6148-030) was mounted. Unless otherwise noted, the laser diode was biased by a direct current from the driver (ThorLabs, LDC 210) of 68 mA and the temperature of the diode was held at 25°C by a temperature controller (Thor Labs, TED 200C). The sinusoidally modulated light was delivered to a phantom through a 200 μm diameter, 3 m long optical fiber that was bundled in a 10 cm coil to overfill the fiber. Overfilling the fiber ensured that some of the higher order modes escape through the jacket of the fiber and remaining modes are filled. This makes the average distance traveled by light constant and insensitive to fiber movement. Light was detected with a 1000 μm diameter, 2 m long optical fiber, also overfilled. The detected signal was focused with an objective, OBJ, (10x 0.3NA) onto an avalanche photodiode, APD, (ThorLabs, APD 210) where it was converted to voltage and fed back into the network analyzer.

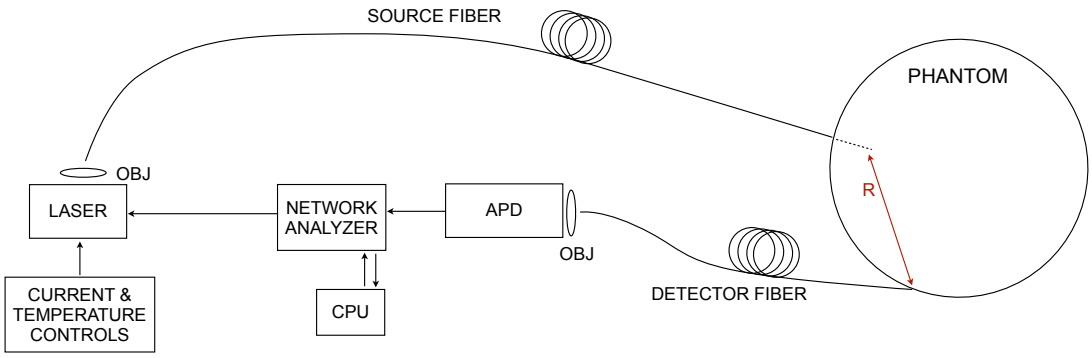

Figure 7.2: The intensity modulation system.

7.2.3 System Stability

The stability of the system was analyzed over time. In one experiment, the repeatability of data collection after system shut down was tested. The network analyzer was set to modulate at 70 MHz. The temperature, laser diode current, APD gain, and network analyzer power were held constant. Data sets were collected four times, between each data set the entire system was shut down and re-started. Phantom 4 ($\mu_a = 0.005\,\mathrm{mm}^{-1}$ & $\mu_s' = 1.3\,\mathrm{mm}^{-1}$) was used as scattering medium; the

source and detector fibers were 33.5 mm apart. Data sets 1–3 were collected on the same day, data set 4 was collected on the following day and the fibers were re-aligned between days.

In another experiment, the effect of running the system for prolonged periods of time was evaluated. The source and detector fibers were aligned 33 mm apart with only air between them. The network analyzer was set to collect data while sweeping the frequency of modulation from 50–350 MHz. The network analyzer was zeroed to this configuration so that any later measurements were expected to be zero. Data were collected at 0, 6, 12, 38 & 41 minutes. Since the set-up was not altered over the course of the experiment any deviation from zero would be a result of system drift or instability. The temperature was held constant at 18 ^{o}C.

7.2.4 Modulation Frequency

The slope of phase lag as a function of distance increases with modulation frequency. The amplitude of the detected signal decreases with modulation frequency and distance. This suggests there is a modulation frequency range where the slope of phase as a function of distance can be maximized while the loss of signal for higher frequencies can be minimized. A maximum measurement of 50 mm during lumpectomy would be sufficient to provide guidance to the surgeon. In addition, if a frequency range less than 100 MHz could be used for this application, the necessary equipment for determining distance could be inexpensive and readily available.

An experiment was conducted to find a frequency range that accurately measured distance in phantom 4 to 50 mm. The source fiber was placed 20 mm from the top of the phantom and the detector fiber was placed on the surface of the phantom at 5–50 mm in 5 mm increments as shown in Figure 7.3. At each detector location, 101 measurements of phase and amplitude were collected and the mean and standard deviation were recorded. One set of 101 phase and amplitude data took less than 10 seconds to complete. One modulation frequency was tested at each detector location, then the network analyzer was set to another modulation frequency and the corresponding phase lag was measured at the detector locations again. Modulation frequencies of 30, 50, 70, 90, 120, & 160 MHz were evaluated.

7.2.5 Diffusion Approximation

An experiment was performed to verify that the phase measurements collected corresponded to the expected values of phase calculated using the diffusion approximation. This was done to ensure the system behaved as expected and to verify that modeling of phase using the diffusion approximation

could be used to predict system response. Phase lag (Equation 5.4) between two points 15 mm apart, μ_a=0.002 mm^{-1}, μ_s'=0.5 mm^{-1}, and frequencies between 0–300 MHz was calculated. These optical properties correspond to phantom 2. The system in Figure 7.2 was used to collect phase in phantom 2 with source and detector fibers 15 mm apart between modulation frequencies of 0 & 300 MHz.

7.2.6 Linear Phase Response

Two measurement configurations were used to measure phase lag as a function of distance in phantom 4. This was done to collect light that had been scattered in different directions from the source fiber. In one configuration, the source fiber was placed 30, 20, and 10 mm deep within the phantom from the top. In the other configuration, the source was placed 20, and 10 mm deep within the phantom from the side. In both configurations, the detector fiber was moved in 5 mm increments within a fiber holder along the top of the phantom. The network analyzer modulated the laser at 70 MHz and the mean and standard deviation of 101 phase lag measurements were recorded at each location.

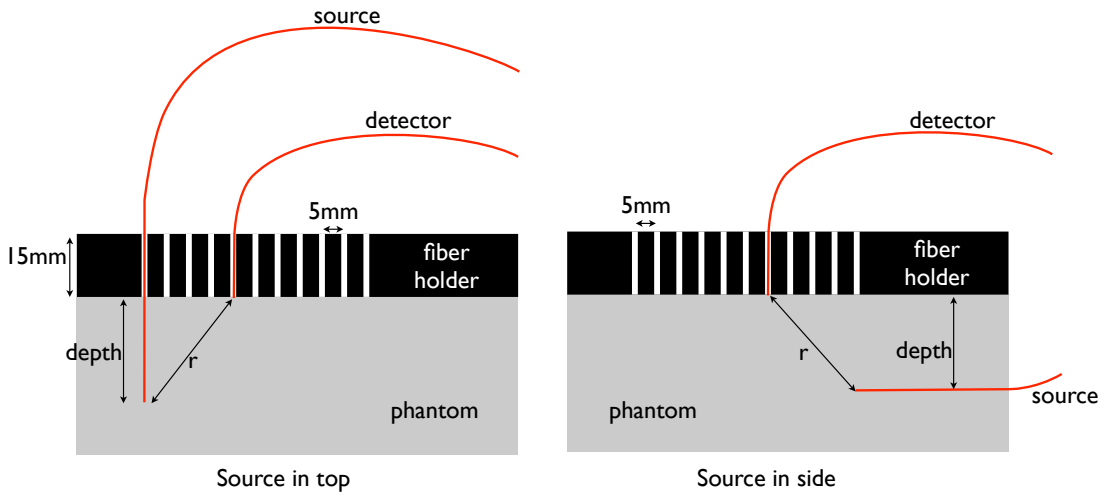

Figure 7.3: Two measurement configurations used to measure the phase lag as a function of source detector separation distance, r.

7.2.7 System Offset

In Equation 5.6 $r = \gamma_a \cdot \theta + C_a$, the distance is dependent on the measured phase and C_a. Since C_a depends on the phase lag introduced by the instrumentation of the modulated light source and is constant, it was determined experimentally. Phase lag was measured at source depths of 28, 28, & 32 mm in phantoms 2, 3, & 4 respectively as shown in the left of Figure 7.3. The network analyzer modulated the laser at 70 MHz and the mean of 101 phase lag measurements were recorded at each location.

7.3 Results

7.3.1 System Stability

The repeatability of data collection after system shut down was demonstrated. Figure 7.4 shows the phase measured at 70 MHz in phantom 4 with 33.5 mm between source and detector. The entire system was shut down between data sets 1–4. The mean and standard deviation of all four data sets was -129.7 ± 0.4 deg.

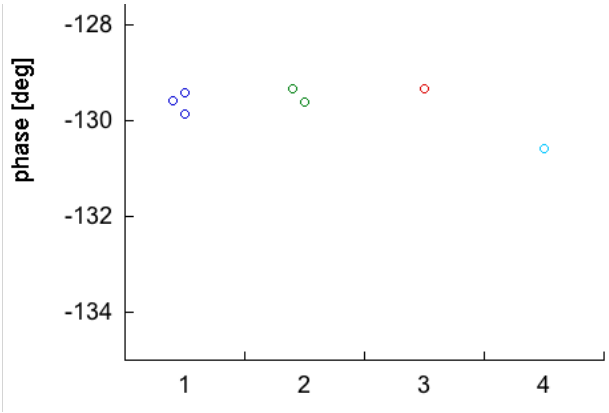

Figure 7.4: Stability of measured phase. The entire system was shut down and then re-started between measurements data sets 1–4.

The effect of running the system for prolonged periods of time was negligible, Figure 7.5. There was no apparent shift in the data collected over a 41 minute time frame. The standard deviation of each data set was less than 0.2 deg. However, there was consistent instability at frequencies of 92, 128, & 200 MHz. These frequencies were avoided in future experiments.

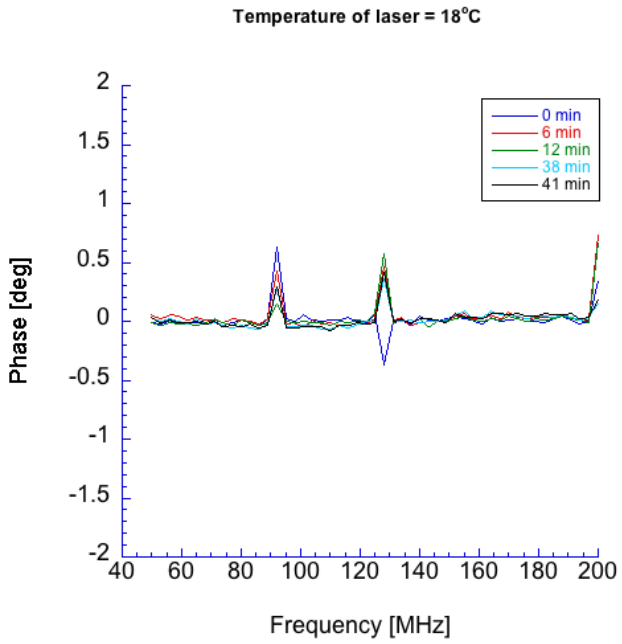

Figure 7.5: The phase was stable over a period of 41 minutes. Data was collected at the time points indicated in the legend while sweeping the modulation frequency of the network analyzer.

7.3.2 Modulation Frequency

To determine the best frequency range to measure distances up to 50 mm , phase lag was measured at modulation frequencies between 30 & 160 MHz. Phantom 4, which has optical properties of breast tissue was used. Each data point in Figure 7.6 shows the mean and standard deviation of 101 phase measurements.. For both 120 & 160 MHz the phase deviated from linearity beyond 40 mm from the source and was not included in the plot. Figure 7.7 shows the standard error of the mean, ε [deg], normalized by the slope, β [deg/mm], of the phase as a function of distance and by the distance, r [mm], ($\varepsilon/(\beta r) * 100$ [%]). From this normalized error, it was found that a modulation frequency of 70 MHz maintained error less than 1% up to 50 mm in this phantom and was chosen as a default modulation frequency for subsequent experiments.

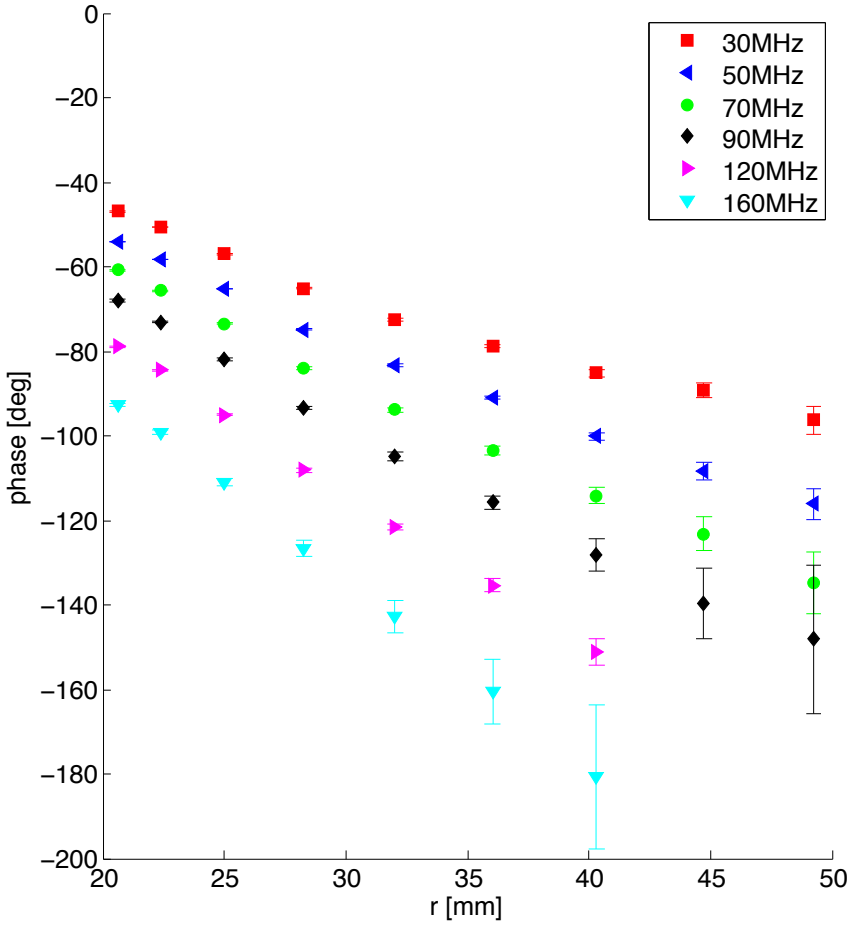

Figure 7.6: Measured phase as a function of distance from the source. Each point represents the mean of 101 phase measurements, error bars are the standard deviation.

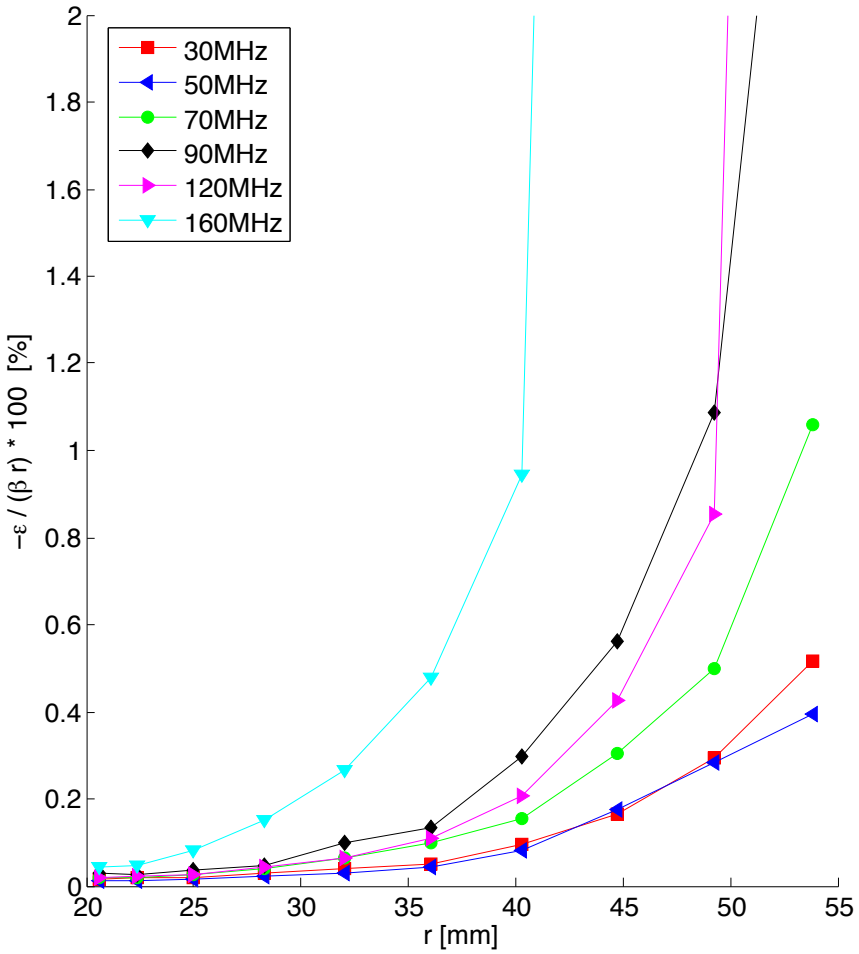

Figure 7.7: Standard Error of the mean, ε, normalized by distance, r, and corresponding slope, β, of phase as a function of distance.

7.3.3 Diffusion Approximation

The measured phase lag with the source and detector separated by 15mm for frequencies between 0–300 MHz in phantom 2 was compared to diffusion theory (Equation 5.4) with the known optical properties of phantom 2. Agreement between the diffusion theory approximation and phase lag was best between 30 and 150 MHz. The phase lag at modulation frequencies above approximately 150 MHz was noisy, most likely due to low signal.

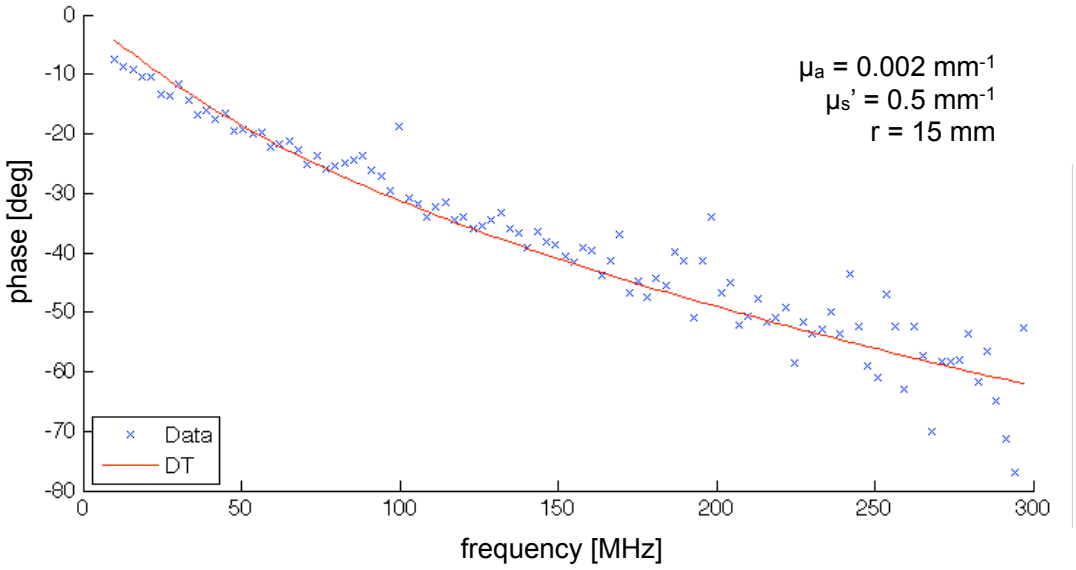

Figure 7.8: Data: Measured phase lag with source and detector separated by 15mm for frequencies between 0–300 MHz in phantom 2. DT: Diffusion theory approximation generated using Equation 5.4 with the known optical properties of phantom 2.

7.3.4 Linear Phase Response

The linear phase response as a function of distance was measured at a modulation frequency of 70 MHz in phantom 4, Figure 7.9. Where error bars are not shown, the standard deviation was smaller than the size of the point, approximately 2.5 deg. The agreement between data sets shown in this plot suggests that a consistent phase response can be measured between 20 & 50 mm regardless of orientation to the launch angle of the source fiber.

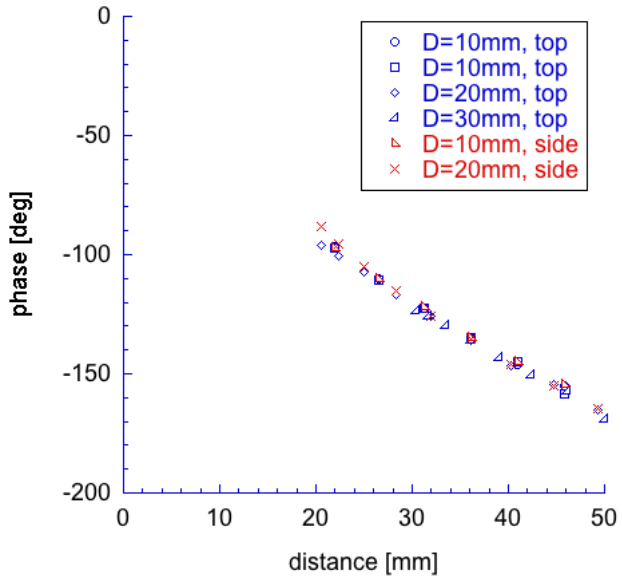

Figure 7.9: Linear phase response as a function of distance from source. The source fiber was located within phantom 4 at depths, D, from the side and top of the phantom while the detector fiber was moved along the top of the phantom in 5 mm increments.

7.3.5 System Offset

A linear phase response as a function of distance from the source in 3 phantoms is shown in Figure 7.10. The lines were drawn to illustrate the system offset, C_a, was independent of the optical properties of the phantoms. The lines converge at a distance of zero and phase of C_a=45 deg.

7.4 Conclusions

Polyurethane optical phantoms with optical properties similar to breast tissue were fabricated and a modulated optical system was assembled. The optical system relied on a network analyzer to modulate the intensity of a red laser and to compare the phase of a source signal to a detected signal. The stability of the system was tested by shutting it down and re-starting it while component settings remained constant. The phase was measured between 4 start-up/shut-down cycles and resulted in a phase of -129.7 $\pm$ 0.4 deg (mean $\pm$ standard deviation) over a distance of 33 mm, the error in deg/mm was 1%. System drift was also tested over 41 minutes and the noise floor was less than 0.2 deg over the entire time.

Once the system was found to be stable, a single modulation frequency was chosen. In general,

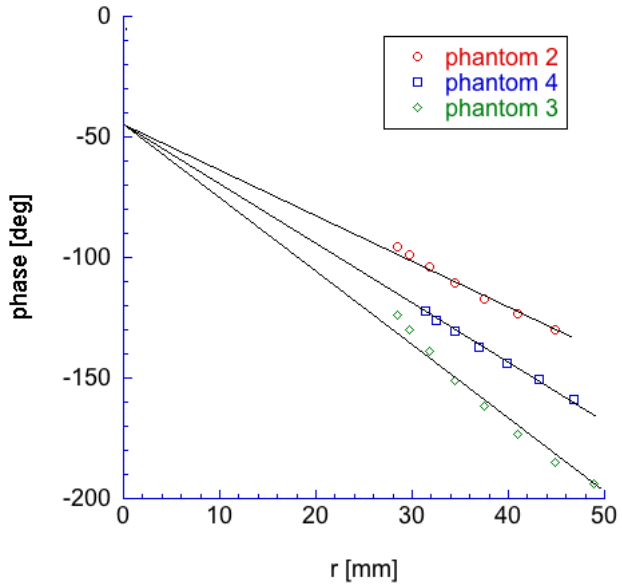

Figure 7.10: Linear phase response as a function of distance from the source in 3 phantoms. The lines were drawn to illustrate the system offset, C_a.

a low modulation frequency would mean a handled probe such as the one proposed in Chapter 6 could be made inexpensively with off-the-shelf components. In addition, lower frequencies attenuate slower and travel farther through scattering medium. However, the drawback to a low frequency is reduced sensitivity to distance. Phase was measured as a function of distance at many modulation frequencies between 50 & 300 MHz. 70 MHz was chosen because it was the lowest frequency where the phase was measured at 50 mm with less than 1 % error.

Critical to the design of the probe in Chapter 6 was the linear relationship between phase and distance and the ability to precisely measure phase when the detector was moved. With the source and detector fibers in two different configurations and 3 source depths, the phase was measured as 10 distances. A consistent phase was measured between 20 & 50 mm regardless of detector orientation to the source. In addition, a constant value for the phase lag of the optical system fas found to be C_a=45 deg. This system phase lag was found by measuring phase in three phantoms of different optical properties and extrapolating the phase lag at a distance of zero.

8

Measuring Distance Through Breast Tissue

8.1 Introduction

The objectives were to evaluate the linearity of phase lag measured as a function of distance from the source in tissue and to determine the error of calculating the distance between the light source and tissue surface using the methods proposed in Chapter 6.

Optical phantoms are useful for characterizing optical devices, but are far more homogeneous than real tissue. Therefore device performance using phantoms is not a realistic representation of how it will perform in tissue. The modulated optical system presented and tested in Chapter 7 was tested in *ex vivo* breast tissue to ensure it measures distance through breast tissue. Three prophylactic mastectomy specimens were tested after resection but before examination by a pathologist. An optical fiber delivered red light within the breast tissue, modulated at 70 MHz. As the 70 MHz wave propagated through the tissue a phase lag developed between the source fiber and the surface of the tissue. During the investigations, the optical fiber was inserted stereotactically through a needle and the phase lag from the fiber tip to the tissue surface was measured with an optical probe. The separation between the fiber tip and the edge of the tissue was calculated using the phase lag and compared to the known stereotactic distance.

8.2 Materials & Methods

8.2.1 Study Design

This was a clinical trial approved by the Providence Health & Services IRB and conducted at Providence St. Vincent Medical Center according to common protocol. No disruption in patient care occurred. No risk to patients was produced by this study. Furthermore, the results of the analysis were not part of the patients medical diagnosis or treatment. The patients were identified in the consent form and in no other part of the study. The data collected was de-identified. Three prophylactic mastectomy specimens were studied after the tissue was removed during surgery and before examination by pathology.

All enrolled subjects met all of the inclusion criteria and none of the exclusion criteria. The only inclusion criteria was that the patient was undergoing prophylactic mastectomy surgery at Providence St. Vincent Medical Center. The only exclusion criteria was that the specimen size was smaller than 6 cm in width (superior-inferior) at its widest point.

8.2.2 Measurement System

The same modulated system used to make measurements in phantoms in Chapter 7 was used here, Figure 8.1. A computer running LabView (National Instruments, v. 2009) was used to control a network analyzer (Hewlett Packard, 8752C) which generated a radio frequency (RF) signal. The RF signal was delivered to a laser diode mount (ThorLabs,TCLDM9) on which an 638 nm laser diode (Sanyo, DL6148-030) was mounted. The laser diode was biased by direct current from the driver (ThorLabs, LDC 210) of 68 mA and the temperature of the diode was held at 25°C by a temperature controller (Thor Labs, TED 200C). The sinusoidally modulated light was delivered within the tissue through a 600 μm diameter that was bundled in a 10 cm coil to overfill the fiber. Over filling the fiber resulted in the majority of the non-primary modes escape through the jacket of the fiber and the primary mode traveling the length of the fiber to escape at the tip. When overfilled, the light escaping the fiber at the tip is insensitive to fiber movement and has a uniform phase lag. Light was detected with a 600 μm diameter, 2 m long optical fiber, also overfilled. The detected signal was focused with an objective, OBJ, (10x, 0.3NA) onto an avalanche photodiode, APD, (ThorLabs, APD 210) where it was converted to voltage and fed back into the network analyzer.

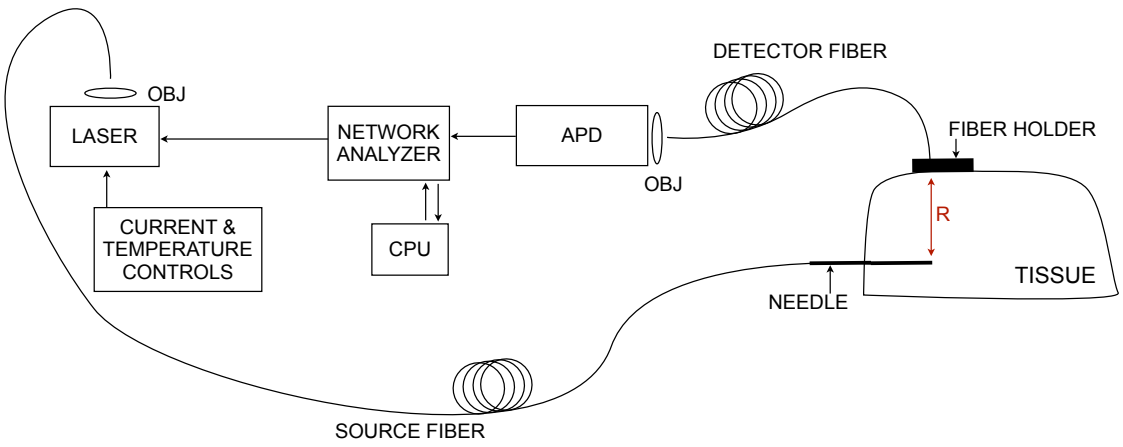

Figure 8.1: The intensity modulation system as used in the perpendicular measurement geometry. Only the location of the needle was changed for the coaxial measurement geometry and is illustrated below.

A 14-gauge needle with 5 mm depth markings was inserted stereotactically into the breast tissue so that it could be moved to a depth of 10–50 mm from the tissue surface in increments of 5 mm. Inside the needle was the 600 μm diameter optical fiber illuminated by the laser. The tip of the optical fiber extended approximately 1–2 mm beyond the tip of the needle and was taped in place to ensure the fiber tip was beyond the tip of the needle. This created a glowball centered just beyond the needle tip within the breast. The detector optical fiber was placed on the surface of the tissue to collect light. The phase lag of the 70 MHz modulated light was measured between the source and detector fibers.

8.2.3 Coaxial Measurement Geometry

A black delrin fiber holder, 15 mm in depth with eleven 800 μm holes drilled 5 mm apart along a straight line was used for all data collected. In addition to measurements in *ex vivo* breast tissue, the phase lag was also measured in phantom 4 from Table 7.1. For each distance between source and detector 101 phase and amplitude measurements were collected by the computer. The mean of the 101 phase measurements was plotted as a function of stereotactic distance from the source.

Coaxial measurements of phase as a function of distance in phantom 4 with a source depth of 20 mm and 10 detector fiber locations were made. The coaxial measurements of phase were linear as a function of distance and the extrapolated phase at distance zero was 45 deg and was subtracted from the raw phase measured in phantoms and tissue.

The coaxial geometry is illustrated in Figure 8.2 which shows the cross-section of the fiber holder on top of tissue. The source fiber and needle were placed in the fiber holder and travel into the tissue at a known depth while the detector fiber is placed in the other holes of the fiber holder to collect data. The source fiber was placed at one of the ends and a measurement was made at each detector location, this resulted in 10 measurements per depth. Seven source depths were measured in sample 1, five depths in sample 2, and two depths in sample 3.

In order to prevent delaying the pathology analysis of the tissue, there was a time constraint of 1 hour to collect data in the tissue samples. Subjects were enrolled who underwent surgery in the morning so I could test the tissue and then deliver it to pathology to be processed the same afternoon. Due to the time constraint, fewer coaxial measurements were made on samples 2 and 3 so that perpendicular measurements could also be collected.

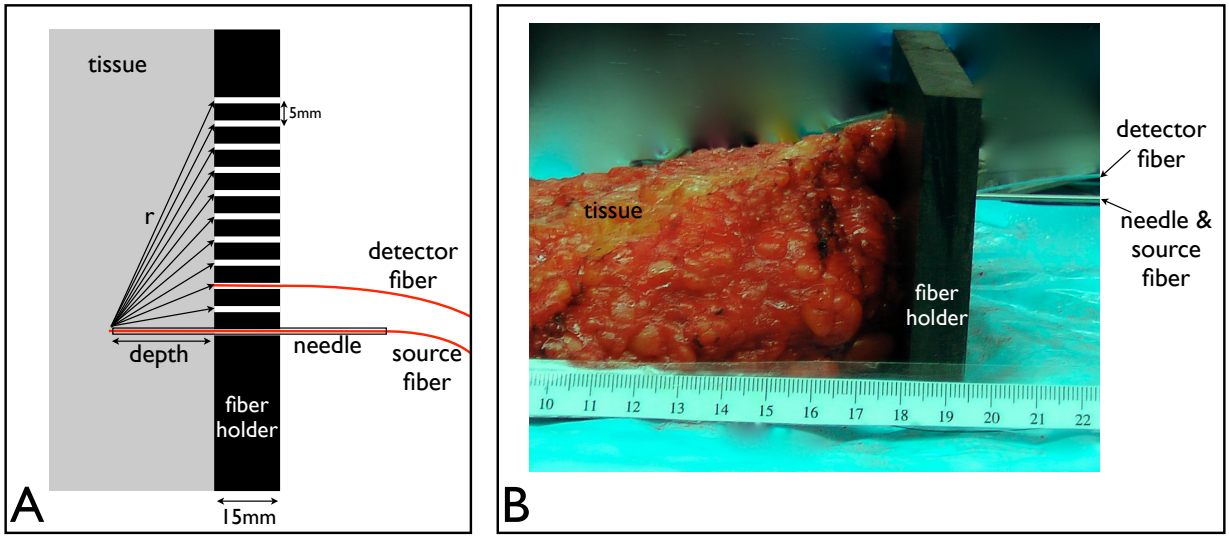

Figure 8.2: Coaxial Measurement geometry: The source fiber was stereotactically inserted in the tissue through a needle in a black delrin fiber holder. The detector fiber was placed on the surface in 5 mm increments as indicated by the arrows, r, extending from the source to the surface.

8.2.4 Perpendicular Measurement Geometry

A black delrin fiber holder, 15 mm in depth with eleven 800 μm holes drilled 5 mm apart along a straight line was used for all data collected. Data was collected at two modulation frequencies of 70 & 110 MHz. For each distance between source and detector 101 phase and amplitude measurements

were collected by the computer. The mean of the 101 phase measurements was used to calculate the distance between the source and the center detector as follows.

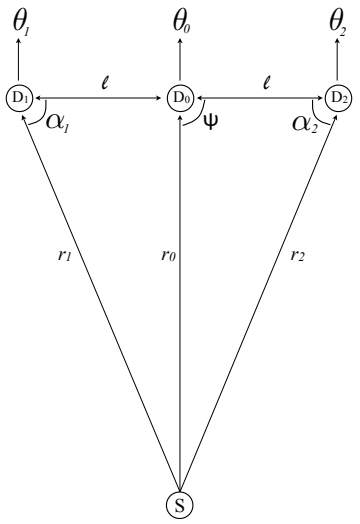

Figure 8.3: In this diagram the light source (S) is below the probe detectors ($D_{1,2,3}$). The distance between detectors (l) and the distance from source to detectors ($r_{1,2,3}$) are drawn as lines. The angle ψ is between the face of the probe and the normal to the light source. The angles $\alpha_{1,2}$ are between the face of the probe and the hypotenuse of the triangle formed between the detectors and the source.

The perpendicular geometry was utilized to test the probe discussed in Chapter 6 and is described again here. Figure 8.3 is a cross section of the light path from the source, S, to the detectors, $D_{1,2,3}$. The distance, r_0, is from the source to the middle of the probe is the depth of the source fiber and is the distance of interest. The detectors D_1 & D_2 are separated from D_0 by a distance l and the angle, ψ, between r_0 and the face of the probe is ninety degrees. Figure 8.4 is the cross section of the full face of the probe with a third outer detector, D_3, orthogonal to the line between the other three detectors. The detectors shown are the minimum needed to determine the distance; in reality many more detectors could be used to reduce the error in the measurement.

From Equation 5.6,

$$r = \gamma_a \cdot \theta + C_a$$

the distance between fibers is linearly dependent on the measured phase and C_a is dependent on the measurement system and not the properties of the tissue being measured. Since C_a depends on the phase lag introduced by the instrumentation of the modulated light source and is constant, it was determined and subtracted from the measured phase at each detector. To determine C_a,

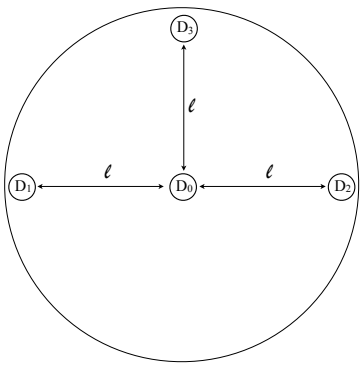

Figure 8.4: The face of the probe has a center detector, D_0, and three surrounding detectors, $D_{1,2,3}$, each a distance, l, from the center detector and located at 0, 90, and 180 degrees from each other.

coaxial measurements of phase as a function of distance in phantom 4 with a source depth of 20 mm and 10 detector fiber locations were made. The coaxial measurements of phase were linear as a function of distance and the extrapolated phase at distance zero was $C_a = 45\,\text{deg}$ and subtracted from the raw phase measured in phantoms and tissue. After subtracting $C_a = 45\,\text{deg}$ from the raw phase, Equation 5.6 can be reduced to

$$r = \gamma_a \cdot \theta$$

which leaves the distance dependent only on the phase lag introduced by the scattering of light through the breast.

When the position of the probe was adjusted to the geometry in Figure 6.2 r_1, r_2 and r_3 (not shown) are equal which means the phase measured at the respective detectors are also equal ($\theta_1 = \theta_2 = \theta_3$). In this position the probe is pointing directly at the source, and a measurement of the distance, r_0, from the source to the middle detector can be made independent of the optical properties of the tissue. If $\bar{\theta}$ is the mean of the phase at the outer detectors it follows that the distance can be calculated directly from $\bar{\theta}$, θ_0, and the distance between detectors, l, where:

$$\alpha_1 = \arcsin \frac{\theta_0}{\bar{\theta}} \tag{8.1}$$

and

$$r_0 = l \cdot \tan \alpha \tag{8.2}$$

$$r_0 = l \cdot \frac{\theta_0}{\sqrt{\bar{\theta}^2 - \theta_0^2}} \tag{8.3}$$

The needle and source fiber were inserted in the tissue parallel to the fiber holder at a known depth from the fiber holder. This configuration made the source fiber and detector fiber perpendicular to each other. The detector fiber was then used to collect data at locations indicated for r_1, r_0, & r_2 in Figure 8.5. Equation 8.3 was used to calculate the distance between the source and the surface at r_0. The phase, $\bar{\theta}$ was the average of the phase measured on each side of θ_0 at each l of 5, 10 & 15 mm.

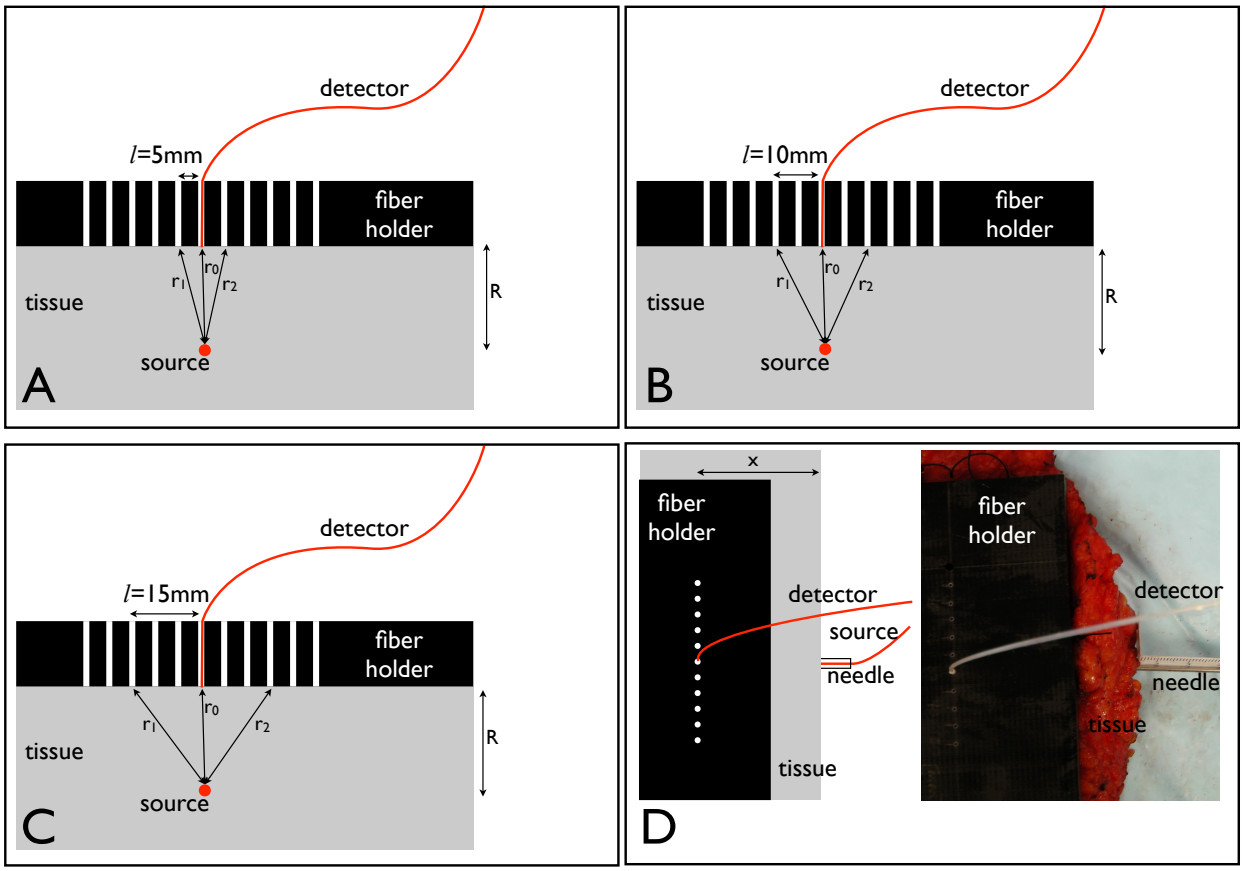

Figure 8.5: Perpendicular Measurement geometry: A, B, & C are cross sectional views in the plane of the fiber tips. D shows the top view of this geometry. The source fiber was stereotactically inserted in the tissue parallel to the fiber holder at a fixed depth, R=8 or 21 mm, from the bottom of the fiber holder (A, B & C). The needle was placed so it was perpendicular to the holes in the fiber holder and with tip of the fiber in the same plane as the holes at a distance x from the needle insertion point (D). The detector fiber was placed on the surface where r_1, r_0, & r_2 are indicated using the fiber holder.

8.3 Results

8.3.1 Coaxial Measurement Geometry

The coaxial measurement geometry was used to collect the phase lag in three different breast tissue samples. Figure 8.6 shows this data for the tissue samples and also for phantom 4. Both media show a linear relationship between phase lag and distance. The mean slope ± standard deviation of the tissue measurements was -1.8±0.2 [deg/mm] and the phantom was -2.4±0.1 [deg/mm]. The residuals were also plotted. In the tissue samples there is a linear trend in the residuals which suggests the phase lag introduced by the system, C_a, may not have been measured accurately or changed slightly between measurements of the phantom and the tissue.

Figure 8.7 shows the data from the tissue samples 1–3 separately. The mean slope ± standard deviation of the tissue measurements was -1.8±0.2 [deg/mm] for both samples 1 & 2 and -1.7±0.1 [deg/mm] for sample 3.

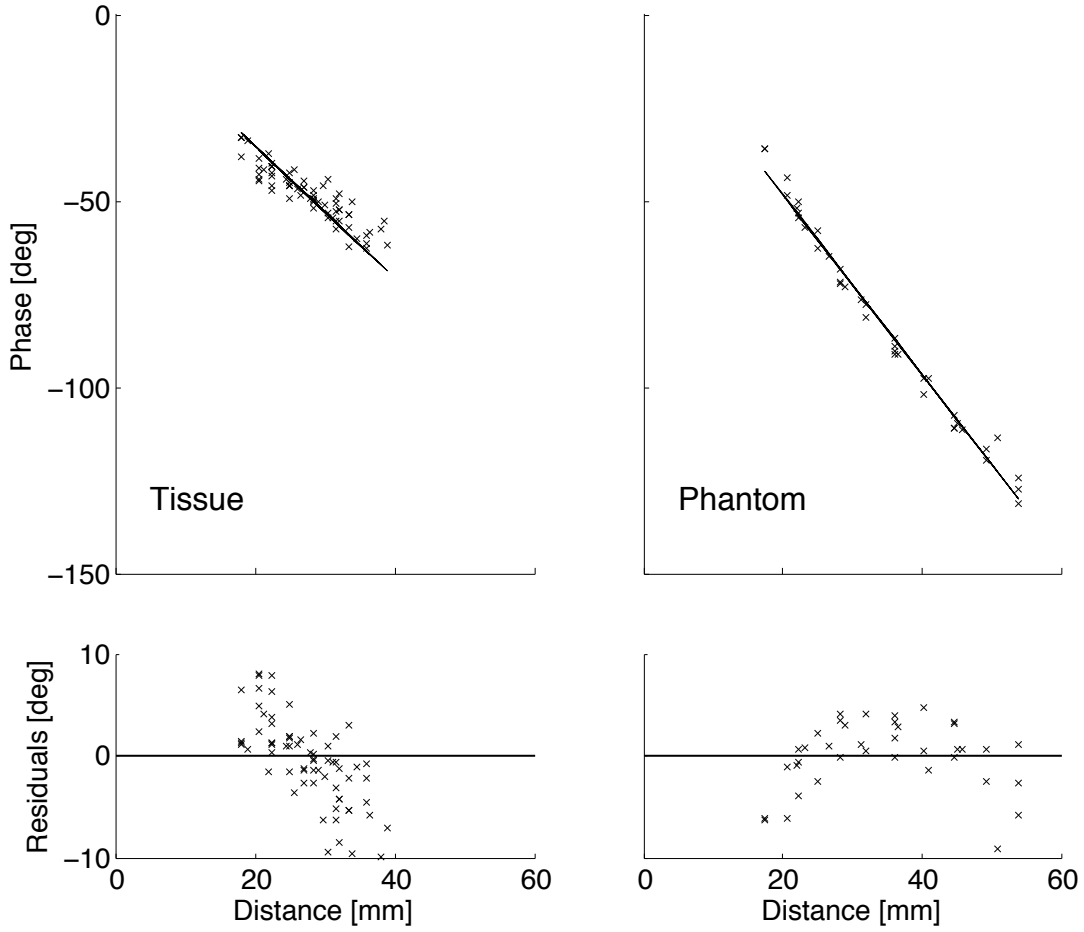

Figure 8.6: *Left column:* Tissue. *Right column:* Phantom. *Top row:* The phase lag from the source of light to the probe as a function of the stereotactically measured distance between the two fibers. The lines are fit to Equation 5.6 ($r = \gamma_a \cdot \theta + C_a$) with $C_a = 0$. *Bottom row:* The difference between fit line and data.

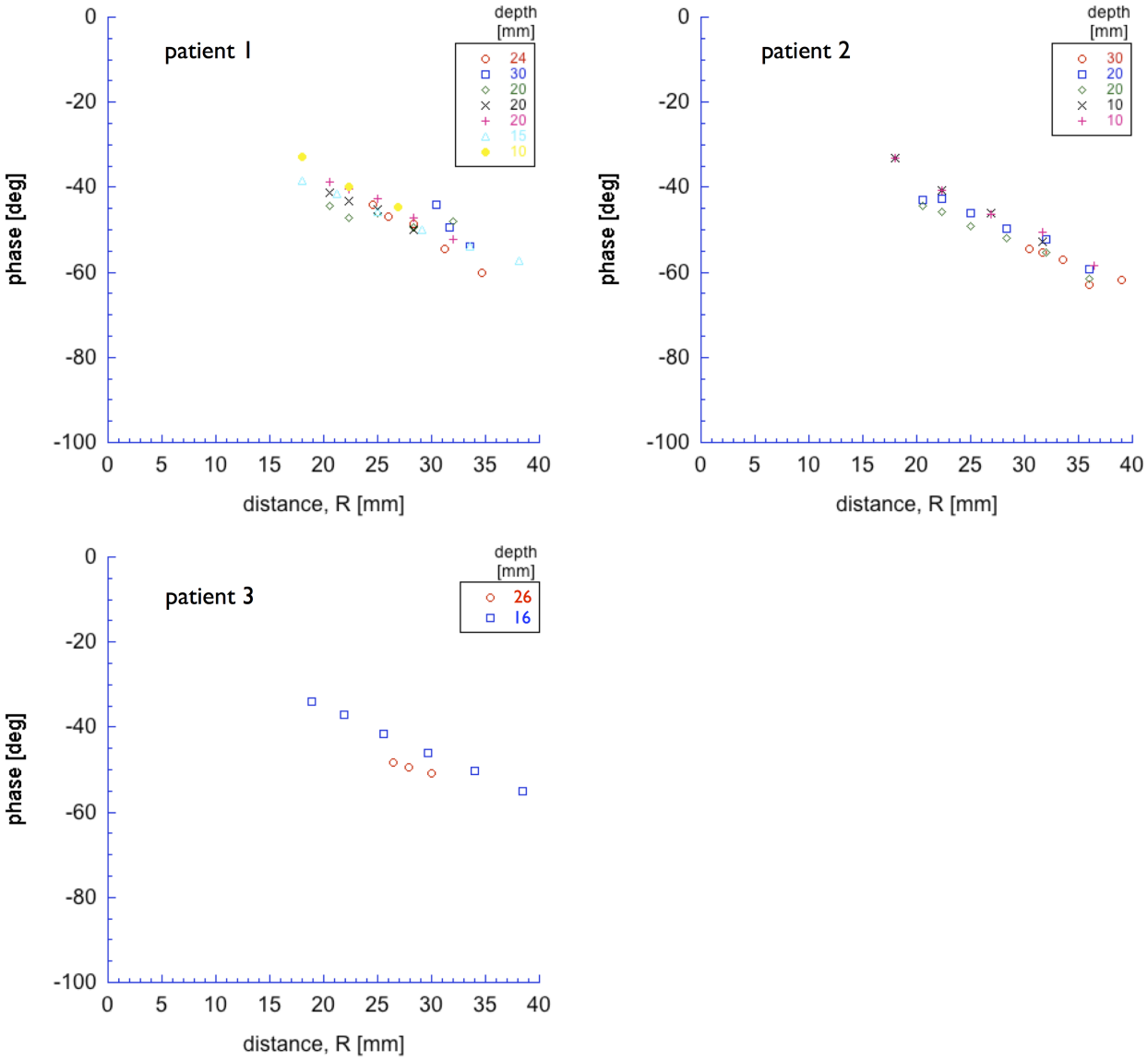

Figure 8.7: The phase lag from the source of light to the probe as a function of the stereotactically measured distance, R between the two fibers in the coaxial configuration for three tissue samples. The intensity of light was modulated at 70 MHz. The different markers each represent the indicated source fiber depth within the tissue.

8.3.2 Perpendicular Measurement Geometry

The perpendicular measurement geometry was used to test the feasibility of the probe described in Chapter 6. Table 8.1 and Figure 8.8 show the distance calculated between source and detector using Equation 8.3. This data suggests a probe detector separation distance, l of 5 mm was too small to provide accurate determination of source depth. However l of 10 and 15 mm both provided a source depth measurement, r_0, within 15% of the actual value.

l mm	sample	f MHz	θ_1 deg	θ_0 deg	θ_2 deg	R mm	r_0 mm	error %
5	3	70	-18.4	-12.3	-14.5	8	6	25
5	3	110	-17.5	-15.0	-17.8	8	8	0
5	3	70	-39.5	-35.9	-40.5	21	10	52
5	3	70	-39.3	-37.2	-40.6	21	13	38
5	3	110	-44.3	-42.1	-45.4	21	14	33
10	3	110	-25.9	-15.0	-25.6	8	7	13
10	3	70	-41.3	-35.9	-41.4	21	18	14
10	3	70	-40.9	-37.2	-42.2	21	20	5
10	3	110	-46.9	-42.1	-47.3	21	20	5
15	3	110	-34.6	-15.0	-34.0	8	7	13
15	3	70	-46.4	-35.9	-45.2	21	19	10
15	3	110	-54.8	-42.1	-50.3	21	20	5

Table 8.1: Summary of data collected in breast tissue sample 3 in the perpendicular configuration. The separation distance between detector fibers, l, is shown as well as the phase lag measured, $\theta_{1,2,3}$ at each detector with modulation frequency, f indicated. Also shown is the stereotactically measured source depth, R and the calculated distance between source and detector, r_0. r_0 was determined by Equation 8.3 where $\bar{\theta}$ is the average of θ_1 and θ_2. The error was calculated as the difference between R and r_0 divided by R.

8.4 Conclusions

The phase lag as a function of distance from an intensity modulated point source was measured in 3 specimens of human breast tissue. The coaxial measurement geometry showed a linear response of phase to distance from the source in both tissue and phantom. The mean slope ± standard deviation of the tissue measurements was -1.8±0.2 [deg/mm] and the phantom was -2.4±0.1 [deg/mm]. The standard deviation of the data collected in tissue was twice as large as in the phantom.

The perpendicular measurement geometry was used to test the feasibility of using the probe described in Chapter 6 as well as to determine if 5, 10 or 15 mm could be used as a detector fiber

separation distance in tissue samples. In tissue sample 3, a probe detector separation distance of 5 mm was not accurate in tissue, the error was 30±20 % (mean± standard deviation). However, probe detector separation distances of both 10 and 15 mm provided more accurate estimates of the stereotactically measured source depth with an error of 9±5 % (mean± standard deviation) for each.

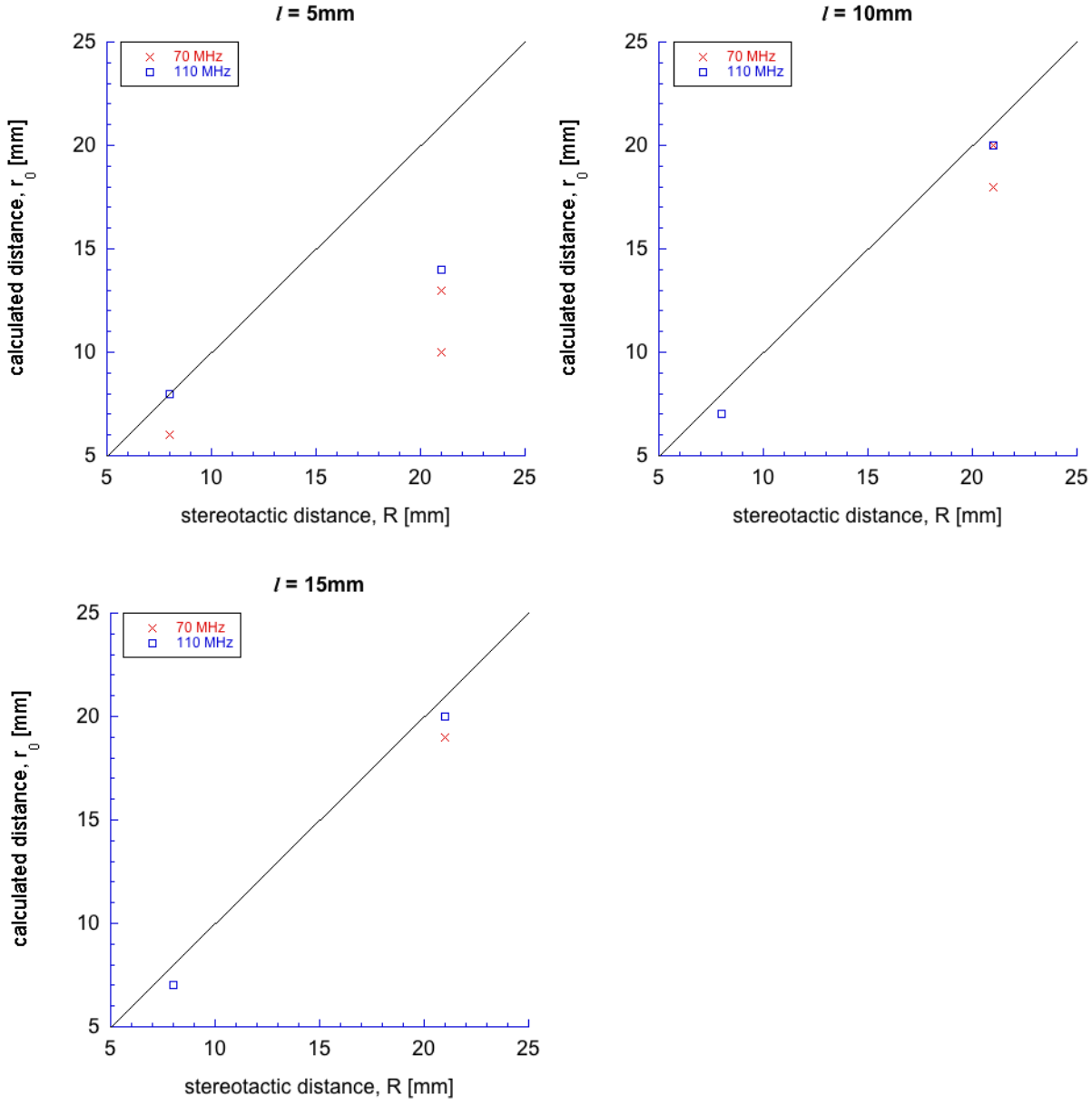

Figure 8.8: The calculated distance between source and detector, r_0 is plotted against the stereotactically measured source depth, R. Equation 8.3 was used to determine r_0 where $\bar{\theta}$ is the average of θ_1 and θ_2. The line indicates equality between the ordinate and abscissa. Each plot represents one of the tested separation distances between detector fibers, l=5, 10, 15 mm.

9

General Discussion & Conclusions

9.1 Light Guided Lumpectomy and First Generation Optical Wire

With a long term goal of reducing the number of repeat lumpectomies due to positive margins, an optical wire was designed to be used as a visual localization technique during lumpectomy surgery. The optical wire made the area of tissue around the lesion glow red during surgery. The optical wire was designed and tested so that a 200 μm optical fiber was axially attached to a standard Kopans wire with medical grade epoxy. The tip of the optical fiber was 3 mm proximal from the tip of the Kopans wire. The goal was that the optical wire could be placed by a radiologist in exactly the same manner as a Kopans wire with the tip within the lesion to be removed. After placement of the wire, the lumpectomy surgery was performed using standard methods but with the additional assistance of being able to see a red glow-ball of light surrounding the lesion. It was determined that red light (specifically 630–660 nm) would be the most visible wavelength in breast tissue. A light delivery system was designed and the optical wire was tested in prophylactic mastectomy specimens to confirm the red light was visible through 30–50 mm of breast tissue. After bench top testing was completed, the optical wire was used clinically in one 65 year old patient undergoing lumpectomy. Given the known location and approximate size of the lesion from previous imaging, the surgeon was able to identify the area of breast tissue to remove. The glow-ball provided immediate visualization at the end of the optical wire and the surgeon used it to estimate proximity to the wire tip. Pathology analysis provided final confirmation of negative margin status.

Given the promising clinical implementation of the optical wire, a clinical study of 8 patients was conducted where an optical wire was used during lumpectomy surgery. Patients with non-palpable

breast cancer (< 2 cm diameter) undergoing lumpectomy for biopsy-proven radiographically identifiable disease were eligible. Patients were between the ages of 41 & 68 diagnosed with either invasive ductal carcinoma or ductal carcinoma *in situ*. Each wire was placed within 4 mm of the lesion by a radiologist. The light emitted from the optical wire was used in each surgery to assist in locating the area of tissue to be removed. This allowed the surgeon to choose a direct plane of dissection towards the lesion. In addition, after approaching the area to be removed, the glow-ball was used to dissect around the lesion. Seven of the eight lumpectomies resulted in negative margins upon pathology review.

9.2 Second Generation Optical Wire

The optical wire was re-designed to create a second generation device. Although the optical wire study resulted in good clinical outcomes, the wire was made more comfortable for the patient and more user friendly for the radiologist placing the wire, the operating surgeon and the engineer controlling the light source. Since the first generation optical wire had 3 m of optical fiber permanently attached to the Kopans wire, it required extra time to be placed by the radiologist, then the fiber had to be wound and carefully taped to the patient's chest. Once the patient was in the operating room, the fiber had to be carefully untaped and unwound, then manually coupled and aligned with the red laser. None of the fibers broke in clinical testing, however, it was likely to occur due to the fragile nature of the small fiber.

To address the issue of potential fiber breakage and in an overall effort to make the device more comfortable for the patient and easier to use, a second generation optical wire was designed, tested, and manufactured. The second generation device was designed with a custom extruded Pebax dual lumen tube with dimensions of 0.0196×0.0334 inches ($500 \times 850\,\mu$m). One lumen of the tube was permanently adhered to a Kopans wire and the other lumen was left open so a fiber could be slid in and out. The second generation device underwent thorough tensile testing and third party sterility validation. It was found to be at least 4 times as strong as the Kopans wire and a steam cycle of 6 minutes at 132 °C was found sufficient to sterilize the wire.

This second generation device allowed the radiologist to place the wire without the fiber attached. The second generation device was more comfortable for the patient because the fiber did not have to be taped to their chest between placement and surgery. From both the radiologist and patient perspective, the optical wire was simply a slightly larger diameter Kopans wire. During

surgery, the optical fiber was placed within one lumen of the dual lumen tube and taped in place during the surgery.

9.3 Intensity Modulation: Modeling & Diffusion Theory

Frequency domain measurements are based on sinusoidally modulating a light source, usually within a bandwidth of hundreds of megahertz. Upon photon propagation through highly scattering material, such as tissue, the sinusoidal signal becomes demodulated, both the amplitude (A) of the wave and the average intensity (DC) decrease and a phase lag develops between the source and the propagating wave. The diffusion approximation to the radiative transport equation was used to model the propagation of a modulated light source through highly scattering medium. In an infinite medium, phase has a linear dependence on distance with the slope of the line dependent on the frequency of modulation and the optical properties of the medium. However, the optical properties of the medium did not need to be explicitly determined in order to calculate the distance from the source as shown in Equation 5.6.

In most work in biomedical optics the effect of a boundary on the behavior of light is carefully considered. Farrell described the extrapolated boundary method for handling a refractive index mis-match. Haskell expanded on Ferrell's method to solve for the phase of a modulated light source at a boundary. Both of these methods model a light source incident on the surface of a scattering medium and detect light that has escaped the medium some distance from the source. The models both place an imaginary point source within the medium and a negative point source outside the medium. Haskell's method was used to model the phase of a modulated light source propagating through an infinite medium and a bounded medium. The effect of the boundary was negligible when the light source was more than 5 mm from a boundary. This meant an infinite medium analysis of the phase lag twas sufficient to determine the distance between source and detector during light-guided lumpectomy.

9.4 Self Calibrating Distance Measurement Probe

Ideally, a handheld probe could be used in conjunction with light-guided lumpectomy to give the operating surgeon a quick measurement of the distance from the dissection plane to the light source within the breast. The primary goal of this measurement probe was to determine the distance from a modulated light source without *a priori* knowledge of the tissue optical properties. A major

problem of measuring the distance from a light source within breast tissue is the optical properties of the tissue will change as the probe is moved to different locations. Therefore, the probe was designed to adjust to changing optical properties in real time. Due to the geometry of the detectors in the probe, the optical properties of the scattering medium do not need to be determined to make a measurement of the distance. Phase lag was modeled in a homogeneous medium and the expected error in the distance calculation was less than 4 % with a detector separation of 5 mm or greater and with the face of the probe less than 15 degrees from normal to the light source.

This probe was designed to be used primarily during a lumpectomy and may not be ideal for measurements through the skin. Both scattering and absorption in the skin will significantly decrease the amount of light reaching the probe. There will be an especially dramatic decrease in signal with high melanin content. A dark spot on the skin such as a freckle, mole, or part of the areola will also create error in the distance measurement of this probe. A goal of future work is to determine the number of detectors needed to minimize error while maintaining the small size of the probe.

In addition to error from skin pigment, perturbations in the breast tissue such as calcifications, fibrous tissue, cysts, or bleeding could cause error in the distance measurement. If the perturbation is within 10–15 mm of the probe and affecting some but not all of the detectors, error will be introduced. One way to minimize the error caused by perturbations would be to use a probe with more than 4 detectors. Perhaps 10–20 detectors or even a fiber bundle could be implemented. Since the average phase lag of the outer detectors was being compared to the central detector, the error will be reduced with the addition of more detectors. More work is needed to determine how perturbations in the tissue will influence the phase lag measured at the detectors.

9.5 Measuring Distance Through Optical Phantoms

Polyurethane optical phantoms with optical properties similar to breast tissue were fabricated and a modulated optical system was assembled. The optical system relied on a network analyzer to modulate the intensity of a red laser and to compare the phase of a source signal to a detected signal. The stability of the system was tested by shutting it down and re-starting it while component settings remained constant. The phase was measured between 4 start-up/shut-down cycles and resulted in a phase of -129.7 $\pm$ 0.4 deg (mean $\pm$ standard deviation) over a distance of 33 mm, the error in deg/mm was 1%. System drift was also tested over 41 minutes and the noise floor was less than 0.2 deg over the entire time.

Once the system was found to be stable, a single modulation frequency was chosen. In general, a low modulation frequency would mean a handled probe such as the one proposed in Chapter 6 could be made inexpensively with off-the-shelf components. In addition, lower frequencies attenuate slower and travel farther through scattering medium. However, the drawback to a low frequency is reduced sensitivity to distance. Phase was measured as a function of distance at many modulation frequencies between 30 & 160 MHz. 70 MHz was chosen because it was the lowest frequency where the phase was measured at 50 mm with less than 1 % error.

Critical to the design of the probe in Chapter 6 was the linear relationship between phase and distance and the ability to precisely measure phase when the detector was moved. With the source and detector fibers in two different configurations and 3 source depths, the phase was measured as 10 distances. A consistent phase was measured between 20 & 50 mm regardless of detector orientation to the source. In addition, a constant value for the phase lag of the optical system fas found to be C_a=45 deg. This system phase lag was found by measuring phase in three phantoms of different optical properties and extrapolating the phase lag at a distance of zero.

9.6 Measuring Distance Through Breast Tissue

The phase lag as a function of distance from an intensity modulated point source was measured in 3 specimens of human breast tissue. A linear response of phase to distance from the source in both tissue and phantoms was shown. The mean slope ± standard deviation of the tissue measurements was -1.8±0.2 [deg/mm] and the phantom was -2.4±0.1 [deg/mm]. The standard deviation of the data collected in tissue was twice as large as in the phantom.

The feasibility of using the probe described in Chapter 6 as well as to determine if 5, 10 or 15 mm could be used as a detector fiber separation distance in tissue samples. In tissue sample 3, a probe detector separation distance of 5 mm was not accurate in tissue, the error was 30%. However, probe detector separation distances of both 10 and 15 mm provided more accurate estimates of the stereotactically measured source depth with an error of 9% for each.

9.7 Discussion

The positive margin rate of lumpectomy surgeries should be improved. One potential way to reduce the number of positive margins following lumpectomy is to make the lesion and tissue surrounding the lesion visible during surgery with a glow-ball of light. The concept of such a light-guided

surgery was tested in 8 patients with the use of an optical wire. Seven of the 8 patients had negative margins.

The concept of a light-guided lumpectomy seemed very promising so further development began on both a second generation optical wire as well as a method to measure the distance between the lesion and the surface of the tissue during surgery. Once completed, the second generation optical wire was more comfortable for the patient and easier for physicians to use. The method developed to measure distance through breast tissue made use of the linear relationship between distance and phase lag of a modulated light source. A probe was designed to make real time measurements of distance during a light-guided lumpectomy. The concepts of the probe were tested in homogeneous optical phantoms as well as in breast tissue. Distance was measured in breast tissue with less than 9 % error.

Prior to evaluation in a clinical setting, the probe needs to be further developed. Experiments in phantoms and computer modeling should be conducted to determine how many detectors are ideal. Device development with the goal of a prototype for use in the operating room also needs to occur. The probe should be hand held with visual and perhaps audio feedback of the distance measured. During a lumpectomy, the probe will likely be used after a skin incision is made as the surgeon is approaching the lesion. It is intended to be an adjunct to the glow-ball during light-guided lumpectomy and will probably be used a few times during the surgery to give the distance from the lesion. After a clinical prototype is ready, a trial in prophylactic mastectomy specimens should be conducted to verify the accuracy of the device when measuring distance in breast tissue. If the mastectomy trial is successful, a larger clinical trial should be conducted to determine if the positive margin rate of lumpectomies could be reduced with light-guided lumpectomy.

References

[1] Lorenzo Spinelli, Alessandro Torricelli, Antonio Pifferi, Paola Taroni, Gian Maria Danesini, and Rinaldo Cubeddu. **Bulk optical properties and tissue components in the female breast from multiwavelength time-resolved optical mammography**. *J Biomed Opt*, **9**(6):1137–1142, 2004. xi, 46, 47

[2] N Shah, AE Cerussi, D Jakubowski, D Hsiang, J Butler, and BJ Tromberg. **Spatial variations in optical and, physiological properties of healthy breast tissue**. *Journal of Biomedical Optics*, **9**(3):534–540, May-Jun 2004. xi, 46, 47

[3] R. L. P. van Veen, H. J. C. M. Sterenborg, A. W. K. S. Marinelli, and M. Menke-Pluymers. **Intraoperatively assessed optical properties of malignant and healthy breast tissue used to determine the optimum wavelength of contrast for optical mammography**. *J Biomed Opt*, **9**(6):1129–1136, 2004. xi, 13, 46, 48

[4] A. B. Nattinger, M. S. Gottlieb, R. G. Hoffman, A. P. Walker, and J. S. Goodwin. **Minimal increase in use of breast-conserving surgery from 1986–1990**. *Med Care*, **34**:479–89, 1996. 2, 4

[5] B. Jerome-D'Emilia and J. W. Begun. **Diffusion of breast conserving surgery in medical communities**. *Soc Sci Med*, **60**:143–51, 2005. 1, 2, 4, 11, 23

[6] L. J. Pierce, J. Moughan, J. White, D. P. Winchester, J. Owen, and J. F. Wilson. **1998–1999 patterns of care study process survey of national practice patterns using breast-conserving surgery and radiotherapy in the management of stage I-II breast cancer**. *Int J Radiat Oncol Biol Phys*, **62**:183–92, 2005. 2, 4

[7] Florian Fitzal and Michael Gnant. **Breast conservation: Evolution of surgical strategies**. *Breast J*, **12**(5, Suppl. 2):S165–S173, Sep-Oct 2006. 1, 2, 4, 11, 23

[8] Alberto Luini, Giovanna Gatti, Stefano Zurrida, Nina Talakhadze, Fabricio Brenelli, Daniela Gilardi, Giovanni Paganelli, Roberto Orecchia, Enrico Cassano, Giuseppe Viale, Claudia Sangalli, Bettina Ballardini, Gabriela Rosali dos Santos, and Umberto Veronesi. **The evolution of the conservative approach to breast cancer**. *Breast*, **16**(2):120–129, Apr 2007. 1, 2, 4, 6, 11, 23

[9] SC Renton, JC Gazet, HT Ford, C Corbishley, and R Sutcliffe. **The importance of the resection margin in conservative surgery for breast cancer**. *European Journal of Surgical Oncology*, **22**(1):17–22, Feb 1996. 2, 4, 12

[10] HH Luu, CN Otis, WP Reed, JL Garb, and JL Frank. **The unsatisfactory margin in breast cancer surgery**. *Am J Surg*, **178**(5):362–366, Nov 1999. 2, 4, 12

[11] Edward Obedian and Bruce G. Haffty. **Negative Margin Status Improves Local Control in Conservatively Managed Breast Cancer Patients**. *The Cancer Journal from Scientific American*, **6**(1):28–33, Jan-Feb 2000. 2, 4, 12

[12] PI Tartter, J Kaplan, I Bleiweiss, C Gajdos, A Kong, S Ahmed, and D Zapetti. **Lumpectomy margins, reexcision, and local recurrence of breast cancer**. *Am J Surg*, **179**(2):81–85, Feb 2000. 2, 4, 12

[13] SE Singletary. **Surgical margins in patients with early-stage breast cancer treated with breast conservation therapy**. *Am J Surg*, **184**(5):383–393, 2002. 2, 4, 12

[14] C. D. Scopa, P. Aroukatos, A. C. Tsamandas, and C. Aletra. **Evaluation of margin status in lumpectomy specimens and residual breast carcinoma**. *Breast J*, **12**:150–3, 2006. 2, 4, 12

[15] Cyrus Kotwall, Mark Ranson, Anquonette Stiles, and Mary Sue Hamann. **Relationship between initial margin status for invasive breast cancer and residual carcinoma after re-excision**. *American Surgeon*, **73**(4):337–343, Apr 2007. 2, 4, 12

[16] LAG Ries, D Melbert, M Krapcho, DG Stinchcomb, N Howlader, MJ Horner, A Mariotto, BA Miller, EJ Feuer, SF Altekruse, DR Lewis, L Clegg, MP Eisner, M Reichman, and BK Edwards. **SEER Cancer Statistics Review, 1975-2005**. *National Cancer Institute. Bethesda, MD.* 2

[17] **HCUP Clinical Classifications Software (CCS) for ICD-9-CM. Healthcare Cost and Utilization Project (HCUP). 2006.** *Agency for Healthcare Research and Quality, Rockville, MD.*, pages www.hcup–us.ahrq.gov/toolssoftware/ccs/ccs.jsp., Accessed October, 26 2009. 1, 11, 23

[18] C. Kotwall, D. Covington, P. Churchill, C. Brinker, D. Weintritt, and J. G. Maxwell. **Breast conservation surgery for breast cancer at a regional medical center**. *Am J Surg*, **176**:510–4, 1998. 1, 11

[19] L. M. Apantaku. **Breast-conserving surgery for breast cancer**. *Am Fam Physician*, **66**:2271–8, 2002. 1, 11

[20] B. Fisher, C. Redmond, E. R. Fisher, M. Bauer, N. Wolmark, D. L. Wickerham, M. Deutsch, E. Montague, R. Margolese, and R. Foster. **Ten-year results of a randomized clinical trial comparing radical mastectomy and total mastectomy with or without radiation**. *N Engl J Med*, **312**:674–81, 1985. 2

[21] B. Fisher, S. Anderson, C. K. Redmond, N. Wolmark, D. L. Wickerham, and W. M. Cronin. **Reanalysis and results after 12 years of follow-up in a randomized clinical trial comparing total mastectomy with lumpectomy with or without irradiation in the treatment of breast cancer**. *N Engl J Med*, **333**:1456–61, 1995. 2, 24

[22] Daniel B. Kopans. *Breast Imaging*. Lippincott Williams & Wilkins, third edition, 2007. 2, 5, 12

[23] M.D. Lagios, F.R. Margolin, P.R. Westdahl, and M.R. Rose. **Mammographically detected duct carcinoma in situ. Frequency of local recurrence following tylectomy and prognostic effect of nuclear grade on local recurrence**. *Cancer*, **63**:618–624, Feb 1989. 4

[24] D.L. Page, W.D. Dupont, L.W. Rogers, R.A. Jensen, and P.A. Schuyler. **Continued local recurrence of carcinoma 15-25 years after a diagnosis of low grade ductal carcinoma in situ of the breast treated only by biopsy**. *Cancer*, **76**:1197–1200, Oct 1995. 4

[25] B.O. Anderson, K.E. Calhoun, and E.L. Rosen. **Evolving concepts in the management of lobular neoplasia**. *J Natl Compr Canc Netw*, **4**:511–522, May 2006. 4

[26] S.M. Brandt, G.Q. Young, and S.A. Hoda. **The "Rosen Triad": tubular carcinoma, lobular carcinoma in situ, and columnar cell lesions**. *Adv Anat Pathol*, **15**:140–146, May 2008. 4

[27] P.P. Rosen. **Lobular carcinoma in situ and intraductal carcinoma of the breast**. *Monogr Pathol*, pages 59–105, 1984. 4

[28] S.J. Shin and P.P. Rosen. **Excisional biopsy should be performed if lobular carcinoma in situ is seen on needle core biopsy**. *Arch. Pathol. Lab. Med.*, **126**:697–701, Jun 2002. 4

[29] H. R. MacDonald, M. J. Silverstein, H. Mabry, B. Moorthy, W. Ye, M. S. Epstein, D. Holmes, H. Silberman, and M. Lagios. **Local control in ductal carcinoma *in situ* treated by excision alone: incremental benefit of larger margins**. *Am J Surg*, **190**:521–5, 2005. 5

[30] Berry Cleffken, Job Postelmans, Steven Olde Damink, Marius Nap, Ineke Schreutelkamp, and Hans van der Bijl. **Breast-conserving therapy for palpable and nonpalpable breast cancer: Can surgical residents do the job irrespective of experience?** *World J Surg*, **31**(9):1731–1736, Sep 2007. 5, 24

[31] Daniel B. Kopans and Salvatore DeLuca. **A Modified Needle-Hookwire Technique to Simplify Preoperative Localization of Occult Breast Lesions**. *Radiology*, **134**:781, 1980. 5, 12, 25

[32] Pamela R. Benitez, Oscar Streeter, Frank Vicini, Vivek Mehta, Coral Quiet, Robert Kuske, Mary Katherine Hayes, Doug Arthur, Henry Kuerer, Gary Freedman, Martin Keisch, Thomas DiPetrillo, David Khan, and Richard Hudes. **Preliminary results and evaluation of MammoSite balloon brachytherapy for partial breast irradiation for pure ductal carcinoma in situ: a phase II clinical study**. *American Journal of Surgery*, **192**(4):427–433, Oct 2006. 6

[33] F Vicini, VR Kini, P Chen, E Horwitz, G Gustafson, P Benitez, G Edmundson, N Goldstein, K McCarthy, and A Martinez. **Irradiation of the tumor bed alone after lumpectomy in selected patients with early-stage breast cancer treated with breast conserving therapy**. *Journal of Surgical Oncology*, **70**(1):33–40, Jan 1999. 6

[34] M. Cutler. **Transillumination as an aid in the daignosis of breast lesions. With special reference to its value in case of bleeding nipple**. *Surg. Gynecol. Obste.*, **48**:721–729, 1929.

[35] M. Cutler. **Trasillumination of the breast**. *Annals of Surgery*, **93**:223–234, 1931.

[36] Amanda Dayton, Laurel Soot, Ronald Wolf, Christina Gougoutas-Fox, and Scott Prahl. **Light-guided lumpectomy: device and case report**. *J Biomed Opt*, **15**(6):061706, 2010. 11, 24, 25

[37] Karen A. Cullen, Margaret J. Hall, and Aleksandr Golosinskiy. **Ambulatory Surgery in the United States, 2006**. National Health Statistics Reports 11, Division of Health Care Statistics, U.S. Department of Health and Human Services, Centers for Disease Control and Prevention, National Center for Health Statistics, January 2009. 11, 23

[38] V. G. Peters, D. R. Wyman, M. S. Patterson, and G. L. Frank. **Optical properties of normal and diseased human breast tissues in the visible and near infrared**. *Phys Med Biol*, **35**:1317–34, 1990. 13

[39] D. Grosenick, K. T. Moesta, H. Wabnitz, J. Mucke, C. Stroszczynski, R. Macdonald, P. M. Schlag, and H. Rinneberg. **Time-domain optical mammography: initial clinical results on detection and characterization of breast tumors**. *Appl Opt*, **42**:3170–86, 2003. 13

[40] T. Durduran, R. Choe, J. P. Culver, L. Zubkov, M. J. Holboke, J. Giammarco, B. Chance, and A. G. Yodh. **Bulk optical properties of healthy female breast tissue**. *Phys Med Biol*, **47**:2847–61, 2002. 13

[41] T. Svensson, J. Swartling, P. Taroni, A. Torricelli, P. Lindblom, C. Ingvar, and S. Andersson-Engels. **Characterization of normal breast tissue heterogeneity using time-resolved near-infrared spectroscopy**. *Phys Med Biol*, **50**:2559–71, 2005. 13

[42] L. Spinelli, A. Torricelli, A. Pifferi, P. Taroni, G. M. Danesini, and R. Cubeddu. **Bulk optical properties and tissue components in the female breast from multiwavelength time-resolved optical mammography**. *J Biomed Opt*, **9**:1137–42, 2004. 13

[43] G. Zacharakis, A. Zolindaki, V. Sakkalis, G. Filippidis, T. G. Papazoglou, D. D. Tsiftsis, and E. Koumantakis. **In vitro optical characterization and discrimination of female breast tissue during near infrared femtosecond laser pulses propagation**. *J Biomed Opt*, **6**:446–9, 2001. 13

[44] A. Ishimaru. *Wave Propagation and Scattering in Random Media*, **1**. Academic Press, New York, 1978. 14

[45] P. Moon and D. E. Spencer. *The Photic Field*. MIT Press, Cambridge, MA, 1981. 14

[46] Karl L. Hussman, Barbara A. Ward, Charles F. McKhann, Steven M. Pustilnick, Irena Tocina, Laura J. Horvath, Liane E. Philpotts, and Carol H. Lee. **Optical Breast Lesion Localization Fiber: Preclinical Testing of a New Device**. *Radiology*, **200**:865–866, 1996. 15, 24

[47] A. Dayton, L. Soot, R. Wolf, C. Gougoutas-Fox, and S. Prahl. **Light Guided Lumpectomy: First Clinical Experience**. *Journal of Biophotonics Special Issue: Clinical Biophotonics*, **4**(10):752758, 2011. 23

[48] Bernard Fisher, Stewart Anderson, John Bryant, Richard G. Margolese, Melvin Deutsch, Edwin R. Fisher, Jong-Hyeon Jeong, and Norman Wolmark. **Twenty-Year Follow-up of a Randomized Trial Comparing Total Mastectomy, Lumpectomy, and Lumpectomy plus Irradiation for the Treatment of Invasive Breast Cancer**. *New England Journal of Medicine*, **347**(16):1233–1241, 10 2002. 24

[49] Rick Pleijhuis, Maurits Graafland, Jakob de Vries, Joost Bart, Johannes de Jong, and Gooitzen van Dam. **Obtaining Adequate Surgical Margins in Breast-Conserving Therapy for Patients with Early-Stage Breast Cancer: Current Modalities and Future Directions**. *Ann Surg Oncol*, **16**:2717–2730, 2009. 24

[50] Seema A. Khan, MD and Firas Eladoumikdachi, MD. **Optimal Surgical Treatment of Breast Cancer: Implications for Local Control and Survival**. *J. Surg. Oncol.*, **101**:677–686, 2010. 24

[51] Nehmat Houssami, Petra Macaskill, M. Luke Marinovich, J. Michael Dixon, Les Irwig, Meagan E. Brennan, and Lawrence J. Solin. **Meta-analysis of the impact of surgical margins on local recurrence in women with early-stage invasive breast cancer treated with breast-conserving therapy**. *European Journal of Cancer*, **46**(18):3219 – 3232, 2010. 24

[52] Rinaa S. Punglia, Monica Morrow, Eric P. Winer, and Jay R. Harris. **Local Therapy and Survival in Breast Cancer**. *New England Journal of Medicine*, **356**(23):2399–2405, 2007. 24

[53] C Dunne, JP Burke, M Morrow, and MR Kell. **Effect of margin status on local recurrence after breast conservation and radiation therapy for ductal carcinoma in situ**. *J Clin Oncol*, **27**:1615–1620, 2009. 28

[54] A. L. Dayton, V. T. Keranen, and S. A. Prahl. **Optical wire guided lumpectomy: frequency domain measurements**. **7173**, page 71730M. SPIE, 2009. 31

[55] Daniel Leff, Oliver Warren, Louise Enfield, Adam Gibson, Thanos Athanasiou, Darren Patten, Jem Hebden, Guang Yang, and Ara Darzi. **Diffuse optical imaging of the healthy and diseased breast: A systematic review**. *Breast Cancer Research and Treatment*, **108**:9–22, 2008. 10.1007/s10549-007-9582-z. 32, 49

[56] V. G. Peters, D. R. Wyman, M. S. Patterson, and G. L. Frank. **Optical properties of normal and diseased human breast tissues in the visible and near infrared**. *Phys Med Biol*, **35**:1317–34, 1990. 46

[57] WF Cheong, SA Prahl, and AJ Welch. **A Review of the Optical-Properties of Biological Tissues**. *IEEE Journal of Quantum Electronics*, **26**(12):2166–2185, Dec 1990. 46

[58] A Kienle, L Lilge, MS Patterson, R Hibst, R Steiner, and BC Wilson. **Spatially resolved absolute diffuse reflectance measurements for noninvasive determination of the optical scattering and absorption coefficients of biological tissue**. *Applied Optics*, **35**(13):2304–2314, May 1 1996. 46

[59] Kazunori Suzuki, Yutaka Yamashita, Kazuyoshi Ohta, Masao Kaneko, Masayuki Yoshida, and Britton Chance. **Quantitative Measurement of Optical Parameters in Normal Breasts Using Time-resolved Spectroscopy: In Vivo Results of 30 Japanese Women**. *J Biomed Opt*, **1**(3):330 – 334, July 1996. 46

[60] VV Tuchin. **Light scattering study of tissues**. *Phys-Usp*, **40**(5):495–515, May 1997. 46

[61] BJ Tromberg, O Coquoz, J Fishkin, T Pham, ER Anderson, J Butler, M Cahn, JD Gross, V Venugopalan, and D Pham. **Non-invasive measurements of breast tissue optical properties using frequency-domain photon migration**. *Philosophical Transactions of the Royal Society of London Series B-Biological Sciences*, **352**(1354):661–668, Jun 29 1997. 46

[62] G. Zacharakis, A. Zolindaki, V. Sakkalis, G. Filippidis, T. G. Papazoglou, D. D. Tsiftsis, and E. Koumantakis. **In vitro optical characterization and discrimination of female breast tissue during near infrared femtosecond laser pulses propagation**. *J Biomed Opt*, **6**:446–9, 2001. 46

[63] N Shah, A Cerussi, C Eker, J Espinoza, J Butler, J Fishkin, R Hornung, and B Tromberg. **Noninvasive functional optical spectroscopy of human breast tissue**. *Proceedings of the National Academy of Sciences of the United States of America*, **98**(8):4420–4425, Apr 10 2001. 46

[64] V Chernomordik, DW Hattery, D Grosenick, H Wabnitz, H Rinneberg, KT Moesta, PM Schlag, and A Gandjbakhche. **Quantification of optical properties of a breast tumor using random walk theory**. *J Biomed Opt*, **7**(1):80–87, Jan 2002. 46

[65] MS Nair, N Ghosh, NS Raju, and A Pradhan. **Determination of optical parameters of human breast tissue from spatially resolved fluorescence: a diffusion theory model**. *Applied Optics*, **41**(19):4024–4035, Jul 1 2002. 46

[66] T Durduran, R Choe, JP Culver, L Zubkov, MJ Holboke, J Giammarco, B Chance, and AG Yodh. **Bulk optical properties of healthy female breast tissue**. *Phys Med Biol*, **47**(16):2847–2861, Aug 21 2002. 46

[67] Antonio Pifferi, Johannes Swartling, Ekaterine Chikoidze, Alessandro Torricelli, Paola Taroni, Andrea Bassi, Stefan Andersson-Engels, and Rinaldo Cubeddu. **Spectroscopic time-resolved diffuse reflectance and transmittance measurements of the female breast at different interfiber distances**. *J Biomed Opt*, **9**(6):1143–1151, 2004. 46, 49

[68] DB Jakubowski, AE Cerussi, F Bevilacqua, N Shah, D Hsiang, J Butler, and BJ Tromberg. **Monitoring neoadjuvant chemotherapy in breast cancer using quantitative diffuse optical spectroscopy: a case study**. *Journal of Biomedical Optics*, **9**(1):230–238, Jan-Feb 2004. 46

[69] D. Grosenick, H. Wabnitz, K. T. Moesta, J. Mucke, M. Moller, C. Stroszczynski, J. Stossel, B. Wassermann, P. M. Schlag, and H. Rinneberg. **Concentration and oxygen saturation of haemoglobin of 50 breast tumours determined by time-domain optical mammography**. *Physics in Medicine and Biology*, **49**(7):1165–1181, Apr 2004. 46

[70] MK Simick, R Jong, B Wilson, and L Lilge. **Non-ionizing near-infrared radiation transillumination spectroscopy for breast tissue density and assessment of breast cancer risk**. *Journal of Biomedical Optics*, **9**(4):794–803, Jul - Aug 2004. 46

[71] D. Grosenick, H. Wabnitz, K. T. Moesta, J. Mucke, P. M. Schlag, and H. Rinneberg. **Time-domain scanning optical mammography: II. Optical properties and tissue parameters of 87 carcinomas**. *Phys Med Biol*, **50**:2451–68, 2005. 46

[72] T. Svensson, J. Swartling, P. Taroni, A. Torricelli, P. Lindblom, C. Ingvar, and S. Andersson-Engels. **Characterization of normal breast tissue heterogeneity using time-resolved near-infrared spectroscopy**. *Phys Med Biol*, **50**:2559–71, 2005. 46

[73] CF Zhu, GM Palmer, TM Breslin, FS Xu, and N Ramanujam. **Use of a multiseparation fiber optic probe for the optical diagnosis of breast cancer**. *J Biomed Opt*, **10**(2), Mar - Apr 2005. 46

[74] A Garofalakis, G Zacharakis, G Filippidis, E Sanidas, DD Tsiftsis, E Stathopoulos, M Kafousi, J Ripoll, and TG Papazoglou. **Optical characterization of thin female breast biopsies based on the reduced scattering coefficient**. *Phys Med Biol*, **50**(11):2583–2596, Jun 7 2005. 46

[75] L. Spinelli, A. Torricelli, A. Pifferi, P. Taroni, G. Danesini, and R. Cubeddu. **Characterization of female breast lesions from multi-wavelength time-resolved optical mammography**. *Phys Med Biol*, **50**(11):2489–2502, Jun 2005. 46

[76] R. L. P. van Veen, A. Amelink, M. Menke-Pluymers, C. van der Pol, and H. J. C. M. Sterenborg. **Optical biopsy of breast tissue using differential path-length spectroscopy**. *Phys Med Biol*, **50**(11):2573–2581, Jun 2005. 46

[77] N Shah, J Gibbs, D Wolverton, A Cerussi, N Hylton, and BJ Tromberg. **Combined diffuse optical spectroscopy and contrast-enhanced magnetic resonance imaging for monitoring breast cancer neoadjuvant chemotherapy: a case study**. *Journal of Biomedical Optics*, **10**(5), Sep - Oct 2005. 46

[78] Albert Cerussi, Natasha Shah, David Hsiang, Amanda Durkin, John Butler, and Bruce J. Tromberg. **In vivo absorption, scattering, and physiologic properties of 58 malignant breast tumors determined by broadband diffuse optical spectroscopy**. *Journal of Biomedical Optics*, **11**(4), Jul - Aug 2006. 46

[79] Stefan A. Carp, Tina Kauffman, Qianqian Fang, Elizabeth Rafferty, Richard Moore, Daniel Kopans, and David Boas. **Compression-induced changes in the physiological state of the breast as observed through frequency domain photon migration measurements**. *Journal of Biomedical Optics*, **11**(6), Nov - Dec 2006. 46, 49

[80] Scott A. Prahl. **Optical Spectra** [online]. 2008 [cited 2008]. 46

[81] D. Segelstein. *The Complex Refractive Index of Water*. Master's thesis, University of Missouri–Kansas City, 1981. 46

[82] Albert E. Cerussi, Andrew J. Berger, Frederic Bevilacqua, Natasha Shah, Dorota Jakubowski, John Butler, Randall F.Holcombe, and Bruce J. Tromberg. **Sources of Absorption and Scattering Contrast for Near-Infrared Optical Mammography**. *Acad Radiol*, **8**:211–218, 2001. 46

[83] K. M. Case and P.F. Zweifel. *Linear Transport Theory*. Addison-Wesley Publishing Co., 1967. 8, 45, 49

[84] MS Patterson, B Chance, and BC Wilson. **Time Resolved Reflectance and Transmittance for the Noninvasive Measurement of Tissue Optical-Properties**. *Applied Optics*, **28**(12):2331–2336, Jun 15 1989. 8, 45, 49, 50

[85] LV Wang and SL Jacques. **Sources of error in calculation of optical diffuse reflectance from turbid media using diffusion theory**. *Computer Methods and Programs in Biomedicine*, **61**:163–170, 2000. 49

[86] M.S. Patterson. **Principles and Applications of Frequency-Domain Measurements of Light Propagation**. In A.J. Welch and M.J.C. vanGemert, editors, *Optical-Thermal Response of Laser-Irradiated Tissue*. Plenum Press, New York, 1995. 50, 51

[87] TJ FARRELL, MS PATTERSON, AND B WILSON. **A DIFFUSION-THEORY MODEL OF SPATIALLY RESOLVED, STEADY-STATE DIFFUSE REFLECTANCE FOR THE NONINVASIVE DETERMINATION OF TISSUE OPTICAL-PROPERTIES INVIVO**. *MEDICAL PHYSICS*, **19**(4):879–888, JUL-AUG 1992. 52

[88] RICHARD C. HASKELL, LARS O. SVAASAND, TSONG-TSEH TSAY, TI-CHEN FENG, MATHEY S. MCADAMS, AND BRUCE J. TROMBERG. **Boundary conditions for the diffusion equation in radiative transfer**. *J. Opt. Soc. Am. A*, **11**(10):2727–2741, Oct 1994. 52, 54

[89] SCOTT A. PRAHL. **Time Based Monte Carlo Code.** [online]. August 2011 [cited 2011]. 54, 66

[90] T. MOFFITT, Y. CHEN, AND S. PRAHL. **Preparation and characterization of polyurethane optical phantoms**. *Journal of Biomedical Optics*, **11**(4):041103, July/August 2006. 75, 77

Appendices

Appendix A

Steam Sterilization Study of the Optical Wire

Steam Sterilization Efficacy Study of the Optical Wire Device

December 13, 2010

This protocol is an ammendment of Protocol 09G_54391_01 prepared by Nichole Jackson, consultant, at NAMSA Advisory Services. The optical wire in protocol 09G_54391_01 had one lumen; the optical wire in this protocol has two lumens, however only one lumen will be tested in this protocol. No testing parameters have changed.

Prepared by:

Amanda Dayton — Date
Biomedical Engineer
Oregon Medical Laser Center

Approved by:

Scott Prahl — Date
Senior Scientist
Oregon Medical Laser Center

SPONSOR:

Oregon Medical Laser Center

Providence St. Vincent Medical Center

9555 SW Barnes Road Suite 210

Portland, OR 97225

A.1 Purpose

The purpose of this study is to verify the effectiveness of steam sterilization for the Optical Wire Device using autoclave half cycles with prevacuum air removal in a double-pouched configuration.

The study will evaluate the resistance of biological indicators (products inoculated with 10^6 *Geobacillus stearothermophilus* spores[1]) to 132°C steam autoclave half cycle exposures.

The intent of this study is to develop guidelines for sterilization of the product and to provide a sterility assurance level (SAL) of at least 10^{-6}. The overkill sterilization method, which is based on the premise that the sterilization cycles will be able to inactivate an appropriate microbial challenge plus provide an additional safety factor, will be used in this study.

The study will be based on the guidelines of AAMI TIR12:2004 *Designing, testing, and labeling reusable medical devices for reprocessing in healthcare facilities: A guide for medical device manufacturers* and ISO 17665-1:2006 *Sterilization of health care products Moist heat Part 1: Requirements for the development, validation and routine control of a sterilization process for medical devices.*

A.2 Scope

In the overkill method of validation, the objective is to develop a sterilant exposure that will consistently reduce, at a minimum, 12 logarithms of a microorganism with a D-value[2], specific to that sterilant, of 1.0 minute. For steam sterilization studies, *Geobacillus stearothermophilus*, an organism known for its resistance to moist heat, is selected.

This study is limited to providing sterilization efficiency data. Device and sterilization compatibility studies are beyond the scope of this protocol.

A.3 Product Description

The Optical Wire Device consists of an anchor wire secured within one lumen of a pebax 7233 dual lumen tube (19 cm length) and a removable placement wire within the other lumen of the tube. The optical wire is packaged in a heat sealable double-pouch (paper/film: 3" wide inner and 4"

[1]Different populations may be utilized depending on the D-value in order to represent a minimum of a six-log reduction.

[2]The term D-value denotes the exposure time required to cause a 1 logarithm (90 percent) reduction in the population of a microorganism under specified conditions.

wide outer). The second component is a solid glass / polyimide optical fiber (3 meters) which is housed within a Teflon tube coil; the coil is packaged in a double pouch (paper/film: 13" x 18" folded inner and 13" x 18" outer).

The placement wire lumen of the dual lumen tube has been deemed to be worst-case (most difficult to sterilize) and will therefore be challenged with BIs. The Optical Fiber will be present during the sterilization cycles to simulate a realistic exposure configuration.

Ten Optical Wires and three Optical Fibers will be required for testing; samples will be submitted in packaging along with extra pouches for exposures. See Appendix for product diagram.

All products used for testing are representative of normal production quality and were produced under Quality Systems Regulations (QSR). Detailed information about the product will be provided on the NAMSA Sample Submission Form.

A.4 Responsibility

Responsible to supply test samples, to prepare protocol, to prepare final report, and to address requirements of applicable regulatory agencies: Amanda Dayton, Biomedical Engineer, Oregon Medical Laser Center, Providence St. Vincent Medical Center, 9555 SW Barnes Road Suite 210, Portland, OR 97225

Responsible for performing the validation and reporting laboratory results to Oregon Medical Laser Center: NAMSA, 9 Morgan Irvine, CA 92618

A.5 Test Procedures

A.5.1 Product Inoculation

A study total of ten Optical Wires will be innoculated. The placement wire (removed from the tube) will be directly inoculated with SPORTROL spore suspension on the area deemed to be most difficult to sterilize (see Appendix). An appropriate aliquot of *Geobacillus stearothermophilus* will be inoculated onto each device to achieve 10^6 (or equivalent population based on a D-value of 1.0) spores per device.

As it is not always possible to obtain *Geobacillus stearothermophilus* with a D-value of exactly 1.0 minutes, alternative combinations of resistance and population may be used, so long as they represent an equivalent or greater challenge to the sterilant. In practice, the population of a challenge organism with a D-value greater than 1.0 minutes may be reduced to compensate for its

greater resistance. Acceptable combinations can be calculated using the following equation:

$$(\textit{Challenge Population } \textit{Log}_{10}) \cdot (\textit{D-value}) \geq 6$$

(*Challenge Population* Log_{10})	(*D-value*) Range
10^6	1.0–1.1
10^5	1.2–1.4
10^4	1.5–1.9
10^3	2.0–2.9

Inoculation will be performed per NAMSA SOP and established NAMSA Test Specification.

Before and after inoculation, a quantitation of the inoculum suspension will be performed to ensure delivery population.

All inoculated products will be dried in a laminar airflow (LAF) hood for a minimum of four hours until visibly dry.

Once products are dry, the placement wire will be returned to original configuration inside tube.

A.5.2 Sterilization

For each of three cycles, three dry inoculated Optical Wires will be individually double-pouched. In addition, three Optical Fibers (inside Teflon coils) will be individually double-pouched. Although the Optical Fibers are not deemed most difficult to sterilize, they will be present in each cycle exposure to simulate practical sterilization configuration during routine use. Three double-pouched Optical Wires and three double-pouched Optical Fibers will be stacked inside the autoclave chamber.

Prior to each half cycle exposure, the autoclave chamber will be reloaded with three inoculated double-pouched Optical Wires. The same three Optical Fibers (dunnage) will be subjected to all half cycle exposures.

Each inner pouch has a steam chemical indicator strip supplied by the sponsor. The technician will document the color of each chemical indicator prior to and post exposure. The chemical indicator should turn from yellow to dark brown after steam exposure. Note: chemical indicators do not provide biological data; only verify the presence of steam.

The half cycle parameters will be **three minutes at 132°C with prevacuum air removal, four pulses, and no dry time.**

A.5.3 Test of Sterility

Immediately following each of three half cycle exposures, three inoculated Optical Wires will be aseptically removed from the pouches and individually tested for sterility in appropriate volumes of prepared Soybean Casein Digest Broth (SCDB).

One unexposed inoculated Optical Wire will be sterility tested upon the completion of the third half cycle to serve as a common positive control for all cycles.

All SCDB cultures will be incubated at 55–60°C until positive for growth or for seven days.

Tests of sterility will be performed per NAMSA SOP and established NAMSA Test Specification.

A.5.4 Reprocessing

All samples including positive controls will be soaked in bleach and dried prior to returning to the Sponsor.

A.6 Acceptance Criteria

If testing of sterility results in the absence of indicator growth for all three consecutive half cycles, then a six-log reduction will be demonstrated. This will qualify the manufacturers recommended full cycle of **six minutes at 132°C using prevacuum air removal in a double-pouched configuration.** The full cycle will demonstrate a twelve-log reduction and provide a sterility assurance level (SAL) of 10^{-6}.

The positive control must result in growth of the indicator organism. Chemical indicators must result in the desired color change. The study will be repeated if either criterion is not met.

If tests of sterility result in one or more positive test cultures (excluding positive controls), then the growth will be verified for the presence of indicator organism. The growth from all positive cultures will be subcultured to Tryptic Soy Agar (TSA) and incubated at 30–35°C and at 55–60°C. Presence of growth at 55–60°C and no growth at 30–35°C confirms the presence of indicator organism. If indicator organism is present, then the autoclave parameters will be examined for any unusual readings and other aspects of the testing may be investigated. Upon completion of the investigation, additional studies may be undertaken to meet the criteria of three consecutive

cycles meeting the acceptance criteria of no indicator growth. Recovery of a single non-indicator organism will not be considered a valid culture and the results of the remaining tests may be used to support sterilization efficacy. Recovery of multiple non-indicator positive cultures will require investigation and failure analysis before interpretation of the test results can be made.

A.7 Documentation

Laboratory data will be issued to OMLC detailing results obtained.

Copies of the autoclave cycle printouts for each half cycle will be filed with the corresponding laboratory data sheets.

A final summary report will be prepared by OMLC upon successful completion of the study.

Any amendment to the protocol must be documented and approved prior to study initiation.

Any deviation to the protocol after study initiation will be documented in the laboratory data sheets.

Any failure investigation will be summarized in a protocol supplement prior to repeating the study.

A.8 Record Storage

All raw data pertaining to this study are to be retained in designated NAMSA archive files for a period of five years.

A.9 References

- AAMI TIR12:2004 – Designing, testing, and labeling reusable medical devices for reprocessing in health care facilities: A guide to device manufacturers.

- ANSI/AAMI ST79:2006 – Comprehensive Guide to steam sterilization and sterility assurance in health care facilities.

- ISO 17664:2004 – Sterilization of medical devices Information to be provided by the manufacturer for the processing of resterilizable medical devices.

- ISO 17665-1:2006 – Sterilization of health care products - Moist heat - Part 1: Requirements for the development, validation and routine control of a sterilization process for medical devices.
- ISO 17665-2:2009 – Sterilization of health care products - Moist heat - Part 2: Guidance of the application of ISO 17665-1.
- United States Pharmacopeia. < 1035 > Biological Indicators for Sterilization.
- AAMI TIR39:2009 – Guidance on selecting a microbial challenge and inoculation sites for sterilization validation of health care products.
- ANSI/AAMI/ISO 11138-3:2006 – Sterilization of health care products Biological indicators Part 3: Biological indicators for moist heat sterilization processes.
- FDA 21 CFR 820 – Quality System Regulations
- NAMSA – Protocol No. 09G_54391_01 prepared by Nichole Jackson of NAMSA Advisory Services.

A.10 Appendix

A.10.1 Product Diagram

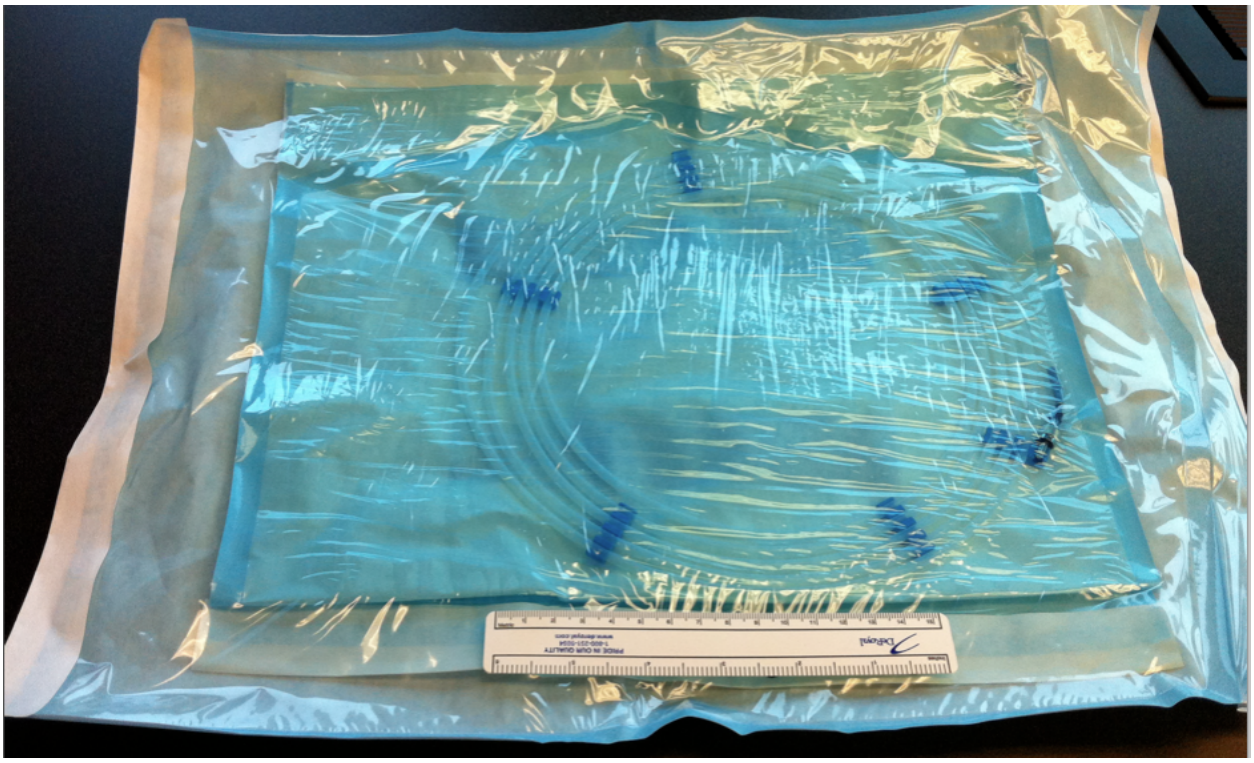

Figure A.1: The optical fiber is not intended for inoculation (dunnage). Note: Optical Fiber is packaged in an outer Teflon coil. Each coil is placed inside a paper/film pouch and sealed. Each inner pouch is placed inside an outer pouch and sealed for exposure.

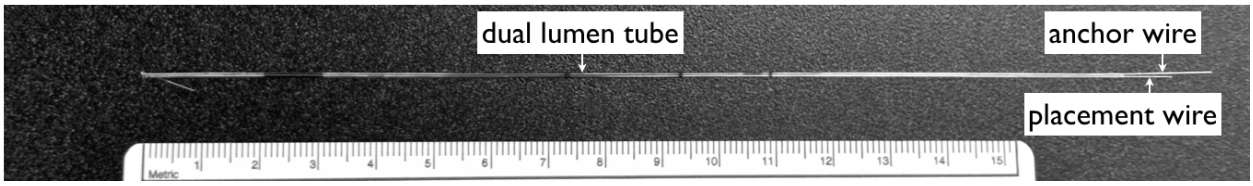

Figure A.2: Optical wire as provided, intended for inoculation; see diagram below.

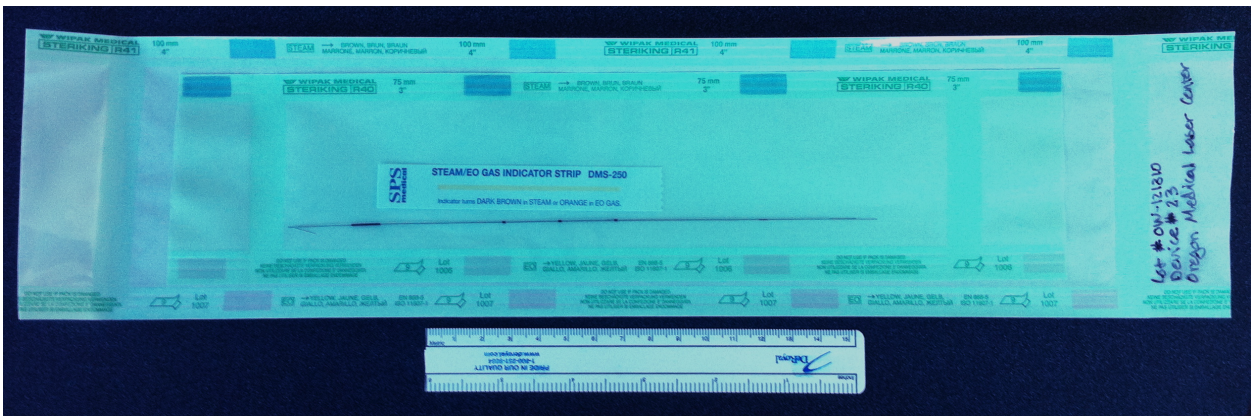

Figure A.3: After inoculation, the optical wire will be packaged in the sponsor supplied paper/film pouches. Each inner pouch is sealed and placed inside an outer pouch which is then sealed for exposure.

A.10.2 Inoculation Diagram

Remove placement wire from dual lumen tube and inoculate placement wire near midpoint. Once dry, return inoculated wire to original configuration inside tube.

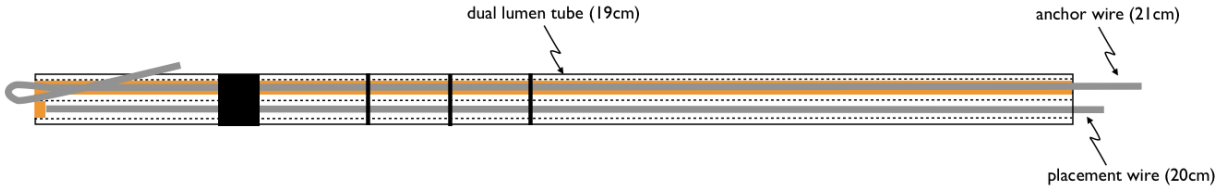

Figure A.4: Optical Wire with placement wire inside tube. The anchor wire is secured within the tube and can not be removed. For clarity, drawing is not to scale.

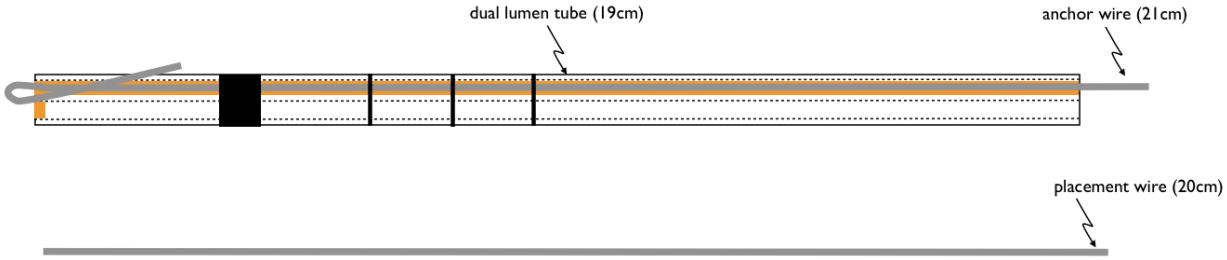

Figure A.5: Optical Wire with placement wire removed from tube. For clarity, drawing is not to scale.

Appendix B

Code

B.1 Time Resolved Monte Carlo

```
char  t1[80] = "Time-Resolved Monte Carlo by Scott Prahl (http://omlc.ogi.edu)";
char  t2[80] = "1 J Pulse Irradiation of Semi-Infinite Medium";

#include <stdio.h>
#include <stdlib.h>
#include <math.h>
#include <time.h>

#define TBINS 2049
#define RBINS 15
#define PULSE 200

double refl[RBINS][TBINS];
double x, y, z, t, u, v, w, weight;
double rs, rd, bit, tbins_per_mm;
double ps_per_tbin = 4; /* [ps/bin] 0.3 mm/ps in air, 0.15 mm/ps in glass */
double mm_per_rbin = 2; /* [mm/bin] radial displacement annulus */
double NA = 0.9*(M_PI / 2);        /* [rad] collection angle of fiber */

typedef struct simtype {
    double mu_a, mu_sp, g, n, albedo, mu_s, mu_t;
    double x0,y0,z0,u0,v0,w0;
    double rmin,rmax,NA,collect_angle,crit_angle,longest_distance;
    long photons;
```

```
} simtype;

static double sqr(double x) {
    return x*x;
}

static void get_input(simtype *s)
{
    double c, angle;

    FILE *fp = fopen("input.txt", "r");
    fscanf(fp, "%lf %lf %lf %lf", &s->mu_a, &s->mu_sp, &s->g, &s->n);
    fscanf(fp, "%lf %lf %lf ", &s->x0, &s->y0, &s->z0);
    fscanf(fp, "%lf %lf %lf ", &s->u0, &s->v0, &s->w0);
    fscanf(fp, "%lf %lf %ld ", &s->rmin, &s->rmax, &s->photons);

    c = 3.0E11 / 1.0E12 / s->n;               /* [mm/ps] speed of light in medium */
    tbins_per_mm  = 1/c/ps_per_tbin;          /* [bin/mm] or [ps/mm * bin/ps] */
    s->mu_s      = s->mu_sp / (1-s->g);       /* [1/mm] */
    s->mu_t      = s->mu_s + s->mu_a;         /* [1/mm] */
    s->albedo    = s->mu_s / (s->mu_s + s->mu_a); /* [-] */
    rs           = sqr((s->n-1.0)/(s->n+1.0)); /* [-] specular reflection */
    s->crit_angle = sqrt(1.0-1.0/s->n/s->n);  /* [-] cos of critical angle */
    s->NA        = NA;                    /* [rad] numerical apperture of fiber*/
    angle        = asin(s->NA/s->n);          /* [radians] acceptance angle */
    s->collect_angle = cos(angle);            /* [-] cos of collection angle of fiber */
    s->longest_distance = TBINS / tbins_per_mm; /* max time determines max distance */
}

static void launch(simtype s)
{
    x = s.x0;     /* [mm] position of source in semi-infinite medium */
    y = s.y0;     /*      z = 0 is surface bourdary with air     */
    z = s.z0;
    t = 0.0;      /* [mm] total path length */
    u = s.u0;     /* [-] direction cosines of the photon */
    v = s.v0;     /*      w = 1 is inward normal to surface*/
    w = s.w0;
    weight = 1.0; /* [-] weight of photon packet*/
}
```

```
static void bounce (simtype *s)       /* Interact with top surface */
{
    double radius, tt, temp, temp1, tf, ss, exiting;
    int tbin,rbin;
    w = -w;                                  /* photon is now going down */
    z = -z;                                  /* photon is now in the medium */
    if (w <= s->crit_angle) return;          /* total internal reflection */

    tt     = sqrt(1.0-sqr(s->n)*(1.0-w*w)); /* cos of exit angle */
    temp1  = (w - s->n*tt)/(w + s->n*tt);
    temp   = (tt - s->n*w)/(tt + s->n*w);
    tf     = 1.0-(temp1*temp1+temp*temp)/2.0; /* Fresnel transmission */
    exiting = tf * weight;                   /* fraction of photon weight exiting */

    ss     = fabs(z/w);                      /* distance photon went past surface */
    radius = sqrt(sqr(x-u*ss)+sqr(y-v*ss)); /* true radius at exit */

    rd    += exiting;                        /* add to total reflected light */
    weight -= exiting;                       /* decrease weight by that lost */

    if (w > s->collect_angle) {
      rbin    = radius / mm_per_rbin;     /* mm * bin/mm = # of radial bin */
        if (rbin >= RBINS) rbin = RBINS-1;
        tbin    = (t - ss) * tbins_per_mm;  /* mm * bin/mm = # of time bin */
        if (tbin >= TBINS) tbin = TBINS-1;
        refl[rbin][tbin] += exiting;         /* increment reflected light bin*/
    }
}

static void move(simtype *s) /* move to next scattering or absorption event */
{
    double d = -log((rand()+1.0)/(RAND_MAX+1.0)) / s->mu_t; /* [mm] */
    x += d * u;
    y += d * v;
    z += d * w;
    t += d;               /* [mm] total path length in mm */

    if ( z<=0 ) bounce(s); /* try to bin photon if it reaches surface */
}
```

```
static void absorb (simtype *s) /* Absorb light in the medium */
{
    weight *= s->albedo;
    if (weight < 0.01){ /* Roulette */
        bit -= weight;
        if (rand() > 0.1*RAND_MAX) weight = 0; else weight /= 0.1;
        bit += weight;
    }
}

static void scatter(simtype *s) /* [-] Scatter photon and establish new direction */
{
    double x1, x2, x3, ttt, mu;

    for(;;) {                           /*new direction*/
        x1=2.0*rand()/RAND_MAX - 1.0;
        x2=2.0*rand()/RAND_MAX - 1.0;
        if ((x3=x1*x1+x2*x2)<=1) break;
    }
    if (s->g==0) { /* isotropic */
        u = 2.0 * x3 -1.0;
        v = x1 * sqrt((1-u*u)/x3);
        w = x2 * sqrt((1-u*u)/x3);
        return;
    }

    mu = (1-s->g * s->g)/(1-s->g + 2.0 * s->g * rand()/RAND_MAX);
    mu = (1 + s->g * s->g -mu*mu)/2.0/s->g;
    if ( fabs(w) < 0.9 ) {
        ttt = mu * u + sqrt((1-mu*mu)/(1-w*w)/x3) * (x1*u*w-x2*v);
        v  = mu * v + sqrt((1-mu*mu)/(1-w*w)/x3) * (x1*v*w+x2*u);
        w  = mu * w - sqrt((1-mu*mu)*(1-w*w)/x3) * x1;
    } else {
        ttt = mu * u + sqrt((1-mu*mu)/(1-v*v)/x3) * (x1*u*v + x2*w);
        w  = mu * w + sqrt((1-mu*mu)/(1-v*v)/x3) * (x1*v*w - x2*u);
        v  = mu * v - sqrt((1-mu*mu)*(1-v*v)/x3) * x1;
    }
    u = ttt;
}
```

```
static void print_table(FILE *fp)
{
    int i,j;

    /* first a header line */
    fprintf(fp, "##[ps] ");
    for (i=0; i<RBINS-1; i++)
        fprintf(fp, "\t%4.1f-%4.1f mm", i*mm_per_rbin,(i+1)*mm_per_rbin);
    fprintf(fp, "\n");

    /* now each time point */
    for (j=0; j<TBINS-1; j++){
        fprintf(fp, "%6.2f", j*ps_per_tbin);
      for (i=0; i<RBINS-1; i++)
         fprintf(fp, "\t%12.3f", refl[i][j]);
        fprintf(fp, "\n");
    }
}

static void print_results(simtype s) /* Print the results */
{
    FILE *f1; FILE *f2;
    time_t now;
    struct tm *date;
    char thedate[80],thetime[80];
    char filetemp[132];

    /* name the current date, e.g., mc-11-09-10-15:10.txt */
    now = time(NULL);
    date = localtime(&now);
    strftime(thedate, 80, "%m-%d-%y", date);
    strftime(thetime, 80, "%H-%M", date);

    /*print the experimental parameters and results to one file*/
    snprintf(filetemp, 132, "%s-%s-%02dmm-MC-results.txt", thedate, thetime,(int) s.z0);
    f2 = fopen(filetemp,"w");
    if (f2 == NULL) {
        fprintf(stderr, "could not open %s\n", filetemp);
        exit(1);
```

```
}
fprintf(f2,"# time [month-day-year-hour-min]: %s-%s\n",thedate,thetime);
fprintf(f2,"# %s\n",t1);
fprintf(f2,"#\n");
fprintf(f2,"# Scattering      \t= %8.3f/mm\n",s.mu_s);
fprintf(f2,"# Absorption      \t= %8.3f/mm\n",s.mu_a);
fprintf(f2,"# Anisotropy      \t= %8.3f\n",s.g);
fprintf(f2,"# Refractive Index \t= %8.3f\n",s.n);
fprintf(f2,"# Photons         \t= %8ld\n",s.photons);
fprintf(f2,"# Temporal Bins   \t= %8d\n",TBINS);
fprintf(f2,"#  ps per bin     \t= %8.2f [ps/bin]\n",ps_per_tbin);
fprintf(f2,"#  max time       \t= %8.2f [ps]\n",TBINS*ps_per_tbin);
fprintf(f2,"#  max distance   \t= %8.2f [ps]\n",s.longest_distance);
fprintf(f2,"# Radial Bins     \t= %8d\n",RBINS);
fprintf(f2,"#  mm per bin     \t= %8.2f [mm/bin]\n",mm_per_rbin);
fprintf(f2,"#  min radius     \t= %8.2f [mm]\n",0.0);
fprintf(f2,"#  max radius     \t= %8.2f [mm]\n",RBINS*mm_per_rbin);
fprintf(f2,"#\n");
fprintf(f2,"# Fiber Collection: \n");
fprintf(f2,"#  NA             \t= %8.5f\n",s.NA);
fprintf(f2,"#  Angle Inside   \t= %8.5f degrees\n",asin(s.NA/s.n)*180/M_PI);
fprintf(f2,"#  cos(angle)     \t= %8.5f \n",cos(asin(s.NA/s.n)));
fprintf(f2,"#\n");
fprintf(f2,"# Location of source: \n");
fprintf(f2,"#  x              \t= %10.2f [mm]\n", s.x0);
fprintf(f2,"#  y              \t= %10.2f [mm]\n", s.y0);
fprintf(f2,"#  z              \t= %10.2f [mm]\n", s.z0);
fprintf(f2,"#\n");
fprintf(f2,"# Direction of first launch: \n");
fprintf(f2,"#  u              \t= %10.2f [mm]\n", s.u0);
fprintf(f2,"#  v              \t= %10.2f [mm]\n", s.v0);
fprintf(f2,"#  w              \t= %10.2f [mm]\n", s.w0);
fprintf(f2,"#\n");
fprintf(f2,"# Time \t Backscattered Light\n");
print_table(f2);
fclose(f2);

/*To be read into matlab: print the experimental parameters to file without headings
    */
```

```
    snprintf(filetemp, 132, "%s-%s-%02dmm-MC-variables.txt", thedate, thetime, (int)
        s.z0);
    f1 = fopen(filetemp,"w");
    fprintf(f1, "%10.4f\n %10.2f\n %10.2f\n %10.2f\n %10.2f\n %10.2f\n %8ld\n %8d\n
        %10.2f\n   %8d\n  %10.2f\n     %8.5f\n",
             s.mu_a, s.mu_s,   s.g,    s.n,    s.z0,    s.w0,    s.photons, TBINS,
                 ps_per_tbin, RBINS, mm_per_rbin, asin(s.NA/s.n)*180/M_PI );
    fclose(f1);

    /*To be read by matlab: print the results to file without headings
    snprintf(filetemp, 132, "%s-%02dmm-MC-results-for-matlab.txt", thedate, (int) s.z0);
    f3 = fopen(filetemp, "w");
    print_table(f3);
    fclose(f3);*/
}

static void reset_vals() /* Print the results */
{
    int i,j;
    rd = 0;
    for ( j = 0; j<TBINS; j++) {
      for ( i = 0; i<RBINS; i++)
         refl[i][j] =0;
    }
}

int main ()
{
    long i;
    simtype s;
    double depth;
    struct tm *date;
    char thetime[80];

    for (depth = 5; depth <= 45; depth += 5) {
        reset_vals();
        get_input(&s);
        s.z0 = depth;

      time_t now;
```

```
now = time(NULL);
date = localtime(&now);
strftime(thetime, 80, "%m-%d-%y,%H:%M:%S", date);
  fprintf(stderr, "depth =%3.0f mm, (time: %s)\n",depth,thetime);

  for (i = 1; i <= s.photons; i++){
   if (i == 1000){
      time_t now;
      now = time(NULL);
      date = localtime(&now);
      strftime(thetime, 80, "%m-%d-%y,%H:%M:%S", date);

      fprintf(stderr, "launched photons = %20.0ld,(time: %s)\n",i,thetime);
      /*fprintf(stderr, "launched photons = %20.0ld\n",i);*/
   }
   if (i == 10000){
      time_t now;
      now = time(NULL);
      date = localtime(&now);
      strftime(thetime, 80, "%m-%d-%y,%H:%M:%S", date);

      fprintf(stderr, "launched photons = %20.0ld,(time: %s)\n",i,thetime);
      /*fprintf(stderr, "launched photons = %20.0ld\n",i);*/
   }
   if (i == 100000){
      time_t now;
      now = time(NULL);
      date = localtime(&now);
      strftime(thetime, 80, "%m-%d-%y,%H:%M:%S", date);

      fprintf(stderr, "launched photons = %20.0ld,(time: %s)\n",i,thetime);
      /*fprintf(stderr, "launched photons = %20.0ld\n",i);*/
   }
   if (i == 1000000){
      time_t now;
      now = time(NULL);
      date = localtime(&now);
      strftime(thetime, 80, "%m-%d-%y,%H:%M:%S", date);

      fprintf(stderr, "launched photons = %20.0ld,(time: %s)\n",i,thetime);
```

```
            /*fprintf(stderr, "launched photons = %20.0ld\n",i);*/
         }
         if (i == 10000000){
            time_t now;
            now = time(NULL);
            date = localtime(&now);
            strftime(thetime, 80, "%m-%d-%y,%H:%M:%S", date);

            fprintf(stderr, "launched photons = %20.0ld,(time: %s)\n",i,thetime);
            /*fprintf(stderr, "launched photons = %20.0ld\n",i);*/
         }
         if (i == 100000000){
            time_t now;
            now = time(NULL);
            date = localtime(&now);
            strftime(thetime, 80, "%m-%d-%y,%H:%M:%S", date);

            fprintf(stderr, "launched photons = %20.0ld,(time: %s)\n",i,thetime);
            /*fprintf(stderr, "launched photons = %20.0ld\n",i);*/
         }

            launch (s);
            while (weight > 0 && t+z < s.longest_distance) {
                move (&s);
                absorb (&s);
                scatter (&s);
            }
        }

        print_results(s);
    }
     /* printf("w = %lf", w); */
     return 0;
}
```

B.2 Fourier Transform of Time Resolved Monte Carlo

```
clear all
%%%%%%%%%%%%%
% set the timestamp of the files to call and read the files that were
% output from time-mc-by-r-2 ( a time based Monte Carlo Code )
%%%%%%%%%%%%%
xx = 10;

%change MM,DD,YY,rr to call the correct files
rho = char('03-29-45mm');
MM = sprintf('02');      % Month
DD = sprintf('23');% %s',D(k,:)); % Day
YY = sprintf('11');      % Year
rr = sprintf('%s',rho); % hour

timestamp =  sprintf('%s-%s-%s-%s',MM,DD,YY,rr);

%read files
TbyPhoton = dlmread(sprintf('%s-MC-results.txt', timestamp), '', 35, 0);
var = dlmread(sprintf('%s-MC-variables.txt', timestamp), '', 0, 0);

[Rowt Col] = size(TbyPhoton);

mua    = var(1);     % [1/mm] absorption
mus    = var(2);     % [1/mm] scattering
g      = var(3);     % [-] anisotropy
nr     = var(4);     % [-] refractive index of medium
zz     = var(5);     % [mm] depth of source
ww     = var(6);     % [-] direction cos of photon launch
photons = var(7);    % [-] number of launched photons
tbins  = var(8);     % [bin] number of time bins
psPERbin= var(9);    % [ps/bin] picoseconds per time bin
rbins  = var(10);    % [bin] number of radial bins
mmPERbin= var(11);   % [mm/bin] milimeters per radial bin
colAngle  = var(12);    % [deg] collection angle of fiber

scrsz = get(0,'ScreenSize');

figure('name','TbyPhoton','NumberTitle','off','Position',[scrsz(3)/2 1 scrsz(3)/2
    scrsz(4)]); clf
set(gca, 'FontSize', 16)
```

```
hold all
for i = 2:1:Col;
   plot(TbyPhoton(:,1),TbyPhoton(:,i))
end
xlabel('time [ps]')
ylabel('binned photons')
xlim([0 4000])
legend('0-2mm','2-4mm','4-6mm','6-8mm','8-10mm','10-12mm','12-14mm','14-16mm',
    '16-18mm','18-20mm','20-22mm','22-24mm','24-26mm','26-28mm')
title(sprintf('%s: [units in mm]\n\n mu_a=%g, mu_s^,=%g, g=%g, n=%g, z=%g, w=%g \n\n
    Photons=%g, collection angle=%3.0fdeg, Time bins=%g, %gps/bin, Rbins=%g, %gmm/bin',
    timestamp, mua, mus*(1-g),g,nr, zz, ww,
    photons,colAngle,tbins,psPERbin,rbins,mmPERbin), 'fontsize', 12)
saveas(gcf,sprintf('%s-MC-plot',timestamp),'pdf')

m   = Rowt;               % [-] number of samples
dt  = psPERbin.* 1e-12;       % [s] time increment
fs  = 1./dt;                  % [1/s] sampling frequency
t   = (0:m-1)./fs;            % [s] time range of data
n   = pow2(nextpow2(10000));  % [-] number of points for fft >= m , must be power of 2
f   = ((0:n-1).*(fs/n))';     % [1/s] frequency range
finc= fs./n;                  % [1/s] frequency increment
fny = fs./2;                  % [1/s] nyquist frequency

%%%%%%%%%%%%%
% format data
%%%%%%%%%%%%%
Row = n/2+1;
nn = 50;
Allresults = zeros(nn,5,Col-1);
resultsf0 = zeros(Col-1,8);
resultsfx = zeros(Col-1,8);

for j = 1:1:Col-1;
x   = TbyPhoton(:,j+1);        % signal - time response of pulse wihtin a medium
photonsCol = sum(x);           % total photons collected for this detector location
Pow = (photonsCol .* 3.16e-19 ./ (t(m))) .* 1e9; % [nW] photons * 3.16e-19 Ws/photon *
    1/s -> 1mW for 1s is 3.16e16 photons!!!!!!!!!!!!!!!!!!
```

```
%%%%%%%%%%%%%
% uncomment this section to test if data is formatted correctly, this adds
% a small sin wave to the time domain signal with a frequency of ftest MHz.
% If all is well, a peak should appear in the amplitude plot at ftest MHz
% and amplitude of A. SWITCH THE FILE NAME OF THE PLOT THAT WILL BE SAVED
% IF YOU USE THIS TEST
%%%%%%%%%%%%%

% ftest = 400;           %[MHz] frequency
% A = 10000;               % [-] amplitude
% x = A.*sin(2*pi*ftest.*1e6.*t);%+ x';
% x = x';

%%%%%%%%%%%%%
% find discrete fourier transform of signal
%%%%%%%%%%%%%

y = fft(x,n)./m;

%%%%%%%%%%%%%
% shift fft and frequency range to center on zero and find the amplitude
% and phase of the signal.
%%%%%%%%%%%%%

y0   = y(1:n/2+1);            % Rearrange y values
f00  = ((-n/2:n/2-1).*(fs/n))'; % 0-centered frequency range
f0   = f(1:n/2+1);
mod  = 2*abs(y0);       % abs(X) = sqrt(real(X).^2 + imag(X).^2) ;
mod1 = 2*abs(y0(1));
mod0 = mod ./ mod1;            % [-] modulation
ph00 = angle(y0);       % [rad] phase: angle(z) = imag(log(z)) = atan2(imag(z),real(z))
ph0  = unwrap(ph00);

amp0(j) = abs(y0(1));
%%%%%%%%%%%%%
% Diffusion theory approximation to modulation and phase as a function of frequency
%%%%%%%%%%%%%
R11 = sqrt(zz^2 + ((j*2)-1)^2);
R1 = R11*1;
f00 = f0*1;
```

```
omega1 = 2.*pi.*f00;
musp = mus*(1-g);
%
% Ms1 = 1;
c = 3e11;
ct = c/nr;
%
% d = 1./(3.*(mua+musp));
% a = d.*ct;
% b = mua.*ct;
%
% u1 = sqrt(b ./ a);
% v1 = (1+ (omega1.^2 ./ b.^2)).^(1/4);
% w1 = 0.5 .* atan(omega1 ./ b);
%
% P1 = -R1 .* u1 .* v1 .* sin(w1);
% M1 = Ms1 .* exp(-R1 .* u1 .* (v1 .* cos(w1) - 1) );

mut = musp + mua;
mfppp = 1/mut;
tau = 1/(mua*ct);
delta = 1/(sqrt(3 * mua * mut));

u = sqrt( (3/2) .* mua .* mut);
w = sqrt(1 + (omega1 .* tau).^2);

kreal = u .* sqrt( w + 1);
kimag = u .* sqrt( w - 1);

%infinite medium
Pim = kimag .* R1;
Mim = exp(-u .* (sqrt(w + 1) - sqrt(2)) .* R1);

%zero boundary condition
ri = 0.6081 + 0.0636*n + 0.7099/n - 1.4399/(n^2);
Zb = (2/3) .* R1 .* ((1+ri) ./ (1-ri));
Zi = Zb + R1;
r0 = sqrt(Zi.^2 + ((j*2)-1)^2);
%r0 = R1;
Pzb = kimag .* R1 - atan(kimag ./ (kreal + (1./r0)));
```

```
a = sqrt((kreal + (1./r0)).^2 + kimag.^2 );
b = (1./delta) + (1./r0);
c = -R1 .* (kreal - (1./delta));

Mzb = (a ./ b) .* exp(c);

P1 = -Pzb;
M1 = Mzb;

%create arrays to print

results1 = [f0(1:nn)'/1e6; mod0(1:nn)'; M1(1:nn)'; ph0(1:nn)'; P1(1:nn)'];
Allresults(:,:,j) = results1';
results = results1';
resultsf0(j,:) = [R1 photonsCol Pow results(1,:)];
resultsfx(j,:) = [R1 photonsCol Pow results(xx,:)];


%%%%%%%%%%%%%
% Plot data and results. Save each to pdf file.
%%%%%%%%%%%%%
figure('Name', sprintf('%s',timestamp),'NumberTitle','off','Position',[1 1 scrsz(3)/2
    scrsz(4)]); clf

%plot original time domain signal
subplot(3,1,1);
hold on
set(gca, 'FontSize', 12)
plot(t*1e12,x,'r-')
xlim([ 0 4000])
%ylim([ 0 PMax])
ylabel('photons [-]')
xlabel('time [ps]')
title(sprintf('%s: [units in mm] \n mu_a=%g, mu_s',=%g, g=%g, n=%g, z=%g, r=%g, w=%g,
    Photons=%g, collection angle=%3.0f, Time bins=%g, %gps/bin, Rbins=%g, %gmm/bin',
    timestamp, mua, musp,g,nr, zz, j*2-1, ww,
    photons,colAngle,tbins,psPERbin,rbins,mmPERbin), 'fontsize', 8)

%plot magnitude as a function of frequency
```

```
subplot(3,1,2);
hold on
set(gca, 'FontSize', 12)
plot(results1(1,:),results1(2,:),'bx')
plot(results1(1,:),results1(3,:),'r-')
xlim([0 500])
ylim([0 1])
ylabel('modulation [-]')
%xlabel('frequency [MHz]')
set(gca,'xtick',[])
legend('MC','DT','fontsize' ,'12','location','southwest')

%plot phase as a function of frequency
subplot(3,1,3);
hold on
set(gca, 'FontSize', 12)
plot(results1(1,:),results1(4,:).*(180/pi),'bx')
plot(results1(1,:),results1(5,:).*(180/pi),'r-')
xlim([0 500])
ylim([-400 0])
ylabel('phase [deg]')
xlabel('frequency [MHz]')
legend('MC','DT','fontsize','12','location','southwest')
%saveas(gcf,sprintf('%s_plot_fft_test',timestamp),'pdf')
saveas(gcf,sprintf('%s-%2.1fmm-fft-plot.pdf',timestamp,R1),'pdf')
hold off
end

%%%%%%%%%%%%%
% Print results to text files
%%%%%%%%%%%%%
for i = 1:1:Col-1
fid2 = fopen(sprintf('%s-%2.1fmm-fft-results.txt',timestamp,resultsf0(i,1)),'w');
fprintf(fid2,'# FFT results of Monte Carlo simulation from: %s [M-D-Y-h-m]\n(see setup
    file for details of monte carlo simulation)\n',timestamp);
fprintf(fid2,'# r = %3.2f [mm] \n',resultsf0(i,1));
fprintf(fid2,'# Power = %G [nW] \n',resultsf0(i,3));
fprintf(fid2,'# frequency \t FFTmodulation \t DTmodulation \t FFTphase \t DTphase\n');
fprintf(fid2,'# [MHz]   \t [-]          \t [-]         \t [rad]   \t [rad] \n');
    for j = 1:1:nn
```

```
        for k = 1:1:5
            fprintf(fid2,'%G       \t%G            \t%G           \t%G       \t%G ',
                Allresults(j,k,i));
        end
        fprintf(fid2,'\n');
    end
    fclose(fid2);
end

%%%%%%%%%%%%%
%Plot power, modulation, and phase as a function of distance R
%%%%%%%%%%%%%
R = resultsfx(:,1);
ff = resultsfx(1,4);
figure('Name', sprintf('%s-by-R',timestamp),'NumberTitle','off','Position',[scrsz(3)/2 1
    scrsz(3)/2 scrsz(4)]); clf

%plot Power
subplot(3,1,1);
%hold on
set(gca, 'FontSize', 12)
semilogy(resultsf0(:,1),resultsf0(:,3), 'rx')
%xlabel('r [mm]')
set(gca,'xtick',[])
ylabel('detected power [nW]')
title(sprintf('%s: [units in mm] \n mu_a=%g, mu_s^,=%g, g=%g, n=%g, f=%3.0fMHz, w=%g,
    Photons=%g, collection angle=%3.0f, Time bins=%g, %gps/bin, Rbins=%g, %gmm/bin',
    timestamp, mua, musp,g,nr, ff, ww, photons,colAngle,tbins,psPERbin,rbins,mmPERbin),
    'fontsize', 8)

%plot modulation
subplot(3,1,2);
hold on
set(gca, 'FontSize', 12)
plot(R,resultsfx(:,5), 'bx')
plot(R,resultsfx(:,6),'r-')
%xlabel('r [mm]')
set(gca,'xtick',[])
ylabel('Modulation [-]')
legend('MC','DT','fontsize' ,'12','location','southwest')
```

```
%plot phase
subplot(3,1,3);
hold on
set(gca, 'FontSize', 12)
plot(R,resultsfx(:,7)*180/pi, 'bx')
plot(R,resultsfx(:,8)*180/pi, 'r-')
xlabel('r [mm]')
ylabel('Phase [deg]')
legend('MC','DT','fontsize' ,'12','location','southwest')
saveas(gcf,sprintf('%s-%3.0fMHz-fft-plot-by-R',timestamp,ff),'pdf')

figure('Name', sprintf('%s-ratio',timestamp),'NumberTitle','off','Position',[scrsz(3)/2
    1 scrsz(3)/2 scrsz(4)]); clf
%plot modulation
subplot(2,1,1);
hold on
set(gca, 'FontSize', 12)
plot(R,resultsfx(:,6)./resultsfx(:,5), 'bx')
%xlabel('r [mm]')
ylim([.8 1.2])
set(gca,'xtick',[])
ylabel('DT / MC - Modulation [-]')
title(sprintf('%s: [units in mm] \n mu_a=%g, mu_s',=%g, g=%g, n=%g, f=%3.0fMHz, w=%g,
    Photons=%g, collection angle=%3.0f, Time bins=%g, %gps/bin, Rbins=%g, %gmm/bin',
    timestamp, mua, musp,g,nr, ff, ww, photons,colAngle,tbins,psPERbin,rbins,mmPERbin),
    'fontsize', 8)

%plot phase
subplot(2,1,2);
hold on
set(gca, 'FontSize', 12)
plot(R,resultsfx(:,7)./resultsfx(:,8), 'bx')
ylim([.8 1.2])
xlabel('r [mm]')
ylabel('MC / DT - Phase [-]')
saveas(gcf,sprintf('%s-%3.0fMHz-fft-plot-ratio',timestamp,ff),'pdf')
```

B.3 Error Analysis of Probe Design

```
clear all

r2set = 5:5:50; % actual depth of source
inc = 0:1:30;    % change in psi

r2d = zeros(length(r2set),length(inc)); % calculated depth of source
resid = zeros(length(r2set),length(inc)); % residuals

for i = 1:length(r2set)
    r2 = r2set(i);
l = 5;                % distance between center and outer detectors

psi1 = (90 + inc) * pi/180;
psi3 = (90 - inc) * pi/180;

r1d = sqrt(r2.^2 + l.^2 - (2 .* r2 .* l .* cos(psi1)) );
r3d = sqrt(r2.^2 + l.^2 - (2 .* r2 .* l .* cos(psi3)) );

diff(i,:) = 1 - (r3d ./ r1d);

rd = (r1d + r3d) / 2;

alpha = asin(r2 ./ rd);
r2d(i,:) = l .* tan(alpha);
resid(i,:) = r2 - r2d(i,:);
end

scrsz = get(0,'ScreenSize');
figure('name','error','NumberTitle','off','Position',[scrsz(3)/2 1 scrsz(3)/2
    scrsz(4)]); clf

set(gca,'fontsize',13)
for i = 1:length(r2set)
    hold all
    plot(inc+90,-100 * (resid(i,:)./r2set(i)))
end
xlabel('angle of detector, \psi  [deg]')
ylabel('percent error [mm/mm]')
```

```
title(sprintf('l = %2.0f [mm]',l))
ylim([0 18])
saveas(gcf,sprintf('031011-l-%2.0f-mm-plot',l),'pdf')
```

B.4 Photon Distribution Monte Carlo

```
char  t1[80] = "Position Tracking Monte Carlo by Scott Prahl & Amanda Dayton"
char  t2[80] = "1 J Pulse Within Semi-Infinite Medium";

#include <stdio.h>
#include <stdlib.h>
#include <math.h>
#include <time.h>

#define TBINS 2049
#define RBINS 10
#define PULSE 200
#define EVENT 50000
#define COLS 6

double refl[RBINS][TBINS];
double path[EVENT][COLS];
double x, y, z, t, u, v, w, weight;
double rs, rd, bit, tbins_per_mm;
double ps_per_tbin = 4; /* [ps/bin] 0.3 mm/ps in air, 0.15 mm/ps in glass */
double mm_per_rbin = 1; /* [mm/bin] radial displacement annulus */
double NA = 1.4;        /* [rad] collection angle of fiber: 1.4rad=70deg, 0.6rad=25deg,
    0.22rad=8.5deg*/
double n2 = 1.49;  /* refractive index of probe*/
double photon;
int event;

char thedate[80],thetime[80];
char filetemp[132];

typedef struct simtype {
    double mu_a, mu_sp, g, n, albedo, mu_s, mu_t;
    double x0,y0,z0,u0,v0,w0;
```

```
    double rmin,rmax,NA,collect_angle,crit_angle,longest_distance;
    long photons;
} simtype;

static double sqr(double x) {
    return x*x;
}

static void get_input(simtype *s)
{
   double c, angle;

    FILE *fp = fopen("input.txt", "r");
    fscanf(fp, "%lf %lf %lf %lf", &s->mu_a, &s->mu_sp, &s->g, &s->n);
    fscanf(fp, "%lf %lf %lf ", &s->x0, &s->y0, &s->z0);
    fscanf(fp, "%lf %lf %lf ", &s->u0, &s->v0, &s->w0);
    fscanf(fp, "%lf %lf %ld ", &s->rmin, &s->rmax, &s->photons);

    c = 3.0E11 / 1.0E12 / s->n;               /* [mm/ps] speed of light in medium */
    tbins_per_mm  = 1/c/ps_per_tbin;          /* [bin/mm] or [ps/mm * bin/ps] */
    s->mu_s      = s->mu_sp / (1-s->g);       /* [1/mm] */
    s->mu_t      = s->mu_s + s->mu_a;         /* [1/mm] */
    s->albedo    = s->mu_s / (s->mu_s + s->mu_a); /* [-] */
    s->crit_angle = sqrt(1.0-sqr(n2)/sqr(s->n));  /* [-] cos of critical angle */
    s->NA        = NA;                    /* [rad] numerical apperture of fiber*/
    angle        = asin(s->NA/s->n);          /* [radians] acceptance angle */
    s->collect_angle = cos(angle);            /* [-] cos of collection angle of fiber */
    s->longest_distance = TBINS / tbins_per_mm; /* max time determines max distance */
}

static void launch(simtype s)
{
    x = s.x0;     /* [mm] position of source in semi-infinite medium */
    y = s.y0;     /*     z = 0 is surface bourdary with air     */
    z = s.z0;
    t = 0.0;      /* [mm] total path length */
    u = s.u0;     /* [-] direction cosines of the photon */
    v = s.v0;     /*     w = 1 is inward normal to surface*/
    w = s.w0;
    weight = 1.0; /* [-] weight of photon packet*/
```

```
}

static void bounce (simtype *s)       /* Interact with top surface */
{
    double radius, tt, temp, temp1, tf, ss, exiting;

    w = -w;                                  /* photon is now going down */
    z = -z;                                  /* photon is now in the medium */
    if (w <= s->crit_angle) return;          /* total internal reflection */

    tt     = sqrt(1.0-sqr(s->n/n2)*(1.0-w*w)); /* cos of exit angle */
    temp1  = (s->n*w - n2*tt)/(s->n*w + n2*tt);
    temp   = (s->n*tt - n2*w)/(s->n*tt + n2*w);
    tf     = 1.0-(temp1*temp1+temp*temp)/2.0; /* Fresnel transmission */
    exiting = tf * weight;                   /* fraction of photon weight exiting */

    ss     = fabs(z/w);                      /* distance photon went past surface */
    radius = sqrt(sqr(x-u*ss)+sqr(y-v*ss)); /* true radius at exit */

    rd    += exiting;                        /* add to total reflected light */
    weight -= exiting;                       /* decrease weight by that lost */

   if (w >= s->collect_angle){
     if (x >= -0.5 && x <= 0.5 && y >=-0.5 && y <=0.5) {path[event][5] = 1;weight =0;}
     if (x >= -0.5 && x <= 0.5 && y >=4.5 && y <=5.5) {path[event][5] = 5;weight =0;}
     if (x >= -0.5 && x <= 0.5 && y >=9.5 && y <=10.5) {path[event][5] = 10;weight =0;}
   }
}

static void move(simtype *s) /* move to next scattering or absorption event */
{
   if ( event == 1) { srand(photon);}
   /*if ( event == 1) { srandomdev(photon);}*/

    double d = -log((rand()+1.0)/(RAND_MAX+1.0)) / s->mu_t; /* [mm] */
    x += d * u;
    y += d * v;
    z += d * w;
    t += d;               /* [mm] total path length in mm */
```

```
   event += 1;
   path[event][0] = photon;
   path[event][1] = event;
   path[event][2] = x;
   path[event][3] = y;
   path[event][4] = z;

    if ( z<=0 ) {bounce(s); } /* try to bin photon if it reaches surface */

}

static void absorb (simtype *s) /* Absorb light in the medium */
{
    weight *= s->albedo;
    if (weight < 0.01){ /* Roulette */
        bit -= weight;
        if (rand() > 0.1*RAND_MAX) weight = 0; else weight /= 0.1;
        bit += weight;
    }
}

static void scatter(simtype *s) /* [-] Scatter photon and establish new direction */
{
    double x1, x2, x3, ttt, mu;

    for(;;) {                           /*new direction*/
        x1=2.0*rand()/RAND_MAX - 1.0;
        x2=2.0*rand()/RAND_MAX - 1.0;
        if ((x3=x1*x1+x2*x2)<=1) break;
    }
    if (s->g==0) { /* isotropic */
        u = 2.0 * x3 -1.0;
        v = x1 * sqrt((1-u*u)/x3);
        w = x2 * sqrt((1-u*u)/x3);
        return;
    }

    mu = (1-s->g * s->g)/(1-s->g + 2.0 * s->g * rand()/RAND_MAX);
    mu = (1 + s->g * s->g -mu*mu)/2.0/s->g;
    if ( fabs(w) < 0.9 ) {
```

```
        ttt = mu * u + sqrt((1-mu*mu)/(1-w*w)/x3) * (x1*u*w-x2*v);
        v  = mu * v + sqrt((1-mu*mu)/(1-w*w)/x3) * (x1*v*w+x2*u);
        w  = mu * w - sqrt((1-mu*mu)*(1-w*w)/x3) * x1;
    } else {
        ttt = mu * u + sqrt((1-mu*mu)/(1-v*v)/x3) * (x1*u*v + x2*w);
        w  = mu * w + sqrt((1-mu*mu)/(1-v*v)/x3) * (x1*v*w - x2*u);
        v  = mu * v - sqrt((1-mu*mu)*(1-v*v)/x3) * x1;
    }
    u = ttt;
}

static void print_table(FILE *fp)
{
    int j;

    /* write each point */
    for (j=0; j<event+1; j++){
        fprintf(fp, "%6.0f", path[j][0]);
      fprintf(fp, "\t %12.0f", path[j][1]);
      fprintf(fp, "\t %6.2f", path[j][2]);
      fprintf(fp, "\t %6.2f", path[j][3]);
      fprintf(fp, "\t %6.2f", path[j][4]);
      fprintf(fp, "\t %6.0f \n", path[j][5]);

    }
}



static void get_timestamp() /* create timestamp */
{
    time_t now;
   struct tm *date;

    /* name the current date and time, e.g., mc-11-09-10-15:10.txt */
    now = time(NULL);
   date = localtime(&now);
   strftime(thedate, 80, "%m-%d-%y", date);
   strftime(thetime, 80, "%H-%M", date);
   snprintf(filetemp, 132, "%s-%s-MC-path-results.txt", thedate, thetime);
```

```
}

static void print_files(simtype s) /* Print the results */
{
    FILE *f2;

    /*print the experimental parameters and results to one file*/
    f2 = fopen(filetemp,"w");
    if (f2 == NULL) {
        fprintf(stderr, "could not open %s\n", filetemp);
        exit(1);
    }
   fprintf(f2,"%4.3f\t%4.3f\t%4.3f\t%4.3f\t%8ld\t%4.2f\t%4.2f\t%4.2f\t%4.2f\t%4.2f\t%4.2f\n",
       s.mu_s,s.mu_a,s.g,s.n,s.photons,s.x0,s.y0,s.z0,s.u0,s.v0,s.w0);
   fprintf(f2,"# time [month-day-year-hour-min]: %s-%s\n",thedate,thetime);
   fprintf(f2,"# %s\n",t1);
   fprintf(f2,"#\n");
    fprintf(f2,"# Scattering      \t= %8.3f/mm\n",s.mu_s);
    fprintf(f2,"# Absorption      \t= %8.3f/mm\n",s.mu_a);
    fprintf(f2,"# Anisotropy      \t= %8.3f\n",s.g);
    fprintf(f2,"# Refractive Index \t= %8.3f\n",s.n);
    fprintf(f2,"# Photons         \t= %8ld\n",s.photons);
   /* fprintf(f2,"# Temporal Bins   \t= %8d\n",TBINS);
    fprintf(f2,"#   ps per bin    \t= %8.2f [ps/bin]\n",ps_per_tbin);
    fprintf(f2,"#   max time      \t= %8.2f [ps]\n",TBINS*ps_per_tbin);
    fprintf(f2,"#   max distance  \t= %8.2f [ps]\n",s.longest_distance);
    fprintf(f2,"# Radial Bins     \t= %8d\n",RBINS);
    fprintf(f2,"#   mm per bin    \t= %8.2f [mm/bin]\n",mm_per_rbin);
    fprintf(f2,"#   min radius    \t= %8.2f [mm]\n",0.0);
    fprintf(f2,"#   max radius    \t= %8.2f [mm]\n",RBINS*mm_per_rbin);*/
    fprintf(f2,"#\n");
    fprintf(f2,"# Fiber Collection: \n");
    fprintf(f2,"#   NA            \t= %8.5f\n",s.NA);
    fprintf(f2,"#   Half Angle    \t= %8.5f degrees\n",asin(s.NA/s.n)*180/M_PI);
    fprintf(f2,"#   cos(angle)    \t= %8.5f \n",cos(asin(s.NA/s.n)));
    fprintf(f2,"#\n");
    fprintf(f2,"# Location of source: \n");
    fprintf(f2,"#   x             \t= %10.2f [mm]\n", s.x0);
    fprintf(f2,"#   y             \t= %10.2f [mm]\n", s.y0);
    fprintf(f2,"#   z             \t= %10.2f [mm]\n", s.z0);
```

```
    fprintf(f2,"#\n");
    fprintf(f2,"# Direction of first launch: \n");
    fprintf(f2,"#   u              \t= %10.2f [mm]\n", s.u0);
    fprintf(f2,"#   v              \t= %10.2f [mm]\n", s.v0);
    fprintf(f2,"#   w              \t= %10.2f [mm]\n", s.w0);
    fprintf(f2,"#\n");
   fprintf(f2,"#photon \t event\tx[mm]\ty[mm]\tz[mm]\tdetector radius [mm] \n");
    fclose(f2);

}

static void print_results(simtype s) /* Print the results */
{
    FILE *f1;

    /*print the results to file*/
    f1 = fopen(filetemp,"a");
    if (f1 == NULL) {
        fprintf(stderr, "could not open %s\n", filetemp);
        exit(1);
    }
      print_table(f1);
    fclose(f1);
}

static void reset_vals()
{
    int i,j;
    rd = 0;
    for ( j = 0; j<EVENT; j++) {
      for ( i = 0; i<6; i++)
         path[j][i] =0;
    }
   event = 0;
}

int main ()
{
    long i;
   char thetime[80];
```

```
struct tm *date;
 simtype s;

get_input(&s);
get_timestamp();
print_files(s);

time_t now;
now = time(NULL);
date = localtime(&now);
strftime(thetime, 80, "%m-%d-%y,%H:%M:%S", date);
fprintf(stderr, "(time: %s)\n",thetime);

for (i = 1; i <= s.photons; i++){
   reset_vals();
   photon = i;

         if (i == 1000){
            time_t now;
            now = time(NULL);
            date = localtime(&now);
            strftime(thetime, 80, "%m-%d-%y,%H:%M:%S", date);
            fprintf(stderr, "launched photons = %20.0ld,(time: %s)\n",i,thetime);
         }
         if (i == 10000){
            time_t now;
            now = time(NULL);
            date = localtime(&now);
            strftime(thetime, 80, "%m-%d-%y,%H:%M:%S", date);
            fprintf(stderr, "launched photons = %20.0ld,(time: %s)\n",i,thetime);
         }
         if (i == 100000){
            time_t now;
            now = time(NULL);
            date = localtime(&now);
            strftime(thetime, 80, "%m-%d-%y,%H:%M:%S", date);
            fprintf(stderr, "launched photons = %20.0ld,(time: %s)\n",i,thetime);
         }
         if (i == 1000000){
            time_t now;
```

```
            now = time(NULL);
            date = localtime(&now);
            strftime(thetime, 80, "%m-%d-%y,%H:%M:%S", date);
            fprintf(stderr, "launched photons = %20.0ld,(time: %s)\n",i,thetime);
          }
          if (i == 10000000){
            time_t now;
            now = time(NULL);
            date = localtime(&now);
            strftime(thetime, 80, "%m-%d-%y,%H:%M:%S", date);
            fprintf(stderr, "launched photons = %20.0ld,(time: %s)\n",i,thetime);
          }
          if (i == 100000000){
            time_t now;
            now = time(NULL);
            date = localtime(&now);
            strftime(thetime, 80, "%m-%d-%y,%H:%M:%S", date);
            fprintf(stderr, "launched photons = %20.0ld,(time: %s)\n",i,thetime);
          }
      launch (s);
      while (weight > 0 && t+z < s.longest_distance) {
         move (&s);
         absorb (&s);
         scatter (&s);
      }
      if (path[event][5] == 1) {print_results(s);}
      if (path[event][5] == 5) {print_results(s);}
      if (path[event][5] == 10){print_results(s);}
   }
    return 0;
}
```

B.5 Analysis of Photon Distribution Monte Carlo

```
clear all
% % %%%%%%%%%%%%
% % %set the timestamp of the files to call and read the files that were
% % %output from light-path-mc ( a photon position based based Monte Carlo Code )
```

```
% % %%%%%%%%%%%%

%%%%% change MM,DD,YY,time to call the correct files %%%%%%%%%%%%%%%%%
MM      = sprintf('09');   % Month
DD      = sprintf('05');   % Day
YY      = sprintf('11');   % Year
time    = sprintf('10-02'); % hour-minute

timestamp =  sprintf('%s-%s-%s-%s',MM,DD,YY,time);

%%%%% read file %%%%%%%%%%%%%%%%%%%%%%%%%%%%%%%%%%%%%%%%%%%%%%%%%%%%%%%%
%%% if the time stamp is between 08-18-11 and 08-24-11 start should be 17,
%%% if the time stamp is between 08-26-11 and ? start should be 26
start = 26;
path = dlmread(sprintf('%s-MC-path-results.txt', timestamp), '', start, 0);
var = dlmread(sprintf('%s-MC-path-results.txt', timestamp),'\t', 'a1..k1');

mus     = var(1);      % [1/mm] absorption
mua     = var(2);      % [1/mm] scattering
g       = var(3);      % [-] anisotropy
nr      = var(4);      % [-] refractive index of medium
photons = var(5);      % [-] number of launched photons
zz      = var(8);      % [mm] depth of source
ww      = var(11);     % [-] direction cos of photon launch
musp    = mus * (1-g); % [1/mm] reduced scattering

%%%%%% find index where each photon was collected at the detector %%%%%%%%
ind   = find(path(:,6));    % length of this matrix is number of photons collected at all
    detectors
ind0  = find(path(:,6)==1); % length of this matrix is number of photons collected at 0mm
    detector
ind5  = find(path(:,6)==5); % length of this matrix is number of photons collected at 5mm
    detector
ind10 = find(path(:,6)==10); % length of this matrix is number of photons collected at
    10mm detector


%%%%%%%% create 2 sets of data, ph are m x 3 matrixes with the mean
%%%%%%%% locations ( x, y, z) of each photon in each row, path are n x 3 matrixes with
    all of
```

```
%%%%%%%% the locations of all the photons
ph0 = []; path0 = [];
ph5 = []; path5 = [];
ph10 = [];path10 = [];
  for i = 1:1:length(ind)
     if path(ind(i),6) == 1
         if i == 1
             pm0 = path(1:ind(i), 3:5);
             p0 = path(1:ind(i), 3:5);
         end
         if i > 1
            pm0 = path(ind(i-1):ind(i), 3:5);
            p0 = path(ind(i-1):ind(i), 3:5);
         end
         pmean0 = mean(p0);
         ph0 = cat(1,ph0,pmean0);
         path0 = cat(1,path0,p0);
     end

     if path(ind(i),6) == 5
         if i == 1
             pm5 = path(1:ind(i), 3:5);
             p5 = path(1:ind(i), 3:5);
         end
         if i > 1
            pm5 = path(ind(i-1):ind(i), 3:5);
            p5 = path(ind(i-1):ind(i), 3:5);
         end
         pmean5 = mean(p5);
         ph5 = cat(1,ph5,pmean5);
         path5 = cat(1,path5,p5);
     end

     if path(ind(i),6) == 10
         if i == 1
             pm10 = path(1:ind(i), 3:5);
             p10 = path(1:ind(i), 3:5);
         end
         if i > 1
            pm10 = path(ind(i-1):ind(i), 3:5);
```

```
            p10 = path(ind(i-1):ind(i), 3:5);

        end
        pmean10 = mean(p10);
        ph10 = cat(1,ph10,pmean10);
        path10 = cat(1,path10,p10);
    end
  end



%%%%%%%%%% generate counts for contour plots

s  = 1;
x  = -40.5:s:40.5;
y  = -40.5:s:40.5;
z  = -10.5:s:70.5;
SS = [length(path0(:,1)) length(path5(:,1)) length(path10(:,1))];

XZ0 = hist3([path0(:,1) path0(:,3)],'Edges',{x z});
XZ5 = hist3([path5(:,1) path5(:,3)],'Edges',{x z});
XZ10 = hist3([path10(:,1) path10(:,3)],'Edges',{x z});

XZ0m = hist3([-path0(:,1) path0(:,3)],'Edges',{x z});
XZ5m = hist3([-path5(:,1) path5(:,3)],'Edges',{x z});
XZ10m = hist3([-path10(:,1) path10(:,3)],'Edges',{x z});

YZ0 = hist3([path0(:,2) path0(:,3)],'Edges',{y z});
YZ5 = hist3([path5(:,2) path5(:,3)],'Edges',{y z});
YZ10 = hist3([path10(:,2) path10(:,3)],'Edges',{y z});

YZ0m = hist3([-path0(:,2) path0(:,3)],'Edges',{y z});
YZ5m = hist3([-path5(:,2) path5(:,3)],'Edges',{y z});
YZ10m = hist3([-path10(:,2) path10(:,3)],'Edges',{y z});


XZ0t = XZ0 + XZ0m;
XZ5t = XZ5 + XZ5m;
XZ10t = XZ10 + XZ10m;
```

```
YZ0t = YZ0 + YZ0m;
YZ5t = YZ5 + YZ5m;
YZ10t = YZ10 + YZ10m;
% normalize the count in each bin to the total number of scattering events
% for each detector. Each bin represents the fraction of total photons
% that occupied the space of the bin. Each of these matrices sum to 1.
XZ0n  = XZ0t./(SS(1)*2);
XZ5n  = XZ5t./(SS(2)*2);
XZ10n = XZ10t./(SS(3)*2);

YZ0n = YZ0t./(SS(1)*2);
YZ5n = YZ5t./(SS(2)*2);
YZ10n = YZ10t./(SS(3)*2);

% take the difference between the normailized counts at 0-5 and 0-10. Each
%  number in each bin is the difference between the two detectors being
%  compared, positive numbers are the fraction of scattering events collected at the 0mm
%  detector and not at the other detector, negative numbers were collected in
%  the other detector butwere not collected at 0mm.
XZ05  = XZ0n - XZ5n;
XZ010 = XZ0n - XZ10n;

YZ05  = YZ0n - YZ5n;
YZ010 = YZ0n - YZ10n;

% find the total percent difference between the two detectors.
%           difference / (detector1 + detector2)
XZ05s  = sum(sum(abs(XZ05 )))/2;
XZ010s = sum(sum(abs(XZ010)))/2;
YZ05s  = sum(sum(abs(YZ05 )))/2;
YZ010s = sum(sum(abs(YZ010)))/2;


%%% find the positive (p) and negative (n) percent difference. The
%%% positive values are the percent of scattering events collected at 0mm,
%%% the negative values were collected at the other detector.
XZ05p  = sum(sum( XZ05(XZ05>=0) ))/2;
XZ05n  = sum(sum( XZ05(XZ05<=0) ))/2;
XZ010p = sum(sum( XZ010(XZ010>=0) ))/2;
XZ010n = sum(sum( XZ010(XZ010<=0) ))/2;
```

```
YZ05p = sum(sum( YZ05(YZ05>=0) ))/2;
YZ05n = sum(sum( YZ05(YZ05<=0) ))/2;
YZ010p = sum(sum( YZ010(YZ010>=0) ))/2;
YZ010n = sum(sum( YZ010(YZ010<=0) ))/2;

%%%%%%%%% contour plots and save %%%%%%%%%%%%%%%%%%%%%%%%%%%%%%%%%%%%%%%%%%%%%
scrsz = get(0,'ScreenSize');     % get screen size
fntsz = 12;    % font size
cmap = jet;   % color map for contour plot
a = -0.5;
b = 0.5;
left = -19;
top = 39.8;
o1 = 2;
o2 = 4;
o3 = 6;
o4 = 8;
    %%%%%%%%% XZ contour plots%%%%%%%
figure('name','XZ PROJECTION 0-5mm','NumberTitle','off','Position',[scrsz(3)/2 1
    scrsz(3)/2 scrsz(4)]); clf

    set(gca, 'FontSize', fntsz)
    hold all
    [C h ]= contourf(x+0.5,z+0.5,100*XZ05');
    colormap(cmap)
    colorbar
    caxis([a b])
    %clabel(C,h)
    ylabel('z [mm]')
    xlabel('x [mm]')
    xlim([ -20 20])
    ylim([ 0 40])
    title(sprintf('%s: [units in mm] \n mu_a=%g, mu_s^,=%g, g=%g, n=%g, photons launched
        = %g, Source(x,y,z) = (0,0,%g)', timestamp, mua, musp,g,nr,photons, zz))
    text(left,top ,sprintf('photons detected at (0,0,0) = %g
        ',length(ind0)),'BackgroundColor',[1 1 1])
    text(left,top-o1,sprintf('photons detected at (0,5,0) = %g
        ',length(ind5)),'BackgroundColor',[1 1 1])
    text(left,top-o2,sprintf('total percent difference between 0mm and 5mm = %2.1f
        ',XZ05s*100),'BackgroundColor',[1 1 1])
```

```
    text(left,top-o3,sprintf('percent collected at 0mm and missed at 5mm = %2.1f
        ',XZ05p*100),'BackgroundColor',[1 1 1])
    text(left,top-o4,sprintf('percent collected at 5mm and missed at 0mm = %2.1f
        ',abs(XZ05n)*100),'BackgroundColor',[1 1 1])
    saveas(gcf,sprintf('%s-%2.0fmmDepth-XZ-0-5mm-contour-mirror-plot',timestamp,zz),'pdf')

figure('name','XZ PROJECTION 0-10mm ','NumberTitle','off','Position',[scrsz(3)/2 1
    scrsz(3)/2 scrsz(4)]); clf

    set(gca, 'FontSize', fntsz)
    hold all
    contourf(x+0.5,z+0.5,100*XZ010');
    colormap(cmap)
    colorbar
    caxis([a b])
    ylabel('z [mm]')
    xlabel('x [mm]')
    xlim([ -20 20])
    ylim([ 0 40])
    title(sprintf('%s: [units in mm] \n mu_a=%g, mu_s^,=%g, g=%g, n=%g, photons launched
        = %g, Source(x,y,z) = (0,0,%g)', timestamp, mua, musp,g,nr,photons, zz))
    text(left,top ,sprintf('photons detected at (0,0,0) = %g
        ',length(ind0)),'BackgroundColor',[1 1 1])
    text(left,top-o1,sprintf('photons detected at (0,10,0) = %g
        ',length(ind10)),'BackgroundColor',[1 1 1])
    text(left,top-o2,sprintf('total percent difference between 0mm and 10mm = %2.1f
        ',XZ010s*100),'BackgroundColor',[1 1 1])
    text(left,top-o3,sprintf('percent collected at 0mm and missed at 10mm = %2.1f
        ',XZ010p*100),'BackgroundColor',[1 1 1])
    text(left,top-o4,sprintf('percent collected at 10mm and missed at 0mm = %2.1f
        ',abs(XZ010n)*100),'BackgroundColor',[1 1 1])

    saveas(gcf,sprintf('%s-%2.0fmmDepth-XZ-0-10mm-contour-mirror-plot',timestamp,zz),'pdf')


%%%%%%%%% YZ contour plots
 figure('name','YZ PROJECTION 0-5mm','NumberTitle','off','Position',[scrsz(3)/2 1
     scrsz(3)/2 scrsz(4)]); clf

    set(gca, 'FontSize', fntsz)
```

```
    hold all
    contourf(y+0.5,z+0.5,100*YZ05');
    colormap(cmap)
    colorbar
    caxis([a b])
    ylabel('z [mm]')
    xlabel('y [mm]')
    xlim([ -20 20])
    ylim([ 0 40])
    title(sprintf('%s: [units in mm] \n mu_a=%g, mu_s^,=%g, g=%g, n=%g, photons launched
        = %g, Source(x,y,z) = (0,0,%g)', timestamp, mua, musp,g,nr,photons, zz))
    text(left,top ,sprintf('photons detected at (0,0,0) = %g
        ',length(ind0)),'BackgroundColor',[1 1 1])
    text(left,top-o1,sprintf('photons detected at (0,5,0) = %g
        ',length(ind5)),'BackgroundColor',[1 1 1])
    text(left,top-o2,sprintf('total percent difference between 0mm and 5mm = %2.1f
        ',YZ05s*100),'BackgroundColor',[1 1 1])
    text(left,top-o3,sprintf('percent collected at 0mm and missed at 5mm = %2.1f
        ',YZ05p*100),'BackgroundColor',[1 1 1])
    text(left,top-o4,sprintf('percent collected at 5mm and missed at 0mm = %2.1f
        ',abs(YZ05n)*100),'BackgroundColor',[1 1 1])

    saveas(gcf,sprintf('%s-%2.0fmmDepth-YZ-0-5mm-contour-mirror-plot',timestamp,zz),'pdf')

figure('name','YZ PROJECTION 0-10mm','NumberTitle','off','Position',[scrsz(3)/2 1
    scrsz(3)/2 scrsz(4)]); clf

    set(gca, 'FontSize', fntsz)
    hold all
    contourf(y+0.5,z+0.5,100*YZ010');
    colormap(cmap)
    colorbar
    caxis([a b])
    ylabel('z [mm]')
    xlabel('y [mm]')
    xlim([ -20 20])
    ylim([ 0 40])
    title(sprintf('%s: [units in mm] \n mu_a=%g, mu_s^,=%g, g=%g, n=%g, photons launched
        = %g, Source(x,y,z) = (0,0,%g)', timestamp, mua, musp,g,nr,photons, zz))
```

```
text(left,top ,sprintf('photons detected at (0,0,0) = %g
    ',length(ind0)),'BackgroundColor',[1 1 1])
text(left,top-o1,sprintf('photons detected at (0,10,0) = %g
    ',length(ind10)),'BackgroundColor',[1 1 1])
text(left,top-o2,sprintf('total percent difference between 0mm and 10mm = %2.1f
    ',YZ010s*100),'BackgroundColor',[1 1 1])
text(left,top-o3,sprintf('percent collected at 0mm and missed at 10mm = %2.1f
    ',YZ010p*100),'BackgroundColor',[1 1 1])
text(left,top-o4,sprintf('percent collected at 10mm and missed at 0mm = %2.1f
    ',abs(YZ010n)*100),'BackgroundColor',[1 1 1])

saveas(gcf,sprintf('%s-%2.0fmmDepth-YZ-0-10mm-contour-mirror-plot',timestamp,zz),'pdf')
```